Chiba Institute of Technology

Doctoral Dissertation

Synthesis, thermal, mechanical, and self-healing properties of biodegradable polyester networks

(生分解性ポリエステルネットワークの合成および熱・力学と自己修復特性)

March 2023

Ussama Warunya

要旨

生分解性ポリエステルネットワークの合成および熱・力学と自己修復特性

本論文は生分解性ポリマーとして代表的なポリ乳酸（PLA）、ポリ（ε-カプロラクトン）（PCL）とポリブチレンサクシネート（PBS）の高分子鎖を含む各種ネットワークポリマーの合成、熱・力学物性およびジスルフィドメタセシス反応を利用した自己修復特性の調査について記述したものであり 3 章から構成される。

現在、大量に排出されるプラスチック廃棄物の環境中への流出による環境汚染や、最近では大きさが 5 mm 以下のマイクロプラスチックによる海洋生物の生態系破壊が大きな問題となっている。それらの環境問題を解決する手段として自然環境中で微生物の働きにより炭酸ガスと水に分解される生分解性プラスチックが注目を集めている。また、生分解性ポリマーの多くはバイオマスから誘導可能なポリマー(バイオベースポリマー)であり、中でも PLA と PBS は将来的な石油資源の枯渇やプラスチック廃棄物の焼却処理に伴い発生する炭酸ガスによる地球温暖化を抑制できる材料として開発が進んでいる。しかし、PLA は高分子材料の中では破断点伸び率が約 3%と非常に低く、靭性に乏しい。一方、石油由来の生分解性ポリマーの PCL は高い破断点伸び率(>300%)を示すが、PCL の融点と引張強さは約 60 ℃と 20 MPa と PLA の約 170℃と 50 MPa よりも非常に低い。そこで相補的な熱・力学物性を示す PLA と PCL のポリマーブレンドの研究が行われているが、両者の相容性が悪く、期待された物性が発現しない。そこで本研究の第 1 章において、PLA と PCL の高分子鎖を含んだ櫛型ポリマーの架橋反応によりコネットワークを合成して、PLA 鎖と PCL 鎖の割合を変えることによる相容性や物性の改良について検討した。また、最近、資源の有効利用や材料の長寿命化の観点から環境低負荷高分子材料として自己修復性ポリマーが大きな注目を集めており、生分解性／バイオベースポリマーであっても自己修復性を付与することが重要となっている。第 2 章では 6 本腕星型ラクチドオリゴマーと ε-カプロラクトンオリゴマーを利用して、熱により組換え可能なジスルフィド結合を導入した PLA と PCL の高分子鎖を含んだコネットーワークを合成し、その熱・力学物性と自己修復性の評価を行った。第 3 章では生分解性ポリマーの中では、PLA と PCL の中間的な物性を示す PBS について、ジスルフィド結合を導入した PBS 系ネットワークポリマーを合成し、熱・力学物性と自己修復性の評価を行った。各章のより詳しい概要は以下のとおりである。

第 1 章では、まずヒドロキシエチルメタクリレートを開始剤とした L-ラクチド(LLA)と ε-カプロラクトン(CL)の開環重合により末端にメタクリロイル基をもつラクチドオリゴマー(MALLAO)とカプロラクトンオリゴマー(MACLO)を合成した。ブチルメタクリレート(BMA)と MALLAO および BMA と MACLO のモル比 8/2 でのラジカル共重合によりヒドロキシ末端櫛型共重合体 (PBML と PBMC) を合成し、PBML/PBMC 重量比が 100/0, 75/25, 50/50, 25/75 および 0/100 でヘキサメチレンジイソシアネート (HDI)と架橋反応することによりポリウレタンコネットワーク (PUN-BML/C) を作製した。FT-IR スペクトルとゲル分率の解析によりウレタン化反応が進行しポリマーネットワークが形成されたことを確認した。PUN-BML/C 100/0 と PUN-BML/C 0/100 は、それぞれ PBML と PBMC よりも有意に高いガラス転移温度(T_g)と 5%重量減少温度($T_{d5\%}$)を示した。走査型電子顕微鏡(SEM)および動的粘弾性測定(DMA)により PUN-BML/C

75/25，50/50 および 25/75 コネットワークのオリゴラクチド(LAO)およびオリゴカプロラクトン(CLO)セグメントはある程度相容化しているが完全には混和していないことが明らかとなった。また、PUN-BML/C の引張強さと引張弾性率は PBML 含有量の増加とともに増加し、PUN-BML/C 75/25 が最も高い破断伸びと引張強靭性を示すことが分かった。なお、本研究は櫛型ポリマーからなる架橋ポリマーの最初の報告例である。

第 2 章では、まずジペンタエルスリトールを開始剤とした LLA と CL の開環重合によりヒドロキシ末端 6 本腕星型オリゴマー（H6LAO および H6CLO）を合成した。次に H6LAO、H6CLO、ビス(2-ヒドロキシエチル)ジスルフィド(BHEDS)と HDI のウレタン化反応により架橋させて、ポリエステルウレタンネットワーク(PN-LC*xy*-DS*z*、H6LAO/H6CLO の重量比 *x*/*y* : 1/0, 3/1, 1/1, 1/3, 0/1、 BHEDS/(H6LAO + H6CLO)のモル比 *z* : 0, 1, 3)を合成した。FT-IR およびゲル分率測定により、ウレタン化反応が進行してポリマーネットワークが形成されたことを確認した。さらに、PN-LC*xy*-DS*z* の示差走査熱量測定により、CLO 鎖は結晶化しているが、LAO 鎖は結晶化していないことが確認された。DMA と SEM 測定により PN-LC31-DS1 では LAO 鎖と CLO 鎖は完全に混和しており、CLO 含有量が増加するにつれてコネットワークの相容性が悪くなることが分かった。PN-LC*xy*-DS1（*xy* = 10, 31, 11, 13）フィルムに付けた傷は室温で 24 h 放置することにより修復した。特に、PN-LC31-DS1 は引張強さにおいて最も高い修復率(98.5%)を示した。ジスルフィド結合のない PN-LC10-DS0 と PN-LC01-DS0 では同様の条件で傷の修復な全くみられなかった。なお、本研究は PLA 鎖を含んだ自己修復性ジスルフィド結合含有架橋ポリマーの最初の報告例である。

第 3 章では、主鎖に C=C 結合を有するポリ（ブチレンサクシネート-*co*-ブチレンイタコネート）(PBSI)とジスルフィド結合を有するチオール末端ポリエーテル（LP-3）の C=C/SH 比が 2/1，1/1,1/2 での求核的チオール-エン反応により、ジスルフィド結合含有ポリエステルネットワーク（PBSI-LP）を合成し、熱・力学物性と自己修復性を評価した。FT-IR およびゲル分率測定により、チオール-エン反応が進行してポリマーネットワークが形成されたことを確認した。PBSI-LP の C=C/SH 比が高くなるにつれて、$T_{d5\%}$、T_g、引張強さ、引張弾性率が増加した。すべての PBSI-LP フィルムは 100 ℃，14-24 h および 75 ℃，24　h の加圧(2 MPa)により修復した。PBSI-LP-11 は引張り強さにおいて最も高い修復効率(94.2%)を示した。PBSI-LP-11 の修復率は、比較として合成したジスルフィド結合を有しない PBSI/2,2’-(エチレンジオキシ)ジエタンチオール(EDT) の C=C/SH=1/1 でのチオール-エン反応によるネットワークポリマーの修復率(23.2%)より大幅に高く、修復率の向上にジスルフィド結合の導入が有効であることが分かった。なお、本研究は PBS 鎖を含んだ自己修復性ジスルフィド結合含有 PBS 系ネットワークポリマーの最初の報告例である。

以上、第 1 章と第 2 章の結果から、PLA 鎖と PCL 鎖を含んだ櫛型ポリマーと星型ポリマーの架橋反応により LAO-CLO コネットワークを合成することにより、両成分の相容性と熱・力学物性を改良できることが分かった。さらに第 2 章と第 3 章の結果から、LAO-CLO コネットワークおよび PBS 鎖を含むネットワークポリマーにおいて熱的に組換え可能なジスルフィド結合を導入することにより生分解性ポリエステルに自己修復性を付与できることが分かった。

Summary

Synthesis, thermal, mechanical, and self-healing properties of biodegradable polyester networks

This thesis, composed of three chapters, describes the synthesis, thermal and mechanical properties, and self-healability driven by the disulfide metathesis reaction for various polymer networks composed of the polymer chains of polylactic acid (PLA), poly(ε-caprolactone) (PCL), and poly(butylene succinate) (PBS), which are popular biodegradable polyesters.

In recent years, environmental pollution caused by the plastic wastes to be discorded in a large quantity and ecological destruction of marine organisms caused by microplastics (plastic fragments less than 5 mm) is becoming a significant social problem. As one means for solving the above problems, biodegradable polyesters, which can be finally decomposed into carbon dioxide and water, are gathering considerable attention. Several biodegradable plastics are biomass-derived polymers (biobased polymers). Especially, the research and development of biodegradable/biobased PLA and PBS contributing to the preservation of oil resources and suppressing global warming are actively carried out. However, one of the drawbacks of PLA is the brittle fracture behavior. In contrast, biodegradable/petroleum-based PCL exhibits a much higher elongation at break (>300%) than PLA (ca. 3%), whereas PCL has a much lower melting temperature (ca. 60 °C) and tensile strength (ca. 20 MPa) than those of PLA (ca.170 °C, ca. 50 MPa). In chapter 1, the improvement of thermal and mechanical properties in addition to the compatibility of the PLA and PCL segments was investigated by changing the ratio of PLA/PCL segments of crosslinking comb-shaped polymers. Recently, as polymer materials reducing environmental load, self-healing polymers having the ability to repair physical damage and cracks, thereby leading to the extension of their lifetime and effective use of resources, are attracting the most attention in addition to biodegradable and biobased polymers. In chapter 2, the introduction of disulfide bonds into the conetworks consisting of 6-armed star-shaped L-lactide and ε-caprolactone oligomers was investigated to provide the self-healing properties driven by the disulfide metathesis reaction. In chapter 3, for biodegradable/biobased PBS having intermediate thermal and mechanical properties of PLA and PCL, disulfide-containing PBS-based network polymers were prepared, and their thermal, mechanical, and self-healing properties were investigated. A more detailed overview of each chapter is described below.

In chapter 1, first, methacrylate-terminated L-lactide and ε-caprolactone oligomers (MALLAO and MACLO) were synthesized by the ring-opening polymerizations of L-lactide (LLA) and ε-caprolactone (CL) initiated with hydroxyethyl methacrylate. Next, the radical copolymerizations of butyl methacrylate/MALLAO and butyl methacrylate/MACLO in a molar ratio of 8/2 generated comb-shaped polymers grafted with hydroxy-terminated lactide and ε-caprolactone oligomers (PBML and PBMC). The crosslinking reaction of PBML/PBMC (weight ratios: 100/0, 75/25, 50/50, 25/75, and 0/100) and hexamethylene diisocyanate (HDI) produced polyurethane networks (PUN-BML/Cs). Analyses of FT-IR spectra and gel fractions verified the formation of a polyurethane network structure. PUN-BML/C 100/0 and PUN-BML/C 0/100 had significantly

higher glass transition and 5% weight loss temperatures (T_g and $T_{d5\%}$) than PBML and PBMC, respectively. The results of scanning electron microscopy (SEM) and dynamic mechanical analysis (DMA) revealed that the oligolactide (LAO) and oligocaprolactone (CLO) segments of PUN-BML/C 75/25, 50/50, and 25/75 conetworks are partially miscible but not fully miscible. In addition, the tensile strength and modulus of PUN-BML/Cs increased with increasing feed PBML content, and PUN-BML/C 75/25 exhibited the highest elongation at break and tensile toughness. It is also noted that this study is the first example of crosslinked comb-shaped polymers.

In chapter 2, hydroxy-terminated 6-armed star-shaped L-lactide and ε-caprolactone oligomers (H6LAO and H6CLO) were synthesized by the ring-opening polymerization reactions of LLA and CL initiated with dipentaerythritol. The disulfide-containing polyester-urethane networks (PN-LC*xy*-DS*z*, weight ratios of H6LAO/H6CLO: *x*/*y* = 1/0, 3/1, 1/1, 1/3, and 0/1, BHEDS/(H6LAO + H6CLO) molar ratios: *z* = 0, 1, and 3) were prepared by the reaction of H6LAO, H6CLO, and bis(2-hydroxyethyl) with HDI. The FT-IR and gel fraction analyses demonstrated that the urethanization reaction proceeded smoothly to form polymer networks. Furthermore, according to the differential scanning calorimetric analysis of PN-LC*xy*-DS*z*s, the CLO segments are crystallized, whereas the LAO segments are not. SEM and DMA results revealed that the LAO and CLO segments of PN-LC31-DS1 are fully compatible and that the conetwork compatibility worsens as the CLO fraction increases. The cut lines on PN-LCxy-DS1 (*xy* = 10, 31, 11, and 13) films healed after 24 h at room temperature. Especially, PN-LC31-DS1 demonstrated the highest healing efficiency for tensile strength (98.5%). The cut lines provided to PN-LC10-DS0 and PN-LC01-DS0 without disulfide bonds were not healed at all. It is also noted that this study is the first example of self-healing PLA-based network polymers driven by the disulfide metathesis.

In chapter 3, the nucleophilic thiol-ene reaction of poly(butylene succinate-*co*-butylene itaconate) (PBSI) and a thiol-terminated polyether (LP-3) containing disulfide linkages at C=C/SH ratios of 2/1, 1/1, and 1/2 produced crosslinked polyester networks (PBSI-LPs). For comparison, a PBSI/2,2'-(ethylenedioxy) diethanethiol crosslinked polymer (PBSI-EDT-11, C=C/SH = 1/1) without disulfide bonds was prepared. The crosslinking density, $T_{dx\%}$ (*x* = 5, 10, and 50), T_g, tensile strength, and tensile modulus of PBSI-LPs increased as the C=C/SH ratio increased. PBSI-LPs exhibited healing properties when pressed at 100 °C for 14–24 h or 75 °C for 24 h. PBSI-LP-11 exhibited the highest healing efficiency (94.2%), which was significantly higher than PBSI-EDT-11 (23.2%), indicating the effectiveness of incorporating disulfide bonds into the polymer. It is also noted that this study is the first example of self-healing PBS-based network polymers driven by the disulfide metathesis.

Consequently, the formation of conetwork structure by the crosslinking reactions of comb-shaped and star-shaped LAOs and CLOs is very effective to improve the compatibility, thermal, and mechanical properties. Furthermore, the investigations of chapter 2 and chapter 3 revealed that the introduction of dynamic disulfide bonds into the LAO-CLO conetworks and PBS networks was very effective to attain excellent self-healing properties. The environmentally benign polymer materials possessing excellent thermal, mechanical, and self-healing properties were successfully developed by the formation of biodegradable polyester networks throughout this doctoral thesis.

Table of Contents

General Introduction

1. Background

Plastics are manufactured polymeric molecules with long chains [1]. Synthetic polymers began to replace natural materials in nearly every area more than half a century ago, and plastics are now an indispensable part of our lives. Synthetic plastics are mainly derived from non-degradable petroleum resources. Global plastic consumption increased from 1.5 million tons in the 1950s to 335 million tons in 2016. As the global manufacturing of plastics increases fast, a massive number of plastics are released into the environment during the duration of their life cycle [2], [3]. According to reports, 79% of plastic products have not been treated effectively and are released into landfills or natural environments [4].

In recent years, environmental pollution caused by the plastic wastes to be discorded in a large quantity and ecological destruction of marine organisms caused by microplastics (plastic fragments less than 5 mm) is becoming a significant social problem [2], [5] . As one means for solving the above problems, biodegradable polymers, which can be finally decomposed into carbon dioxide and water, are gathering considerable attention.

Biodegradable polymers and bio-based polymers (or bioplastics) currently contribute less than one percent of the more than 367 million tons of plastic produced annually. In contrast to a minor decline in worldwide plastic consumption, the bioplastics market has steadily increased. This growth is driven by increasing demand and the development of more innovative applications and products. From approximately 2.41 million tones in 2021 to approximately 7.59 million tones in 2026, the global capacity to produce bioplastics will expand dramatically. Consequently, the percentage of bioplastics in worldwide plastic manufacturing will surpass the 2% threshold for the first time [6]. Biodegradable polymers derived from renewable or petroleum-based resources are being designed and developed to have a low carbon footprint, high recycling value, and complete biodegradability or composability [6], [7]. Biodegradable polymers such as polylactic acid or polylactide (PLA), poly(ε-caprolactone) (PCL) and polybutylene succinate (PBS) have numerous applications in the fields of medicine, agriculture, medication release, and packaging [6]. Nevertheless, the majority of biodegradable plastics has lower thermal and mechanical properties than conventional petroleum-based plastics, which leads to the restriction on use. Therefore, research and development efforts are underway to enhance the thermal and mechanical properties of biodegradable/bio-based plastics, which enables the replacement of conventional plastics.

Recently, as polymer materials reducing environmental load, self-heling polymers have the ability to repair physical damage and cracks, thereby leading to the extension of service life and effective use of resources. Zhang et al. reported a new method for chemically modifying dialdehyde starch (DAS) *via* dynamic imine chemistry. The DAS crosslink is produced by diamines through a Schiff-based reaction. They developed a highly dynamic covalent crosslinked DAS-based polyimine (DAS-PI). The obtained DAS-PI demonstrates excellent thermal stability, self-healing ability, water/solvent resistance, and degradability, indicating a high application potential as "greener" packaging material [8]. Leibler et al. have utilized supramolecular assembly to generate a self-healing and thermo-reversible rubber with excellent recoverable elongation and minimal load-induced creep [9]. The Urban research group has developed a self-healing material composed of oxetane-modified chitosan precursors incorporated into polyurethane networks. These systems use ultraviolet light to recombine free radicals into crosslinks; it has been discovered that these systems can repair surface scratch damage in less than one hour [10].

Table 1. Material coordinate system of bioplastics [11]

Classification of bioplastics	**Type of resources**	**Example**
Non-biodegradable	conventional plastics (fossil-based)	PE, PP, PET
	bio-based	bio-based PE, PET, PA, PTT
Biodegradable	bio-based	PLA, PHBH, PBS, Starch blends
	fossil-based	PBAT, PCL

2. Biodegradable polyesters

Biodegradable aliphatic polyesters are one of the most significant biodegradable polymers. Many of these biodegradable polyesters have excellent biodegradability and biocompatibility, making them a significant classification of biodegradable polymers. There are various aliphatic biodegradable polyesters; nonetheless, only a small number are commercially available. PLA, PCL, PBS, and poly(3-hydroxybutyrate-*co*-3-hydroxyhexanoate) (PHBH) are representative and commercially available biodegradable polyesters. Among them, PLA, PBS, and PHBH are derived from biomass, whereas PCL is derived from petroleum resources.

PLA and PCL are biodegradable aliphatic polyesters, which have been widely used for environmentally benign and biomedical materials usable for agriculture, automobile, diary commodities, tissue engineering and controlled drug delivery etc.[12]–[19]. In past studies, homopolymers and copolymers of lactide (LA) and ε-caprolactone (CL) with well-defined macromolecular architectures such as star-shaped [20]–[27], comb-shaped [28]–[37], hyperbranched [27] and dendritic structures [38]–[40] have been synthesized to improve the physicochemical and biodegradable properties of PLA and PCL. Their unique polymers have high terminal functionalities arisen from the highly branched or grafted structure. Although PLA has relatively a higher mechanical strength and melting temperature (T_m) than other biodegradable polyesters, one of the drawbacks of PLA for biomedical applications is the brittle fracture behavior. In contrast, biodegradable/petroleum-based PCL exhibits a much higher elongation at break (>300%) than PLA (ca. 3%), whereas PCL has a much lower melting temperature (ca. 60 °C) and tensile strength (ca. 20 MPa) than those of PLA (ca.170 °C, ca. 50 MPa) [6], [41], [42]. Blends with flexible polymers are commonly utilized to improve the brittleness of PLA. Particularly, blending with biodegradable polycaprolactone (PCL) has been reported the most frequently. However, PLA is incompatible with PCL, and a simple PCL/PLA blend has a coarse morphology and poor adhesion between the two phases. Consequently, the resulting mechanical properties are not those expected.

PBS and its blends have commercial applications in agriculture, fishing, forestry, construction, and other industries. For example, PBS has been utilized as mulch film, packaging, and flushable hygiene goods and as a non-migratory plasticizer for polyvinyl chloride (PVC). In addition, it is utilized for foaming and food packing. PBS is a semicrystalline polyester with intermediate thermal and mechanical properties of PLA and PCL and a higher melting point than PLA. The crystal structure and degree of crystallinity affect mechanical and thermal properties [43]. The glass transition temperature (T_g) of PBS is approximate −32°C, and the melting temperature (T_m)

is approximately 115°C. Compared with PLA, PBS is tougher in nature but has a lower rigidity and Young's modulus. By altering the composition of the monomer, the mechanical properties can be tailored to the specific application [44], [45]. The comparatively low mechanical flexibility of PBS restricts the applications of 100% PBS-based products. However, this can be overcome by blending PBS with PLA or starch to considerably increase the mechanical characteristics, providing properties comparable to polyolefin [46], [47].

PHBH is a promising bacterial polyester with prospective applications in the packaging and biomedical material sector. PHBH is a random copolymer of PHA family [48] that consists of (*R*)-3HB and (*R*)-3HH units, having a propyl (C_3H_7) side chain [49]. In general, the thermal and mechanical properties of PHBH copolymer significantly depend on the content of comonomer ((*R*)-3HB or (*R*)-3HH). PHBH was shown to naturally have a lower tensile strength and higher percentage of elongation at break, while PLA shows a high mechanical strength and good fabricability [50]. Thus, the combination of these two biodegradable polymers can enhance the blend's overall mechanical qualities. Since PHBH is generated by Microbial synthesis, whereas PLA, PCL, and PBS can be generated by chemical synthesis, PLA, PCL, and PBS can be modified more easily than PHBH.

Table 2**.** Properties of popular biodegradable polyesters.

Polyester	T_g (℃)	T_m (℃)	Tensile strength (MPa)	Young's modulus (MPa)	Elongation at break (%)	Reference
PLA	55-65	170-200	15.5-150	2700-4140	3.0-10.0	[6], [41]
PBS	−32	115	33.7	707	94	[43]
PCL	−60	60	15	245	430	[6], [42]
P(3HB-*co*-5% 3HH	0	151	-	-	5	[51]
P(3HB-*co*-10% 3HH	−1	127	21	-	400	[51]
P(3HB-*co*-15% 3HH	0	115	23	-	760	[51]
P(3HB-*co*-20% 3HH	−4	108	18	370	19	[50]

3. Biodegradable polyester networks

The non-degradability of petrochemical-based plastics has caused environmental and ecological problems as their use has increased. Biodegradable aliphatic polyesters such as PLA, PCL, and PBS are environmentally preferable alternative to their synthetic counterparts [13], [14], [52]–[58].

Recent efforts have been made to improve the properties of linear thermoplastic polyesters and make them more competitive with petroleum-based polymers. For this reason, an extensive study on polymer blends, co-polymerizations, composites, and the formation of networks has been carried out [59]–[64]. The formation of crosslinked structures is one of the most intriguing strategies since it offers the opportunity to improve the compatibility of several components leading to the improve of mechanical and thermal properties. According to previous research included homopolymers and copolymers of lactide (LA) and ε-caprolactone (CL) with well-defined macromolecular architectures such as star-shaped [20]–[27], comb-shaped [28]–[37], hyperbranched [27], and dendritic structures [38]–[40] were synthesized to enhance the physicochemical and biodegradable properties of PLA and PCL. Their unique polymers have high terminal functionalities arising from the highly branched or grafted structure. Especially, In order to synthesize PLA and PCL networks, it is necessary to multi-functionalize the polymers and convert them into star-shaped and comb-shaped polymers.

Star-shaped polymers have high symmetry due to the radiate from the center and form a uniform or regular network when crosslinked. Conversely, the star-shaped polymer can be multi-functionalized little, with a maximum of six to eight functionalities, making it challenging to increase the crosslinking density [65], [66]. Compared to star-shaped polymers, comb-shaped polymers have lower symmetry, making it more difficult to obtain a uniform network or regular network. In addition, polymers whose main chains differ from the grafted side chains are easily affected by the main chains' physical properties. Conversely, increasing the grafting rate enables the generation of network polymers that are easily multi-functionalized and possess a high crosslink density. In this investigation, we are conducting the research described in chapter 1 to determine which star- and comb-shaped polymers exhibit superior compatibility and physical properties when network polymers are generated [33], [67].

Shibita et al. synthesized conetworks [MH4(LA/CL)Ons] by The reactions of methylenediphenyl 4,4’-diisocyanate (MDI) with hydroxy-terminated 4-armed star- shaped L-lactide oligomer (H4LAOn) and 4-armed star-shaped ε-caprolactone oligomer (H4CLOn) with the degree of polymerization per one arm, n = 3, 5 or 10 to improve the combability, thermal, and

mechanical properties of PLA and PCL [68]. Younes et al. reported biodegradable elastomeric networks prepared by the ring-opening polymerization of bis(3-caprolactone-4-yl) propane initiated with hydroxy-terminated 3-armed star-shaped random copolymers of LA and CL [69]. Although investigating the characteristics of highly crosslinked networks composed of comb-shaped polymers grafted with lactide and ε-caprolactone oligomers (LAO and CLO) is an intriguing issue, these network polymers have not been reported. In addition, PBS is obtained by polycondensation and is difficult to synthetically multi-functionalities. Regarding the crosslinked PBS networks, Teramoto et al. reported the crosslinking and biodegradation of PBS-based prepolymers containing unsaturated itaconic acid or maleic acid units in the main chain using BPO as an initiator [70]. Kim et al. reported the crosslinking of PBS with dicumyl peroxide (DCP) and investigated its physical and thermal properties and biodegradability. It was found that the mechanical properties of PBS were enhanced while the crystallization temperature increased. This result was explained by the possibility that crosslink points or reaction by-products act as nucleating agents [71].

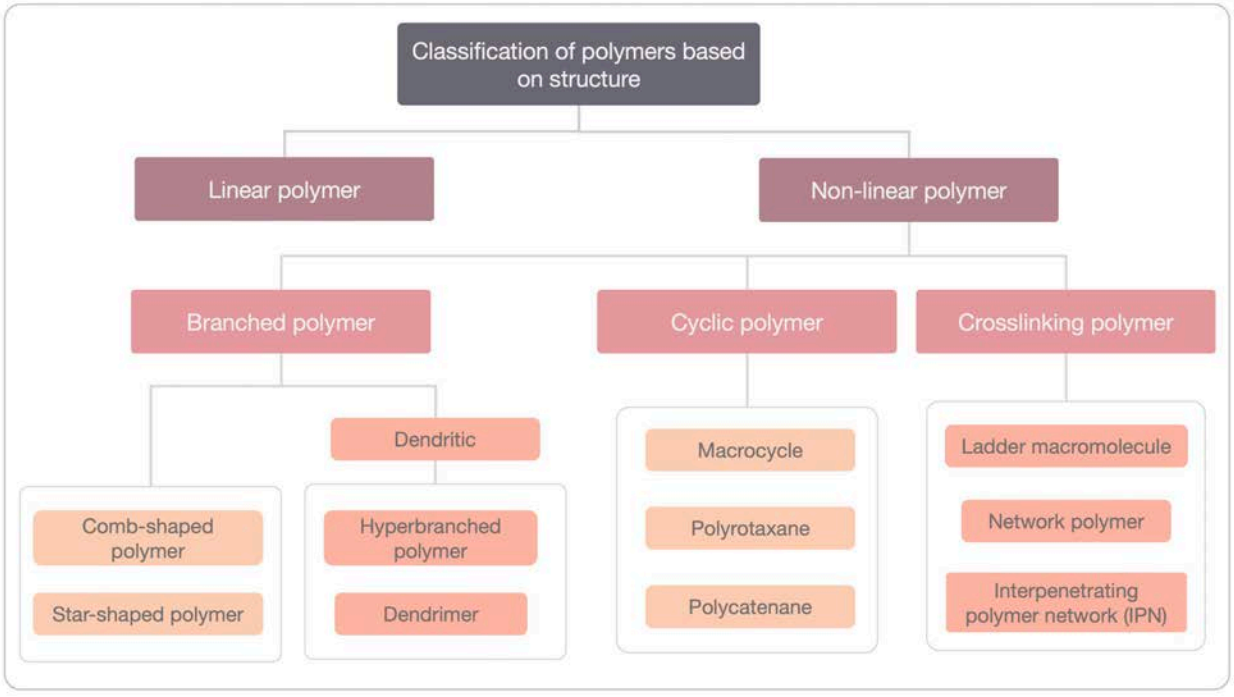

Fig.1. Classification of polymers based on structure [72].

4. Self-healing polymer networks

Since the majority of plastics in use today are composed of irreversible bonds, when polymer chains are broken by mechanical damage or UV light, they cannot be restored, resulting in material degradation. Therefore, self-healing polymers, that is, polymers that can regenerate bonds even when polymer chains are broken, are actively being researched because they can extend the lifetime of materials as functional materials. Self-healing polymers can be divided into two main types. The first type is “Extrinsic self-healing”, a healing agent pre-embedded in the polymer matrix. In extrinsic self-healing systems, the healing agent is typically isolated from the main matrix, such as in microcapsules. These capsules, when broken, release the healing agent into the damaged (cracked) area, which then self-heals through a chemical reaction. This technique allows the repair of relatively extensive damaged areas [73]. However, depletion of the healing agent results in a single healing event. The second type is “Intrinsic self-healing”, in which the polymers themselves repair molecular and macroscopic damage (cracks). Intrinsic self-healing systems can also be categorized according to their type of healing mechanism. The two major categories are chemical bonding (reversible dynamic bond) and physical interaction (reversible supramolecular interactions) [74], [75]. Regarding reversible covalent bonds, a network with reversible covalent bonds is referred to as a covalent adaptive network (CANs) [76]–[79]. CANs are divided into two categories based on their exchange mechanism: (i)dissociative CANs, in which an existing bond is broken, and then a new bond is formed; and (ii) associative CANs (also known as vitrimers), in which the cleavage of the existing bond and formation of the new bond are concerted. The Diels-Alder and its retro reactions are a typical dissociated CANs bond [80]–[82]. The examples of associative CANs polymer networks based on transesterification of epoxy-cured resins [83]–[85], transamination of polyurethanes and/or polyureas [86]–[88], transcarbamoylation of polyhydroxyureas [89], imine/amine exchange [90], [91], olefin metathesis [92], disulfide metathesis [93], [94] and so on. By introducing these dynamic covalent bonds into crosslinked epoxy, polyurethane, and poly(urea-urethane) networks, conventional thermoset polymers could be reprocessed using a hot press technique.The mechanism of chemical self-healing is based on reversible covalent bonding. Chemical reversible bonding methods such as the Diels-Alder (DA) reaction [95]–[98], transesterification [99], [100], disulfide bonds [101], [102], and imine bonds [103]–[105], facilitate excellent mechanical strength and dimensional stability than physical bonding. Physical self-healing (reversible supramolecular interactions) relies on non-covalent interactions, such as diffusion and entanglement, π-π-stacking [106], [107] , host-guest [108]–[112], and hydrogen bonding [113]–[115].

Turkenburg and Fischer reported self-healing epoxy networks by the DA reaction of 4,4'-bismaleimidodiphenylmethane (BMI) and a prepolymer of furfurylamine (FA) and diglycidyl ether of bisphenol A (DGEBA) [98].Wan and Chen reported the three-step polymerization of a β-CD/polyethylene glycol inclusion compound, isophorone diisocyanate, a polycaprolactone diol, 2,2-bis(hydroxymethyl) propionic acid (DMPA), 2-hydroxyethyl disulfide, and ethylene diamine to generate healable waterborne polyurethane networks (EDA). The disulfide metathesis and host-guest interactions-based polyurethane networks were healed by a 65 °C heat treatment [116]. Behara et al. reported the development of specialized functional PU using double dynamic covalent chemistry utilizing the thermoreversible DA "click" (based on furan maleimide cycloaddition) and disulfide metathesis reaction. A functional diol with furfuryl and disulfide functionality was synthesized and utilized as a chain extender in the synthesis of a polyurethane (PU) elastomer based on polycaprolactone (PCL) diol and 4,4'-methylenebis (phenyl diisocyanate) (MDI). This dual-functional PU elastomer was cross-linked with bismaleimide (BM) via DielsAlder (DA) reaction with the furfuryl pendant group in PU. This dual-functional PU with thermoreversible DA linkage and disulfide linkage exhibited high tensile strength (σ = 39.5 MP MPa) and, more significantly, superior self-healing properties (self-healing efficiency, $E_\sigma \approx 97\%$) [117]. Jian et al. reported the synthesis of a self-healing polyurethane material by combining disulfide bonds and H-bonding. Polyurethanes were generated using a one-pot polymerization method. The soft segment was composed of PTMEG, while the hard segments were composed IPDI as the diisocyanate and HEDS as the chain extender. The self-healing ability of synthesized polyurethane comes from the covalent disulfide metathesis and non-covalent H-bonding. The mechanical testing indicates that disulfide metathesis reforms covalent bonds on a longer time scale, whereas H-bonding contributes to an early healing efficiency of approximately 46%. The compromise between mechanical performance and healing capability is reached by modifying the disulfide concentration. The creep testing reveals that the tensile strength of the sample with 100% self-healing efficiency can reach 5.01 MPa, which can be explained by the higher chain mobility at room temperature [118].

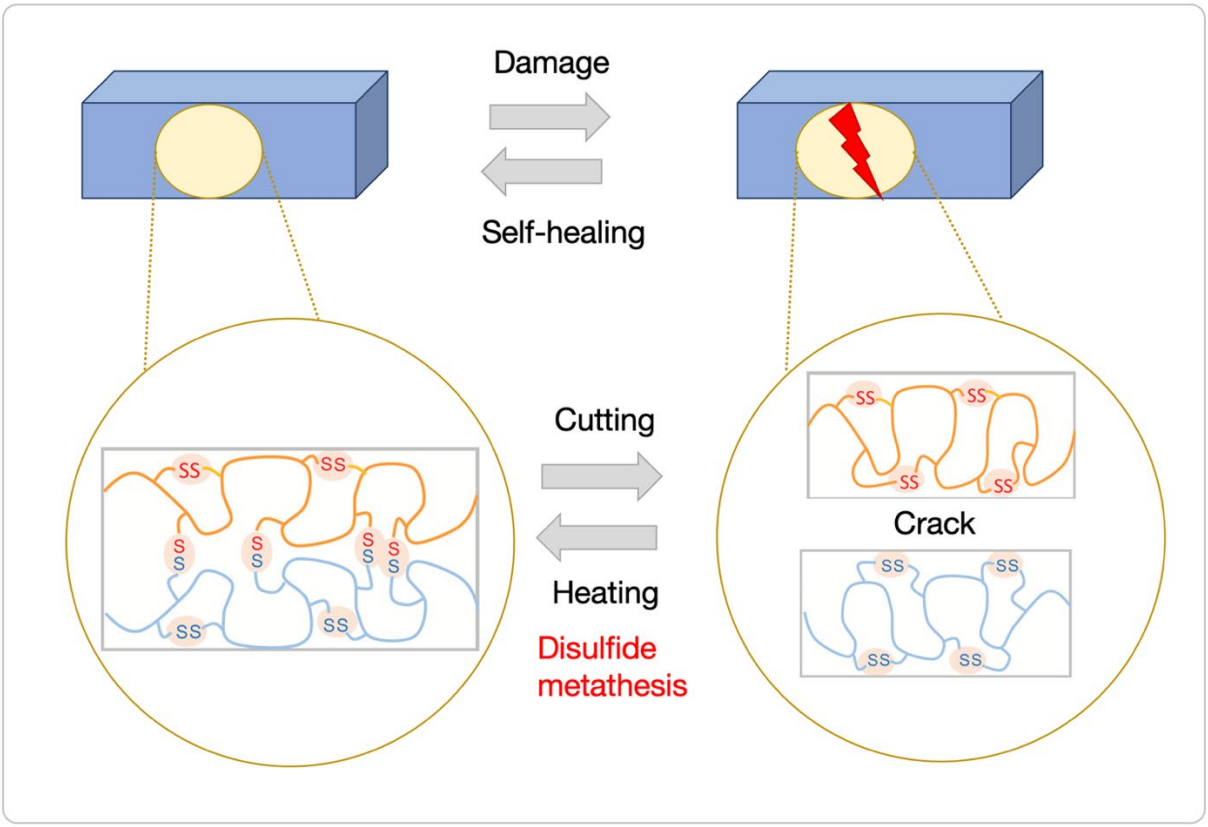

Fig.2. Schematic representation of self-healing polymer network driven by disulfide metathesis reaction.

5. Biodegradable polyester networks exhibiting self-heling properties

Biobased and biodegradable polyesters, such as PBS and PLA, are being developed to overcome the depletion of petroleum resources and the increase in plastic pollution [58], [119]. In addition, PLA and PCL are widely used as biomaterials in the fields of tissue engineering, regenerative medicine, controlled drug delivery, etc. By modifying the crosslinking density, the crystallinity, biodegradability, thermal properties, and mechanical properties of these polymers can be modified to develop tailored biomaterials [19], [120], [121]. However, mechanical fracture of these polymer networks results in irreversible loss of mechanical properties, limiting their practical application in various fields. Therefore, it is essential for bio-based and biodegradable materials to have self-healing properties in order to address the drawbacks and enhance resource utilization and long service life.

Thermo-reversible DA and transesterification reactions have been used to develop the self-healing PLA networks [85], [122]–[124]. Furthermore, The self-healing PCL networks have been

studied and developed using the quadruple hydrogen bonding in 2-ureido-4[1H]-pyrimidinone (UPy), disulfide metathesis, and thermos-reversible DA reaction [125]–[133].

Regarding to self-healimg PLA networks, Borska et al. reported that disulfide bond-containing PLA networks prepared by urethanization of a 4-armed star-shaped lactide oligomer and 2-hydroxyethyl disulfide with HDI possessed self-healing properties [134]. Brutman et al. studied the healing ability by transesterification reaction of renewable polylactide-based vitrimers containing $Sn(Oct)_2$. The PLA vitrimers were produced by cross-linking hydroxyl-terminated 4-arms star-shaped poly((±)-lactide) with methylenediphenyl diisocyanate (MDI). The healing of PLA-based vitrimers fractured during uniaxial tensile testing by compression molding resulted in up to 67% recovery of ultimate elongation, up to 102% recovery of tensile strength, and up to 133% recovery of tensile modulus values [85].

Regarding to self-healing PCL network, Zhang et al. studies on using a thiol-ene "click" reaction, polycaprolactone (PCL) networks containing disulfide bonds are developed. The PCL networks have a variety of functional properties, such as self-healing, shape memory, re-processability, and degradability. After 1h of heating at 60 °C, the PCL networks exhibits a remarkable 92% healing efficiency in terms of yield strength. In the meantime, PCL networks exhibit shape memory with a fixing ratio (R_f) of 98% and a recovery ratio (R_r) of 95%. The PCL network can rapidly decompose via a thiol-disulfide exchange reaction and retains its mechanical properties after repeated processing cycles [133].

Regarding to self-healing PLA/PCL conetwork, Sugane et al. developed 4-Armed star-shaped ε-caprolactone and L-lactide oligomers, which have essentially poor compatibility, were cross-linked by the DA reaction and demonstrated the self-healing ability in PLA and PCL networks by utilizing DA reaction [122].

Regarding to self-healing PBS network, Yoshie et al. synthesized poly(2,5-furandimethylene succinate-co-butylene succinate) (P(FS-co-BS)) through polycondensation of 2,5-bis(hydroxymethyl)furan, 1,4-butanediol (BD), and succinic acid (SA). The crosslinked PBS networks generated by the DA reaction between P(FS-co-BS) and bismaleimide demonstrated self-healing properties [135].

6. Goals of thesis

Nowadays, environmental pollution caused by the plastic wastes to be discorded in a large quantity and ecological destruction of marine organisms caused by microplastics (plastic fragments less than 5 mm) is becoming a significant social problem [2], [5] As one means for solving the above problems, biodegradable polyesters, which can be finally decomposed into carbon dioxide and water, are gathering considerable attention. Several biodegradable plastics are biomass-derived polymers (biobased polymers). Particularly, the research and development of biodegradable/biobased PLA and PBS contributing to preserving oil resources and suppressing global warming are actively carried out. While PLA has similar mechanical properties to traditional polymers, PLA has a relatively higher mechanical strength and melting temperature (T_m) than other biodegradable polyesters; one of the drawbacks of PLA is the brittle fracture behavior. Especially, blending PLA with flexible biodegradable polyesters is one of the most efficient and practical strategies for enhancing the brittleness of PLA. Blends of PLA and flexible poly(ε-caprolactone (PCL) have been intensively researched. However, PLA is immiscible with PCL, and a simple PCL/PLA blend has a coarse morphology and poor adhesion between the two phases. To improve the complementary physicochemical properties of PLA and PCL, a series of network polymers were synthesized by the crosslinking reaction of various hydroxy-terminated star-shaped lactide and ε-caprolactone oligomers with diisocyanates and their thermal and mechanical properties were elucidated in our laboratory. However, the properties of highly crosslinked networks composed of comb-shaped polymers grafted with lactide and ε-caprolactone oligomers (LAO and CLO) have not been reported.

Chapter 1 focused on improving thermal and mechanical properties and the compatibility of the PLA and PCL segments by modifying the ratio of PLA/PCL segments of crosslinking comb-shaped polymers. The polyurethane networks were produced by crosslinking a comb-shaped hydroxy-terminated oligolactide and oligocaprolactone (PBML, PBMC) with hexamethylene diisocyanate (HDI).

Also, as polymer materials reducing environmental load, self-healing polymers having the ability to repair physical damage and cracks, thereby leading to the extension of their lifetime and effective use of resources, are attracting the most attention in addition to biodegradable and biobased polymers. In this study, we considered disulfide metathesis reactions that can be restored under relatively mild conditions. In recent years, several researchers have reported introducing dynamic disulfide bonds into the polymer networks for developing self-healing PCL. Chapter 2 focused on introducing disulfide bonds into the conetworks consisting of 6-armed star-shaped L-

lactide and ε-caprolactone oligomers was investigated to provide the self-healing properties driven by the disulfide metathesis reaction. The disulfide-containing polymer networks were synthesized by crosslinking hydroxy-terminated 6-armed star-shaped L-lactide and ε-caprolactone oligomers (H6LAO and H6CLO) and 2-hydroxyethyl disulfide (BHEDS) were crosslinked with hexamethylene diisocyanate (HDI).

Moreover, to the best of our knowledge, self-healing PBS networks involving disulfide metathesis reactions have not yet been reported. Previously, poly(butylene succinate-co-butylene itaconate) (PBSI) was produced by polycondensation of BD, SA, and itaconic acid (IA) [70]. In chapter 3, the thiol-ene reaction of poly(butylene succinate-*co*-butylene itaconate) (PBSI) and a thiol-terminated polyether (LP-3) containing disulfide linkages generated crosslinked polyester networks (PBSI-LPs). Chapter 3 focused on preparing the disulfide-containing PBS-based network polymer, and their thermal, mechanical, and self-healing properties were investigated.

Consequently, this thesis focused on the synthesis, thermal and mechanical properties, and self-healability driven by the disulfide metathesis reaction for various polymer networks composed of the polymer chains of polylactic acid (PLA), poly(ε-caprolactone) (PCL), and poly(butylene succinate) (PBS), which are popular biodegradable polyesters.

7. References

[1] G. Scott, *Polymers and the Environment*. Royal Society of Chemistry, 1999.

[2] W. C. Li, H. F. Tse, and L. Fok, "Plastic waste in the marine environment: A review of sources, occurrence and effects," *Sci. Total Environ.*, vol. 566–567, pp. 333–349, Oct. 2016, doi: 10.1016/j.scitotenv.2016.05.084.

[3] "Plastic production worldwide 2020," *Statista*, 2020. https://www.statista.com/statistics/282732/global-production-of-plastics-since-1950/ (accessed Aug. 10, 2022).

[4] R. Geyer, J. R. Jambeck, and K. L. Law, "Production, use, and fate of all plastics ever made," *Sci. Adv.*, vol. 3, no. 7, p. e1700782, Jul. 2017, doi: 10.1126/sciadv.1700782.

[5] G. G. N. Thushari and J. D. M. Senevirathna, "Plastic pollution in the marine environment," *Heliyon*, vol. 6, no. 8, p. e04709, Aug. 2020, doi: 10.1016/j.heliyon.2020.e04709.

[6] R. P. Babu, K. O'connor, and R. Seeram, "Current progress on bio-based polymers and their future trends," *Prog. Biomater.*, vol. 2, no. 1, pp. 1–16, 2013.

[7] P. Bhagabati, "Chapter 9 - Biopolymers and biocomposites-mediated sustainable high-performance materials for automobile applications," in *Sustainable Nanocellulose and Nanohydrogels from Natural Sources*, F. Mohammad, H. A. Al-Lohedan, and M. Jawaid, Eds. Elsevier, 2020, pp. 197–216. doi: https://doi.org/10.1016/B978-0-12-816789-2.00009-2.

[8] H. Zhang, Z. Su, and X. Wang, "Starch-Based Rehealable and Degradable Bioplastic Enabled by Dynamic Imine Chemistry," *ACS Sustain. Chem. Eng.*, vol. 10, no. 26, pp. 8650–8657, Jul. 2022, doi: 10.1021/acssuschemeng.2c02537.

[9] P. Cordier, F. Tournilhac, C. Soulié-Ziakovic, and L. Leibler, "Self-healing and thermoreversible rubber from supramolecular assembly," *Nature*, vol. 451, no. 7181, pp. 977–980, 2008.

[10] B. Ghosh and M. W. Urban, "Self-Repairing Oxetane-Substituted Chitosan Polyurethane Networks," *Science*, vol. 323, no. 5920, pp. 1458–1460, Mar. 2009, doi: 10.1126/science.1167391.

[11] C. Manger, "Publications," *European Bioplastics e.V.*, Jul. 2018. https://www.european-bioplastics.org/news/publications/ (accessed Aug. 29, 2022).

[12] F.-L. Jin, R.-R. Hu, and S.-J. Park, "Improvement of thermal behaviors of biodegradable poly(lactic acid) polymer: A review," *Compos. B. Eng.*, vol. 164, pp. 287–296, May 2019, doi: 10.1016/j.compositesb.2018.10.078.

[13] S. Farah, D. G. Anderson, and R. Langer, “Physical and mechanical properties of PLA, and their functions in widespread applications — A comprehensive review,” *Adv. Drug Deliv. Rev.*, vol. 107, pp. 367–392, Dec. 2016, doi: 10.1016/j.addr.2016.06.012.

[14] B. Tyler, D. Gullotti, A. Mangraviti, T. Utsuki, and H. Brem, “Polylactic acid (PLA) controlled delivery carriers for biomedical applications,” *Adv. Drug Deliv. Rev.*, vol. 107, pp. 163–175, Dec. 2016, doi: 10.1016/j.addr.2016.06.018.

[15] H. Liu and J. Zhang, “Research progress in toughening modification of poly(lactic acid),” *J. Polym. Sci. B Polym. Phys.*, vol. 49, no. 15, pp. 1051–1083, Aug. 2011, doi: 10.1002/polb.22283.

[16] R. M. Rasal, A. V. Janorkar, and D. E. Hirt, “Poly(lactic acid) modifications,” *Prog. Polym. Sci.*, vol. 35, no. 3, pp. 338–356, Mar. 2010, doi: 10.1016/j.progpolymsci.2009.12.003.

[17] A. L. Sisson, D. Ekinci, and A. Lendlein, “The contemporary role of ε-caprolactone chemistry to create advanced polymer architectures,” *Polymer*, vol. 54, no. 17, pp. 4333–4350, Aug. 2013, doi: 10.1016/j.polymer.2013.04.045.

[18] M. A. Woodruff and D. W. Hutmacher, “The return of a forgotten polymer—Polycaprolactone in the 21st century,” *Prog. Polym. Sci.*, vol. 35, no. 10, pp. 1217–1256, Oct. 2010, doi: 10.1016/j.progpolymsci.2010.04.002.

[19] L. S. Nair and C. T. Laurencin, “Biodegradable polymers as biomaterials,” *Prog. Polym. Sci.*, vol. 32, no. 8–9, pp. 762–798, Aug. 2007, doi: 10.1016/j.progpolymsci.2007.05.017.

[20] S. H. Kim, Y.-K. Han, Y. H. Kim, and S. I. Hong, “Multifunctional initiation of lactide polymerization by stannous octoate/pentaerythritol,” *Makromol. Chem.*, vol. 193, no. 7, pp. 1623–1631, 1992.

[21] J. S. Lee, D. J. Choo, S. H. Kim, and Y. H. Kim, “Synthesis and degradation property of star-shaped polylactide,” *Polym. (Korea)*, vol. 22, no. 6, pp. 880–889, 1998.

[22] E. S. Kim, B. C. Kim, and S. H. Kim, “Structural effect of linear and star-shaped poly(L-lactic acid) on physical properties,” *J. Polym. Sci. B Polym. Phys.*, vol. 42, no. 6, pp. 939–946, Mar. 2004, doi: 10.1002/polb.10685.

[23] J.-L. Wang, L. Wang, and C.-M. Dong, “Synthesis, crystallization, and morphology of star-shaped poly(ε-caprolactone),” *J. Polym. Sci. A Polym. Chem.*, vol. 43, no. 22, pp. 5449–5457, Nov. 2005, doi: 10.1002/pola.20954.

[24] J.-L. Wang and C.-M. Dong, “Physical properties, crystallization kinetics, and spherulitic growth of well-defined poly(ε-caprolactone)s with different arms,” *Polymer*, vol. 47, no. 9, pp. 3218–3228, Apr. 2006, doi: 10.1016/j.polymer.2006.02.047.

[25] C.-M. Dong, K.-Y. Qiu, Z.-W. Gu, and X.-D. Feng, “Synthesis of Star-Shaped Poly(ε-caprolactone)- *b* -poly(DL -lactic acid- *alt* -glycolic acid) with Multifunctional Initiator and

Stannous Octoate Catalyst," *Macromolecules*, vol. 34, no. 14, pp. 4691–4696, Jul. 2001, doi: 10.1021/ma010005w.

[26] D. J. A. Cameron and M. P. Shaver, "Aliphatic polyester polymer stars: synthesis, properties and applications in biomedicine and nanotechnology," *Chem. Soc. Rev.*, vol. 40, no. 3, pp. 1761–1776, 2011, doi: 10.1039/C0CS00091D.

[27] A. Michalski, M. Brzezinski, G. Lapienis, and T. Biela, "Star-shaped and branched polylactides: Synthesis, characterization, and properties," *Prog. Polym. Sci.*, vol. 89, pp. 159–212, Feb. 2019, doi: 10.1016/j.progpolymsci.2018.10.004.

[28] I. Barakat, P. Dubois, R. Jérôme, P. Teyssié, and E. Goethals, "Macromolecular engineering of polylactones and polylactides. XV. Poly (d, l)-lactide macromonomers as precursors of biocompatible graft copolymers and bioerodible gels," *J. Polym. Sci. A Polym. Chem.*, vol. 32, no. 11, pp. 2099–2110, 1994.

[29] J. Eguiburu, M. J. Fernandez-Berridi, and J. S. Román, "Graft copolymers for biomedical applications prepared by free radical polymerization of poly(l-lactide) macromonomers with vinyl and acrylic monomers," *Polymer*, vol. 37, no. 16, pp. 3615–3622, Aug. 1996, doi: 10.1016/0032-3861(96)00184-X.

[30] D. W. Lim, S. H. Choi, and T. G. Park, "A new class of biodegradable hydrogels stereocomplexed by enantiomeric oligo (lactide) side chains of poly (HEMA-g-OLA) s," *Macromol. Rapid Commun.*, vol. 21, no. 8, pp. 464–471, 2000.

[31] K. Ishimoto *et al.*, "Biobased Polymers: Synthesis of Graft Copolymers and Comb Polymers Using Lactic Acid Macromonomer and Properties of the Product Polymers," *Biomacromolecules*, vol. 13, no. 11, pp. 3757–3768, Nov. 2012, doi: 10.1021/bm301212a.

[32] K. Ishimoto *et al.*, "Biobased Polymer System: Miniemulsion of Poly(alkyl methacrylate-*graft* -lactic acid)s," *Biomacromolecules*, vol. 10, no. 10, pp. 2719–2723, Oct. 2009, doi: 10.1021/bm9007937.

[33] J. Bao, L. Han, G. Shan, Y. Bao, and P. Pan, "Preferential Stereocomplex Crystallization in Enantiomeric Blends of Cellulose Acetate- *g* -Poly(lactic acid)s with Comblike Topology," *J. Phys. Chem. B*, vol. 119, no. 39, pp. 12689–12698, Oct. 2015, doi: 10.1021/acs.jpcb.5b05398.

[34] R. Ferrari, T. R. Rooney, M. Lupi, P. Ubezio, R. A. Hutchinson, and D. Moscatelli, "A Methyl Methacrylate-HEMA-CL $_n$ Copolymerization Investigation: From Kinetics to Bioapplications: A Methyl Methacrylate-HEMA-CL $_n$ Copolymerization Investigation: …," *Macromol. Biosci.*, vol. 13, no. 10, pp. 1347–1357, Oct. 2013, doi: 10.1002/mabi.201300152.

[35] R. Ferrari, Y. Yu, M. Morbidelli, R. A. Hutchinson, and D. Moscatelli, "ε-Caprolactone-Based Macromonomers Suitable for Biodegradable Nanoparticles Synthesis through Free Radical Polymerization," *Macromolecules*, vol. 44, no. 23, pp. 9205–9212, Dec. 2011, doi: 10.1021/ma201955p.

[36] S. Gatti, A. Agostini, R. Ferrari, and D. Moscatelli, “Synthesis and Nanoprecipitation of HEMA-CLn Based Polymers for the Production of Biodegradable Nanoparticles,” *Polymers*, vol. 9, no. 12, p. 389, Aug. 2017, doi: 10.3390/polym9090389.

[37] S. Jiang, H. Liu, X. Zhang, Y. Ren, X. Cui, and X. Song, “Synthesis of PCL-branched P(MMA- *co* -HEMA) to toughen electrospun PLLA fiber membrane,” *Polym. Adv. Technol.*, vol. 29, no. 1, pp. 442–450, Jan. 2018, doi: 10.1002/pat.4133.

[38] S. Corneillie and M. Smet, “PLA architectures: the role of branching,” *Polym. Chem.*, vol. 6, no. 6, pp. 850–867, 2015, doi: 10.1039/C4PY01572J.

[39] C. Gottschalk and H. Frey, “Hyperbranched Polylactide Copolymers,” *Macromolecules*, vol. 39, no. 5, pp. 1719–1723, Mar. 2006, doi: 10.1021/ma0513259.

[40] Z. Li and J. Li, “Control of Hyperbranched Structure of Polycaprolactone/Poly(ethylene glycol) Polyurethane Block Copolymers by Glycerol and Their Hydrogels for Potential Cell Delivery,” *J. Phys. Chem. B*, vol. 117, no. 47, pp. 14763–14774, Nov. 2013, doi: 10.1021/jp4094063.

[41] 柴田充弘 and 山口達明, *E-コンシャス 高分子材料*. 三共出版, 2009.

[42] “Biodegradable Polyesters,” *Polymer database*, 2015. https://polymerdatabase.com/polymer%20classes/Biodegradable%20Polyester%20type.html (accessed Jun. 28, 2022).

[43] N. Jacquel *et al.*, “Synthesis and properties of poly (butylene succinate): Efficiency of different transesterification catalysts,” *J. Polym. Sci. Part A: Polym. Chem.*, vol. 49, no. 24, pp. 5301–5312, 2011.

[44] L. Liu, J. Yu, L. Cheng, and W. Qu, “Mechanical properties of poly(butylene succinate) (PBS) biocomposites reinforced with surface modified jute fibre,” *Compos. Part A Appl. Sci. Manuf.*, vol. 40, no. 5, pp. 669–674, May 2009, doi: 10.1016/j.compositesa.2009.03.002.

[45] L. Liu, J. Yu, L. Cheng, and X. Yang, “Biodegradability of poly(butylene succinate) (PBS) composite reinforced with jute fibre,” *Polym. Degrad. Stab.*, vol. 94, no. 1, pp. 90–94, Jan. 2009, doi: 10.1016/j.polymdegradstab.2008.10.013.

[46] H. Eslami and M. R. Kamal, “Elongational rheology of biodegradable poly(lactic acid)/poly[(butylene succinate)- *co* -adipate] binary blends and poly(lactic acid)/poly[(butylene succinate)- *co* -adipate]/clay ternary nanocomposites,” *J. Appl. Polym. Sci.*, vol. 127, no. 3, pp. 2290–2306, Feb. 2013, doi: 10.1002/app.37928.

[47] P. Zhao, W. Liu, Q. Wu, and J. Ren, “Preparation, Mechanical, and Thermal Properties of Biodegradable Polyesters/Poly(Lactic Acid) Blends,” *J. Nanomater.*, vol. 2010, pp. 1–8, 2010, doi: 10.1155/2010/287082.

[48] Z. Zheng, F.-F. Bei, H.-L. Tian, and G.-Q. Chen, “Effects of crystallization of polyhydroxyalkanoate blend on surface physicochemical properties and interactions with rabbit articular cartilage chondrocytes,” *Biomaterials*, vol. 26, no. 17, pp. 3537–3548, 2005.

[49] K. Sudesh, H. Abe, and Y. Doi, “Synthesis, structure and properties of polyhydroxyalkanoates: biological polyesters,” *Prog. Polym. Sci.*, vol. 25, no. 10, pp. 1503–1555, 2000.

[50] Q. Zhao *et al.*, “Phase morphology, physical properties, and biodegradation behavior of novel PLA/PHBHHx blends,” *J. Biomed. Mater. Res.*, vol. 100, no. 1, pp. 23–31, 2012.

[51] Y. Doi, S. Kitamura, and H. Abe, “Microbial synthesis and characterization of poly (3-hydroxybutyrate-co-3-hydroxyhexanoate),” *Macromolecules*, vol. 28, no. 14, pp. 4822–4828, 1995.

[52] C. W. Pouton and S. Akhtarb, “Biosynthetic polyhydroxyalkanoates and their potential delivery,” *Adv. Drug Deliv. Rev.*, p. 30, 1996.

[53] G.-Q. Chen and M. K. Patel, “Plastics derived from biological sources: present and future: a technical and environmental review,” *Chem. Rev.*, vol. 112, no. 4, pp. 2082–2099, 2012.

[54] K. Hamad, M. Kaseem, H. W. Yang, F. Deri, and Y. G. Ko, “Properties and medical applications of polylactic acid: A review,” *Express Polym. Lett.*, vol. 9, no. 5, pp. 435–455, 2015, doi: 10.3144/expresspolymlett.2015.42.

[55] L. Xiao, B. Wang, G. Yang, and M. Gauthier, “Poly (lactic acid)-based biomaterials: synthesis, modification and applications,” in *Biomedical science, engineering and technology*, vol. 11, InTech Rijeka, Croatia, 2012, pp. 247–282.

[56] V. K. Khatiwala, N. Shekhar, S. Aggarwal, and U. K. Mandal, “Biodegradation of Poly(ε-caprolactone) (PCL) Film by Alcaligenes faecalis,” *J. Polym. Environ.*, vol. 16, no. 1, pp. 61–67, Jan. 2008, doi: 10.1007/s10924-008-0104-9.

[57] M. Funabashi, F. Ninomiya, and M. Kunioka, “Biodegradation of Polycaprolactone Powders Proposed as Reference Test Materials for International Standard of Biodegradation Evaluation Method,” *J. Polym. Environ.*, vol. 15, no. 1, pp. 7–17, Feb. 2007, doi: 10.1007/s10924-006-0041-4.

[58] S. RameshKumar, P. Shaiju, K. E. O’Connor, and R. B. P, “Bio-based and biodegradable polymers - State-of-the-art, challenges and emerging trends,” *Curr. Opin. Green Sustain. Chem.*, vol. 21, pp. 75–81, Feb. 2020, doi: 10.1016/j.cogsc.2019.12.005.

[59] G.-Q. Chen, I. Hajnal, H. Wu, L. Lv, and J. Ye, “Engineering biosynthesis mechanisms for diversifying polyhydroxyalkanoates,” *Trends Biotechnol.*, vol. 33, no. 10, pp. 565–574, 2015.

[60] C. R. Reed *et al.*, “Composite tissue engineering on polycaprolactone nanofiber scaffolds,” *Ann Plast Surg*, vol. 62, no. 5, pp. 505–512, 2009.

[61] L. Timbart, E. Renard, V. Langlois, and P. Guerin, “Novel Biodegradable Copolyesters Containing Blocks of Poly (3-hydroxyoctanoate) and Poly (ε-caprolactone): Synthesis and Characterization,” *Macromol. Biosci.*, vol. 4, no. 11, pp. 1014–1020, 2004.

[62] P. Lemechko, E. Renard, J. Guezennec, C. Simon-Colin, and V. Langlois, “Synthesis of dextran-graft-PHBHV amphiphilic copolymer using click chemistry approach,” *React. Funct. Polym.*, vol. 72, no. 8, pp. 487–494, Aug. 2012, doi: 10.1016/j.reactfunctpolym.2012.04.008.

[63] Y. Wang, S. Chiao, T.-F. Hung, and S.-Y. Yang, “Improvement in toughness and heat resistance of poly (lactic acid)/polycarbonate blend through twin-screw blending: influence of compatibilizer type,” *J. Appl. Polym. Sci.*, vol. 125, no. S2, pp. E402–E412, 2012.

[64] L. Cabedo, J. Luis Feijoo, M. Pilar Villanueva, J. M. Lagarón, and E. Giménez, “Optimization of biodegradable nanocomposites based on aPLA/PCL blends for food packaging applications,” in *Macromolecular Symposia*, 2006, vol. 233, no. 1, pp. 191–197.

[65] T. M. Marsalkó, I. Majoros, and J. P. Kennedy, “Multi-arm Star Polyisobutylenes. V. Characterization of Multi-arm Polyisobutylene Stars by Viscometry, Pour Points, Electron Microscopy, and Ultrasonic Shear Degradation,” *J. Macromol. Sci. A.*, vol. 34, no. 5, pp. 775–792, 1997, doi: 10.1080/10601329708014330.

[66] M. K. Mishra and S. Kobayashi, *Star and Hyperbranched Polymers*. New York : Marcel Dekker, 1999.

[67] N. A. Platé and V. P. Shibaev, *Comb-Shaped Polymers and Liquid Crystals*. Boston, MA: Springer US, 1987. doi: 10.1007/978-1-4613-1951-1.

[68] A. Shibita, T. Shimasaki, N. Teramoto, and M. Shibata, “Conetworks composed of 4-armed star-shaped l-lactide oligomer and 4-armed star-shaped ε-caprolactone oligomer,” *Polymer*, vol. 74, pp. 54–62, Sep. 2015, doi: 10.1016/j.polymer.2015.07.052.

[69] B. G. Amsden, G. Misra, F. Gu, and H. M. Younes, “Synthesis and characterization of a photo-cross-linked biodegradable elastomer,” *Biomacromolecules*, vol. 5, no. 6, pp. 2479–2486, 2004.

[70] N. Teramoto, M. Ozeki, I. Fujiwara, and M. Shibata, “Crosslinking and biodegradation of poly(butylene succinate) prepolymers containing itaconic or maleic acid units in the main chain,” *J. Appl. Polym. Sci.*, vol. 95, no. 6, pp. 1473–1480, Mar. 2005, doi: 10.1002/app.21393.

[71] D. J. Kim *et al.*, “Modification of poly(butylene succinate) with peroxide: Crosslinking, physical and thermal properties, and biodegradation,” *J. Appl. Polym. Sci.*, vol. 81, no. 5, pp. 1115–1124, Aug. 2001, doi: 10.1002/app.1534.

[72] 柴田充弘, 基本高分子化学. 三共出版, 2012.

[73] B. J. Blaiszik, S. L. B. Kramer, S. C. Olugebefola, J. S. Moore, N. R. Sottos, and S. R. White, "Self-Healing Polymers and Composites," *Annu. Rev. Mater. Res.*, vol. 40, no. 1, pp. 179–211, Jun. 2010, doi: 10.1146/annurev-matsci-070909-104532.

[74] P. Michael, D. Doehler, and W. H. Binder, "Improving autonomous self healing via combined chemical/physical principles," *Polymer*, vol. 69, pp. 216–227, 2015.

[75] Y. C. Yuan, T. Yin, M. Z. Rong, and M. Q. Zhang, "Self healing in polymers and polymer composites. Concepts, realization and outlook: A review," *Express Polym. Lett.*, vol. 2, no. 4, pp. 238–250, 2008, doi: 10.3144/expresspolymlett.2008.29.

[76] C. J. Kloxin, T. F. Scott, B. J. Adzima, and C. N. Bowman, "Covalent Adaptable Networks (CANs): A Unique Paradigm in Cross-Linked Polymers," *Macromolecules*, vol. 43, no. 6, pp. 2643–2653, Mar. 2010, doi: 10.1021/ma902596s.

[77] C. N. Bowman and C. J. Kloxin, "Covalent Adaptable Networks: Reversible Bond Structures Incorporated in Polymer Networks," *Angew. Chem. Int. Ed.*, vol. 51, no. 18, pp. 4272–4274, Apr. 2012, doi: 10.1002/anie.201200708.

[78] C. J. Kloxin and C. N. Bowman, "Covalent adaptable networks: smart, reconfigurable and responsive network systems," *Chem. Soc. Rev.*, vol. 42, no. 17, pp. 7161–7173, Apr. 2013, doi: 10.1039/C3CS60046G.

[79] W. Denissen, J. M. Winne, and F. E. Du Prez, "Vitrimers: permanent organic networks with glass-like fluidity," *Chem. Sci.*, vol. 7, no. 1, pp. 30–38, 2016, doi: 10.1039/C5SC02223A.

[80] X. Chen *et al.*, "A thermally re-mendable cross-linked polymeric material," *Science*, vol. 295, no. 5560, pp. 1698–1702, 2002.

[81] X. Chen, F. Wudl, A. K. Mal, H. Shen, and S. R. Nutt, "New Thermally Remendable Highly Cross-Linked Polymeric Materials," *Macromolecules*, vol. 36, no. 6, pp. 1802–1807, Mar. 2003, doi: 10.1021/ma0210675.

[82] J. Zhang *et al.*, "Self-healable and recyclable triple-shape PPDO–PTMEG co-network constructed through thermoreversible Diels–Alder reaction," *Polym. Chem.*, vol. 3, no. 6, p. 1390, 2012, doi: 10.1039/c2py20028g.

[83] D. Montarnal, M. Capelot, F. Tournilhac, and L. Leibler, "Silica-like malleable materials from permanent organic networks," *Science*, vol. 334, no. 6058, pp. 965–968, 2011.

[84] K. Yu, P. Taynton, W. Zhang, M. L. Dunn, and H. J. Qi, "Reprocessing and recycling of thermosetting polymers based on bond exchange reactions," *RSC Adv.*, vol. 4, no. 20, pp. 10108–10117, 2014, doi: 10.1039/C3RA47438K.

[85] J. P. Brutman, P. A. Delgado, and M. A. Hillmyer, "Polylactide Vitrimers," *ACS Macro Lett.*, vol. 3, no. 7, pp. 607–610, Jul. 2014, doi: 10.1021/mz500269w.

[86] W. Denissen, G. Rivero, R. Nicolaÿ, L. Leibler, J. M. Winne, and F. E. Du Prez, "Vinylogous urethane vitrimers," *Advanced Functional Materials*, vol. 25, no. 16, pp. 2451–2457, 2015.

[87] A. Erice *et al.*, "Reprocessable and recyclable crosslinked poly(urea-urethane)s based on dynamic amine/urea exchange," *Polymer*, vol. 145, pp. 127–136, Jun. 2018, doi: 10.1016/j.polymer.2018.04.076.

[88] A. Erice *et al.*, "Effect of Regioisomerism on Processability and Mechanical Properties of Amine/Urea Exchange Based Poly(urea-urethane) Vitrimers," *ACS Appl. Polym. Mater.*, vol. 1, no. 9, pp. 2472–2481, Sep. 2019, doi: 10.1021/acsapm.9b00589.

[89] D. J. Fortman, J. P. Brutman, C. J. Cramer, M. A. Hillmyer, and W. R. Dichtel, "Mechanically Activated, Catalyst-Free Polyhydroxyurethane Vitrimers," *J. Am. Chem. Soc.*, p. 4, 2015.

[90] P. Taynton, K. Yu, R. K. Shoemaker, Y. Jin, H. J. Qi, and W. Zhang, "Heat-or water-driven malleability in a highly recyclable covalent network polymer," *Adv. Mater.*, vol. 26, no. 23, pp. 3938–3942, 2014.

[91] Q. Yu *et al.*, "Vanillin-based degradable epoxy vitrimers: Reprocessability and mechanical properties study," *Eur. Polym. J.*, vol. 117, pp. 55–63, Aug. 2019, doi: 10.1016/j.eurpolymj.2019.04.053.

[92] Y.-X. Lu, F. Tournilhac, L. Leibler, and Z. Guan, "Making Insoluble Polymer Networks Malleable via Olefin Metathesis," *J. Am. Chem. Soc.*, vol. 134, no. 20, pp. 8424–8427, May 2012, doi: 10.1021/ja303356z.

[93] I. Azcune and I. Odriozola, "Aromatic disulfide crosslinks in polymer systems: Self-healing, reprocessability, recyclability and more," *Eur. Polym. J.*, vol. 84, pp. 147–160, Nov. 2016, doi: 10.1016/j.eurpolymj.2016.09.023.

[94] J.-H. Chen, D.-D. Hu, Y.-D. Li, J. Zhu, A.-K. Du, and J.-B. Zeng, "Castor oil-based high performance and reprocessable poly(urethane urea) network," *Polymer Testing*, vol. 70, pp. 174–179, Sep. 2018, doi: 10.1016/j.polymertesting.2018.07.004.

[95] Z. Karami, M. Zolghadr, and M. J. Zohuriaan-Mehr, "Chapter 8 - Self-healing Diels–Alder engineered thermosets," in *Self-Healing Polymer-Based Systems*, S. Thomas and A. Surendran, Eds. Elsevier, 2020, pp. 209–233. doi: https://doi.org/10.1016/B978-0-12-818450-9.00008-8.

[96] D. Ehrhardt, J. Mangialetto, J. Bertouille, K. Van Durme, B. Van Mele, and N. Van den Brande, "Self-Healing in Mobility-Restricted Conditions Maintaining Mechanical Robustness: Furan–Maleimide Diels–Alder Cycloadditions in Polymer Networks for Ambient Applications," *Polymers*, vol. 12, no. 11, p. 2543, Oct. 2020, doi: 10.3390/polym12112543.

[97] K. Yasuda, K. Sugane, and M. Shibata, “Self-healing high-performance thermosets utilizing the furan/maleimide Diels-Alder and amine/maleimide Michael reactions,” *J. Polym. Res.*, vol. 27, no. 1, p. 18, Jan. 2020, doi: 10.1007/s10965-019-1986-z.

[98] D. Turkenburg and H. Fischer, “Diels-Alder based, thermo-reversible cross-linked epoxies for use in self-healing composites,” *Polymer*, vol. 79, pp. 187–194, 2015.

[99] F. Fu, M. Huang, W. Zhang, Y. Zhao, and X. Liu, “Thermally assisted self-healing behavior of anhydride modified polybenzoxazines based on transesterification,” *Sci. Rep.*, vol. 8, no. 1, p. 10325, Dec. 2018, doi: 10.1038/s41598-018-27942-9.

[100] F. I. Altuna, C. E. Hoppe, and R. J. J. Williams, “Epoxy Vitrimers: The Effect of Transesterification Reactions on the Network Structure,” *Polymers*, vol. 10, no. 1, 2018, doi: 10.3390/polym10010043.

[101] X. Li *et al.*, “Self-Healing Polyurethane Elastomers Based on a Disulfide Bond by Digital Light Processing 3D Printing,” *ACS Macro Lett.*, vol. 8, no. 11, pp. 1511–1516, Nov. 2019, doi: 10.1021/acsmacrolett.9b00766.

[102] K. Chang, H. Jia, and S.-Y. Gu, “A transparent, highly stretchable, self-healing polyurethane based on disulfide bonds,” *Eur. Polym. J.*, vol. 112, pp. 822–831, Mar. 2019, doi: 10.1016/j.eurpolymj.2018.11.005.

[103] X. Cao *et al.*, “Self-healing solid polymer electrolyte based on imine bonds for high safety and stable lithium metal batteries,” *RSC Adv.*, vol. 11, no. 5, pp. 2985–2994, 2021, doi: 10.1039/D0RA10035H.

[104] J. Hu, R. Mo, X. Sheng, and X. Zhang, “A self-healing polyurethane elastomer with excellent mechanical properties based on phase-locked dynamic imine bonds,” *Polym. Chem.*, vol. 11, no. 14, pp. 2585–2594, 2020, doi: 10.1039/D0PY00151A.

[105] R. Mo, L. Song, J. Hu, X. Sheng, and X. Zhang, “An acid-degradable biobased epoxy-imine adaptable network polymer for the fabrication of responsive structural color film,” *Polym. Chem.*, vol. 11, no. 5, pp. 974–981, 2020, doi: 10.1039/C9PY01821B.

[106] J. Meurer *et al.*, “In-depth characterization of self-healing polymers based on π–π nteractions,” *Beilstein J. Org. Chem.*, vol. 17, pp. 2496–2504, Sep. 2021, doi: 10.3762/bjoc.17.166.

[107] J.-F. Mei *et al.*, “A highly stretchable and autonomous self-healing polymer based on combination of pt⋯ pt and π–π interactions,” *Macromol. Rapid Commun.*, vol. 37, no. 20, pp. 1667–1675, 2016.

[108] M. Nakahata, Y. Takashima, H. Yamaguchi, and A. Harada, “Redox-responsive self-healing materials formed from host–guest polymers,” *Nat. Commun.*, vol. 2, no. 1, p. 511, Sep. 2011, doi: 10.1038/ncomms1521.

[109] X. Yang *et al.*, "Self-healing polymer materials constructed by macrocycle-based host–guest interactions," *Soft Matter*, vol. 11, no. 7, pp. 1242–1252, 2015, doi: 10.1039/C4SM02372B.

[110] Z. Hu *et al.*, "Multistimuli-Responsive Intrinsic Self-Healing Epoxy Resin Constructed by Host–Guest Interactions," *Macromolecules*, vol. 51, no. 14, pp. 5294–5303, Jul. 2018, doi: 10.1021/acs.macromol.8b01124.

[111] K. Sugane and M. Shibata, "Self-healing thermoset polyurethanes utilizing host–guest interaction of cyclodextrin and adamantane," *Polymer*, vol. 221, p. 123629, Apr. 2021, doi: 10.1016/j.polymer.2021.123629.

[112] K. Sugane, Y. Maruoka, and M. Shibata, "Self-healing epoxy networks based on cyclodextrin–adamantane host–guest interactions," *J. Polym. Res.*, vol. 28, no. 11, pp. 1–10, 2021.

[113] J. Hu, R. Mo, X. Jiang, X. Sheng, and X. Zhang, "Towards mechanical robust yet self-healing polyurethane elastomers via combination of dynamic main chain and dangling quadruple hydrogen bonds," *Polymer*, vol. 183, p. 121912, Nov. 2019, doi: 10.1016/j.polymer.2019.121912.

[114] Z. Xie, B.-L. Hu, R.-W. Li, and Q. Zhang, "Hydrogen Bonding in Self-Healing Elastomers," *ACS Omega*, vol. 6, no. 14, pp. 9319–9333, Apr. 2021, doi: 10.1021/acsomega.1c00462.

[115] I. Gadwal, "A Brief Overview on Preparation of Self-Healing Polymers and Coatings via Hydrogen Bonding Interactions," *Macromol*, vol. 1, no. 1, pp. 18–36, Dec. 2020, doi: 10.3390/macromol1010003.

[116] T. Wan and D. Chen, "Preparation of β-cyclodextrin reinforced waterborne polyurethane nanocomposites with excellent mechanical and self-healing property," *Compos Sci Technol*, vol. 168, pp. 55–62, 2018.

[117] P. K. Behera, S. K. Raut, P. Mondal, S. Sarkar, and N. K. Singha, "Self-Healable Polyurethane Elastomer Based on Dual Dynamic Covalent Chemistry Using Diels–Alder 'Click' and Disulfide Metathesis Reactions," *ACS Appl. Polym. Mater.*, vol. 3, no. 2, pp. 847–856, Feb. 2021, doi: 10.1021/acsapm.0c01179.

[118] X. Jian, Y. Hu, W. Zhou, and L. Xiao, "Self-healing polyurethane based on disulfide bond and hydrogen bond," *Polym. Adv. Technol.*, p. 7, 2017.

[119] S. Lambert and M. Wagner, "Environmental performance of bio-based and biodegradable plastics: the road ahead," *Chem. Soc. Rev.*, vol. 46, no. 22, pp. 6855–6871, 2017, doi: 10.1039/C7CS00149E.

[120] L. Sartore, N. Inverardi, S. Pandini, F. Bignotti, and F. Chiellini, "PLA/PCL-based foams as scaffolds for tissue engineering applications," *Mater. Today.*, vol. 7, pp. 410–417, 2019, doi: 10.1016/j.matpr.2018.11.103.

[121] M. Shahrezaee, M. Salehi, S. Keshtkari, A. Oryan, A. Kamali, and B. Shekarchi, “In vitro and in vivo investigation of PLA/PCL scaffold coated with metformin-loaded gelatin nanocarriers in regeneration of critical-sized bone defects,” *Nanomed.: Nanotechnol. Biol. Med.*, vol. 14, no. 7, pp. 2061–2073, 2018.

[122] K. Sugane, N. Kumai, Y. Yoshioka, A. Shibita, and M. Shibata, “Thermo-responsive alternating conetworks by the Diels-Alder reaction of furan-terminated 4-armed star-shaped ε-caprolactone oligomers and maleimide-terminated 4-armed star-shaped l-lactide oligomers,” *Polymer*, vol. 124, pp. 20–29, Aug. 2017, doi: 10.1016/j.polymer.2017.07.038.

[123] S. Cai, Z. Qiang, C. Zeng, and J. Ren, “Multifunctional poly (lactic acid) copolymers with room temperature self-healing and rewritable shape memory properties via Diels-Alder reaction,” *Mater. Res. Express.*, vol. 6, no. 4, p. 045701, 2019.

[124] Z. Wang, H. Yang, B. D. Fairbanks, H. Liang, J. Ke, and C. Zhu, “Fast self-healing engineered by UV-curable polyurethane contained Diels-Alder structure,” *Prog. Org. Coat.*, vol. 131, pp. 131–136, 2019.

[125] H. Mallek, C. Jegat, N. Mignard, M. Abid, S. Abid, and M. Taha, “Reversibly crosslinked self-healing PCL-based networks,” *J. Appl. Polym. Sci.*, vol. 129, no. 3, pp. 954–964, Aug. 2013, doi: 10.1002/app.38595.

[126] M. Wei *et al.*, “Novel poly (tetramethylene ether) glycol and poly (ε-caprolactone) based dynamic network via quadruple hydrogen bonding with triple-shape effect and self-healing capacity,” *ACS Appl. Mater. Interfaces*, vol. 7, no. 4, pp. 2585–2596, 2015.

[127] L.-T. T. Nguyen *et al.*, “Healable shape memory (thio) urethane thermosets,” *Polym. Chem.*, vol. 6, no. 16, pp. 3143–3154, 2015.

[128] Cs. Lakatos, K. Czifrak, R. Papp, J. Karger-Kocsis, M. Zsuga, and S. Keki, “Segmented linear shape memory polyurethanes with thermoreversible Diels-Alder coupling: Effects of polycaprolactone molecular weight and diisocyanate type,” *Express Polym. Lett.*, vol. 10, no. 4, pp. 324–336, 2016, doi: 10.3144/expresspolymlett.2016.30.

[129] W. Chen *et al.*, “Shape-memory and self-healing polyurethanes based on cyclic poly (ε-caprolactone),” *Polym. Chem.*, vol. 7, no. 44, pp. 6789–6797, 2016.

[130] J. Zhao, R. Xu, G. Luo, J. Wu, and H. Xia, “Self-healing poly (siloxane-urethane) elastomers with remoldability, shape memory and biocompatibility,” *Polym. Chem.*, vol. 7, no. 47, pp. 7278–7286, 2016.

[131] M. Invernizzi, S. Turri, M. Levi, and R. Suriano, “4D printed thermally activated self-healing and shape memory polycaprolactone-based polymers,” *Eur. Polym. J.*, vol. 101, pp. 169–176, Apr. 2018, doi: 10.1016/j.eurpolymj.2018.02.023.

[132] K. Sugane, Y. Yoshioka, T. Shimasaki, N. Teramoto, and M. Shibata, “Self-healing 8-armed star-shaped ε-caprolactone oligomers dually crosslinked by the Diels-Alder and

urethanization reactions," *Polymer*, vol. 144, pp. 92–102, May 2018, doi: 10.1016/j.polymer.2018.04.045.

[133] L. Zhang, T. Qiu, Z. Zhu, L. Guo, and X. Li, "Self-Healing Polycaprolactone Networks through Thermo-Induced Reversible Disulfide Bond Formation," *Macromol. Rapid Commun.*, vol. 39, no. 20, p. 1800121, Oct. 2018, doi: 10.1002/marc.201800121.

[134] K. Borska, M. Bednarek, and A. Pawlak, "Reprocessable polylactide-based networks containing urethane and disulfide linkages," *Eur. Polym. J.*, vol. 156, p. 110636, Aug. 2021, doi: 10.1016/j.eurpolymj.2021.110636.

[135] T. Ikezaki, R. Matsuoka, K. Hatanaka, and N. Yoshie, "Biobased poly(2,5-furandimethylene succinate- *co* -butylene succinate) crosslinked by reversible Diels–Alder reaction," *J. Polym. Sci. Part A: Polym. Chem.*, vol. 52, no. 2, pp. 216–222, Feb. 2014, doi: 10.1002/pola.26990.

Chapter 1

Synthesis and properties of polyurethane networks composed of comb- shaped polymers grafted with L-lactide and ε-caprolactone oligomers.

1.1 Introduction

Polylactide (PLA) and poly(ε-caprolactone) (PCL) are biodegradable aliphatic polyesters that have been extensively used in ecologically friendly materials and biomedical for use in controlled drug delivery tissue engineering, agriculture, automobiles, dairy products, and other applications [1–8]. PLA is a polymer of economic significance due to its similarities to hydrocarbon polymers such as polyethylene terephthalate (PET). In addition, it possesses numerous unique characteristics, including high transparency, a glossy appearance, high rigidity, and the capacity to withstand various processing conditions [9]. However, one of the drawbacks of PLA is the brittle fracture behavior. In contrast, biodegradable/petroleum-based PCL exhibits a much higher elongation at break (>300%) than PLA (ca. 3%), whereas PCL has a much lower melting temperature (ca. 60 °C) and tensile strength (ca. 20 MPa) than those of PLA (ca.170 °C, ca. 50 MPa) [9,10]. Blending PLA with flexible biodegradable polyesters is one of the most effective and practical methods to improve the brittleness of PLA. However, Blends of PLA and ductile PCL have been studied intensively, PLA is incompatible with PCL, and a simple PCL/PLA blend has a coarse morphology and poor adhesion between the two phases. Consequently, the resulting mechanical properties are not those expected. Cross-linking PLA and PCL chains to generate a polymer network is one technique to increase compatibility [11–14]. This technique can considerably enhance compatibility due to the incorporation of PLA and PCL into a single network.

In our lab recently reported the characteristics of a series of network polymers made by crosslinking reactions of various hydroxy-terminated star-shaped lactide and ε-caprolactone oligomers with diisocyanates [15–24]. Although elucidating the characteristics of highly crosslinked networks composed of comb-shaped polymers grafted with lactide and ε-caprolactone oligomers (LAO and CLO) is a fascinating subject, these network polymers have not been published.

Regarding the comb-shaped polymers grafted with LAO, Park et al. reported the generation of enantiomeric macromonomers (MALLAO and MADLAO) through the ring-opening

polymerizations of L- and D-lactides initiated with hydroxyethyl methacrylate (HEMA) and stereocomplex crystallization of copolymer blends of HEMA/MALLAO and HEMA/MADLAO [25].In addition, S. Kobayashi et al. reported on the synthesis and characteristics of comb-shaped polymers (PBMA-*g*-PLAs) generated by the radical co-polymerization of MALLAO and butyl methacrylate (BMA) [26]. According to their research, PBMA-*g*-PLAs synthesized via solution polymerization in toluene or 1,4-dioxane are too brittle to evaluate their physical properties. Moreover, Pan et al. reported the stereo complexation of enantiomeric blends of cellulose acetate-*g*-PLAs as another type of LAO-grafted comb-shaped polymer [27].

Regarding comb-shaped polymers grafted with CLOs, D. Moscatelli et al. described the synthesis of nanoparticles by emulsion polymerization of a macromonomer (MACLO) by ring-opening polymerization of CL initiated with HEMA and emulsion polymerization of MACLO and methyl methacrylate (MMA) for drug delivery applications [28]. However, the paper did not report the thermal and mechanical properties of the MACLO and MMA copolymers.

In this chapter, first, methacrylate-terminated L-lactide and ε-caprolactone oligomers (MALLAO and MACLO) were synthesized by the ring-opening polymerizations of L-lactide (LLA) and ε-caprolactone (CL) initiated with hydroxyethyl methacrylate. Next, the radical copolymerizations of butyl methacrylate/MALLAO and butyl methacrylate/MACLO in a molar ratio of 8/2 generated comb-shaped polymers grafted with hydroxy-terminated lactide and ε-caprolactone oligomers (PBML and PBMC). The crosslinking reaction of PBML/PBMC (weight ratios: 100/0, 75/25, 50/50, 25/75, and 0/100) and hexamethylene diisocyanate (HDI) produced polyurethane networks (PUN-BML/Cs). In this study, we focused on enhancing the thermal and mechanical properties of PBML and PBMC through the cross-linking reaction of the comb-shaped polymers and the network compatibility of lactide and ε-caprolactone oligomers (LAO and CLO) segments.

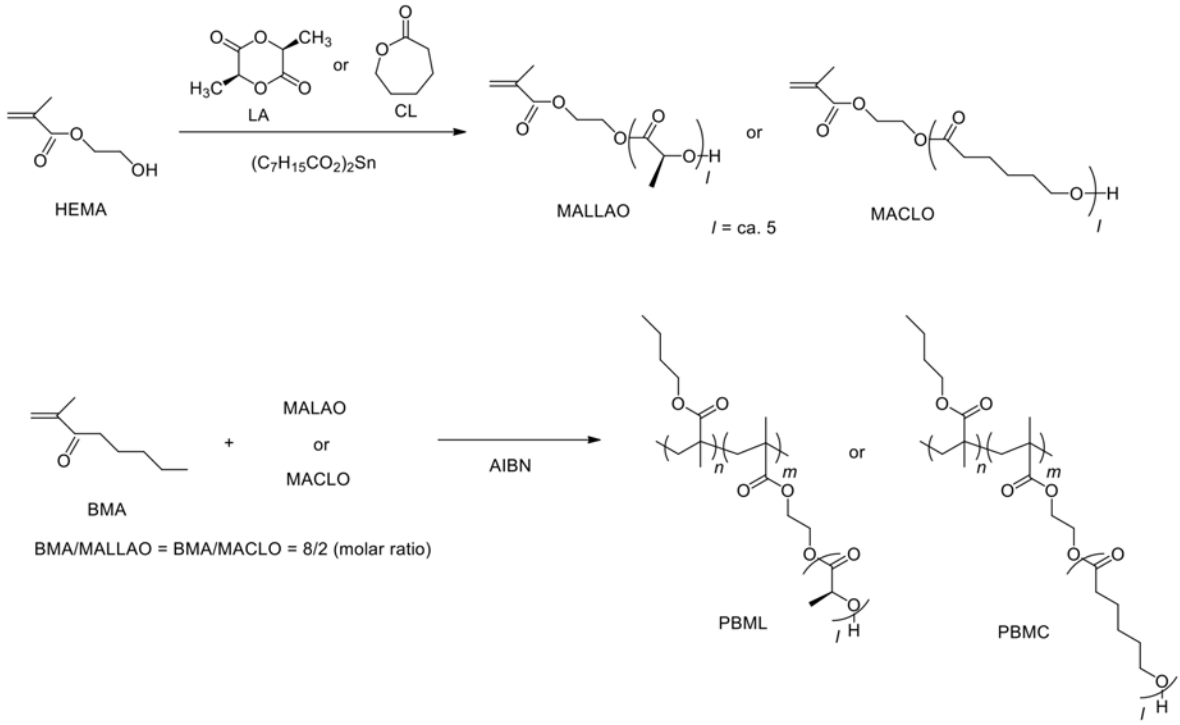

Scheme 1. Synthesis of MALLAO, MACLO, PBML and PBMC.

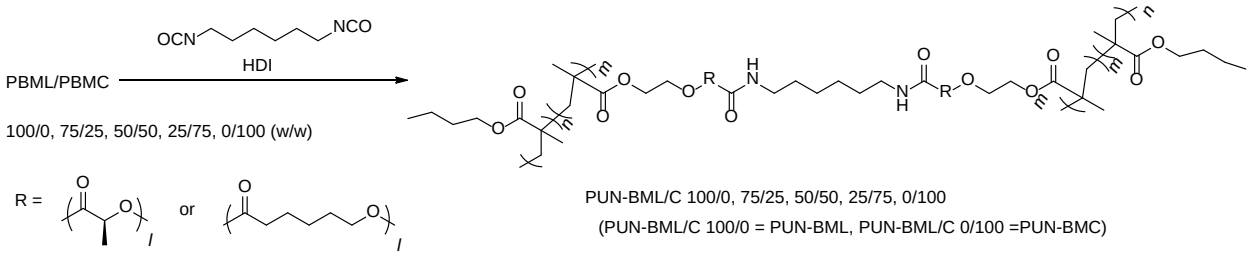

Scheme 2. Synthesis of PUN-BML/Cs.

1.2. Experimental section

1.2.1. Materials

Hydroxyethyl methacrylate (HEMA)
MW: 130.14
m.p.: 85.0 ℃ (5 mmHg)
b.p.: 250 ℃
Tokyo Chemical Industry Co., Ltd.

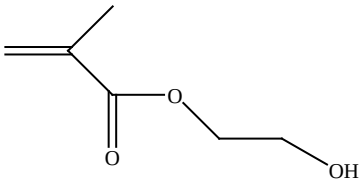

L-lactide (LLA)
MW: 144.13
m.p.: 92.0～94.0 ℃
b.p.: 255 ℃
Daiwakasei Industry Co., Ltd.

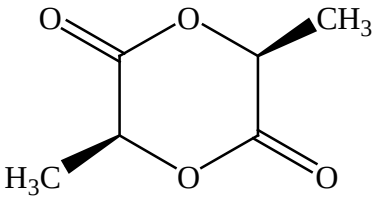

ε-caprolactone (CL)
MW: 114.14
m.p.: −1.00 ℃
b.p.: 140 ℃ (35 mmHg)
Tokyo Chemical Industry Co., Ltd.

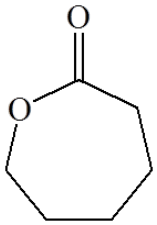

Chlorobenzene
MW: 112.56
m.p.: −45.0 ℃
FUJIFILM Wako Pure Chemical Corporation.

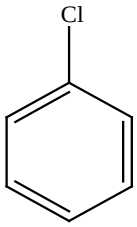

Tin (II) bis(2- ethylhexanoate) ($Sn(Oct)_2$)

MW: 405.12

b.p.: 228 ℃

Nacalai Tesque Inc.

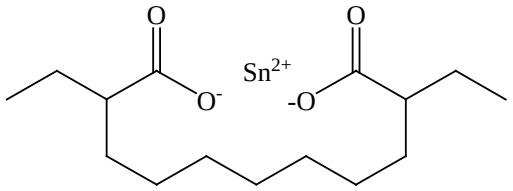

Hexamethylene diisocyanate (HDI)

MW: 168.19

m.p.: −55.0 ℃

Tokyo Chemical Industry Co., Ltd.

1,4-Dioxane

MW: 88.10

m.p.: 11.8 ℃

b.p.: 101.1 ℃

Kanto Chemical Co. Inc.

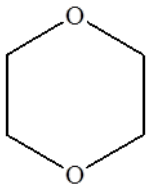

α,α’-Azobisisobutyronitrile(AIBN)

MW: 164.21

b.p.: 102～104 ℃

Kanto Chemical Co. Inc.

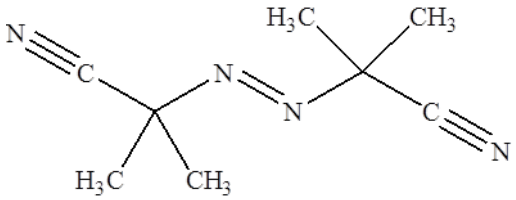

1,2-dichloroethane (DCE)

MW: 98.96

m.p.: −35.0 ℃

b.p.: 83.0～84.0 ℃

Kanto Chemical Co. Inc.

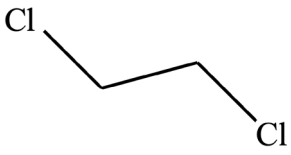

Butyl methacrylate (BMA)
MW: 142.2
m.p.: −75.0 ℃
Tokyo Chemical Industry Co., Ltd.

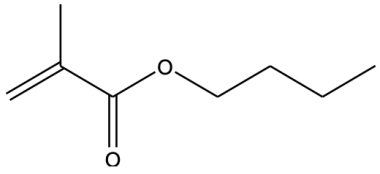

1.2.2. Synthesis of MALLAO

MALLAO was synthesized according to previously reported method except that chlorobenzene was used as a reaction solvent [26],[29]. In a nitrogen-purged three-necked flask were put 9.02 g (69.3 mmol) of HEMA, 20.9 g (145 mmol) of L-LA, and 15 mL of chlorobenzene, respectively. The mixture was heated to 150 °C until the L-LA was completely dissolved, and then 0.299 g (0.738 mmol) of $Sn(Oct)_2$ was added to the flask. The resulting mixture was stirred for 24 hours at 150 °C in an atmosphere of nitrogen. The cooled reaction mixture was added to 300 mL of hexane with stirring. The supernatant hexane phase was decanted, and the separated viscous liquid phase was repeatedly washed with hexane and dried at 40 °C in a vacuum oven to yield MALLAO as a viscous liquid (28.8 g, 96%). The experimental flow chat of MALLAO is shown in Fig.1.1.

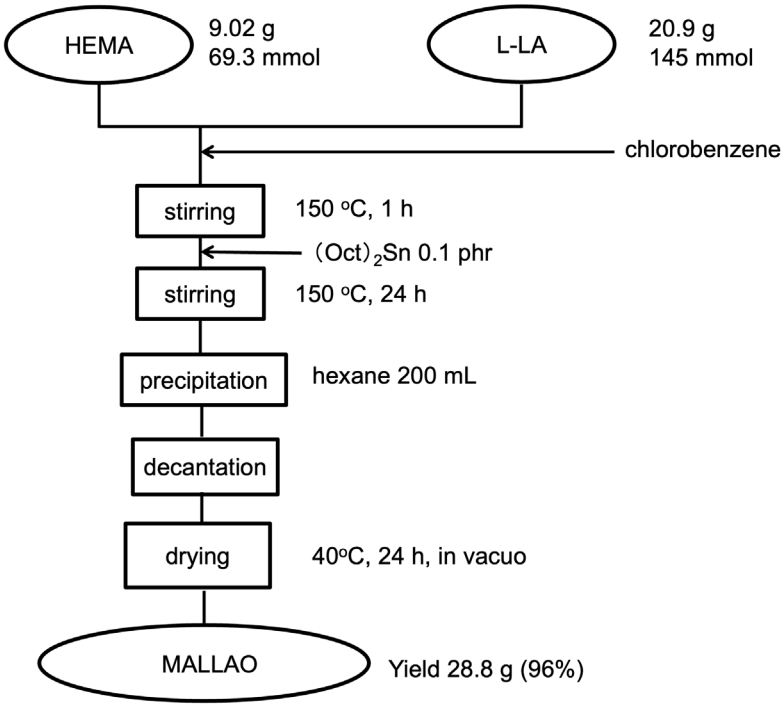

Fig.1.1. The synthesis flow chart of MALLAO.

1.2.3. Synthesis of MACLO

MACLO was synthesized according to the previously reported method except that toluene was used as a reaction solvent [28]. In a nitrogen-purged three-necked flask were put 6.02 g (46.8 mmol) of HEMA, 23.9 g (210 mmol) of CL, and 15 mL of toluene, respectively. The mixture was heated to 110°C, and 0.299 g (0.738 mmol) of $Sn(Oct)_2$ was added to the flask. The resulting mixture was stirred for 24 h at 110 °C in an atmosphere of nitrogen. The cooled reaction mixture was added to 200 mL of hexane with stirring. The supernatant hexane phase was decanted, and the separated viscous liquid phase was repeatedly washed with hexane and dried at 40 °C in a vacuum oven to give MACLO as a viscous liquid (28.8 g, 96%). The synthesis flow chat of MACLO is shown in Fig.1.2.

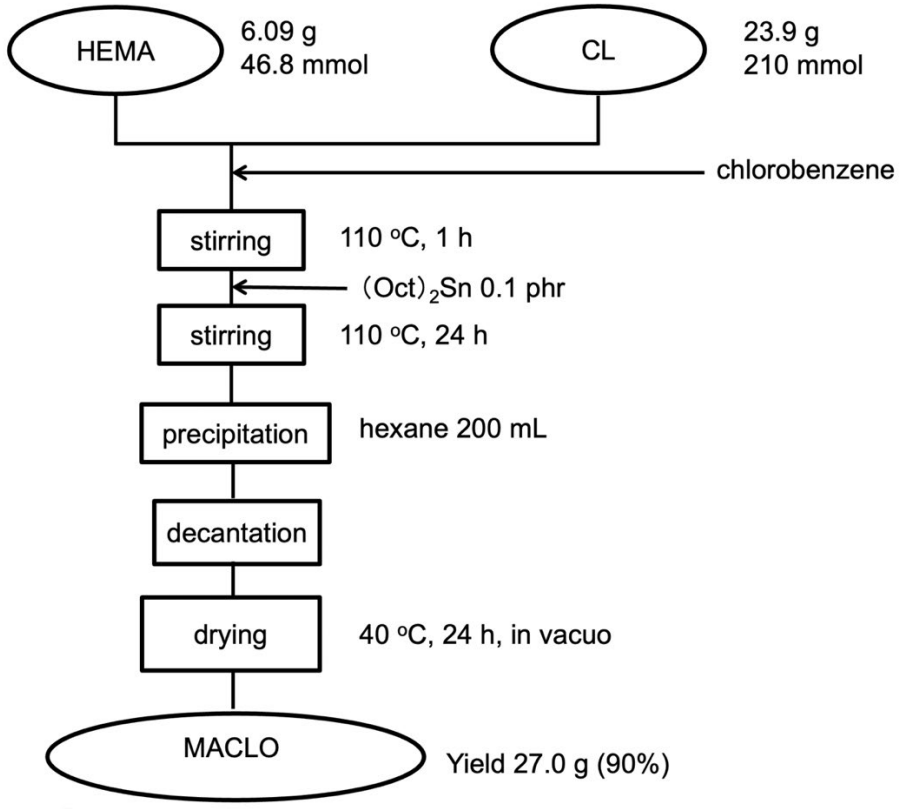

Fig.1.2. The synthesis flow chat of MACLO

.

1.2.4. Synthesis of PBML

According to the previously reported synthetic method, PBML was synthesized using 1,4-dioxane as a reaction solvent [29].In a nitrogen-purged three-necked flask, 2.72 g (19.1 mmol) of BMA, 2.37 g (4.78 mmol) of MALLAO and 1,4-dioxane (10 mL) were added and stirred. 0.392 g, (2.39 mmol) of AIBN (10 mol% of monomers) was added to the flask after the mixture was heated to 70 °C. The molar ratio of BMA/ MALLAO was fixed to 8/2. The resulting mixture was stirred for 24 h at 70 °C in an atmosphere of nitrogen. Next, the cooled reaction mixture was added to 200 mL of hexane with stirring. Finally, the supernatant hexane phase was decanted, and the separated viscous liquid phase was repeatedly washed with hexane and dried at 40 °C in a vacuum to produce PBML as a viscous liquid (4.8 g, 94%). The number and weight-averaged molecular weights (M_n and M_w) of PBML measured by the GPC method were 17,000 and 48,300, respectively. The synthesis flow chat of PBML is shown in Fig.1.3.

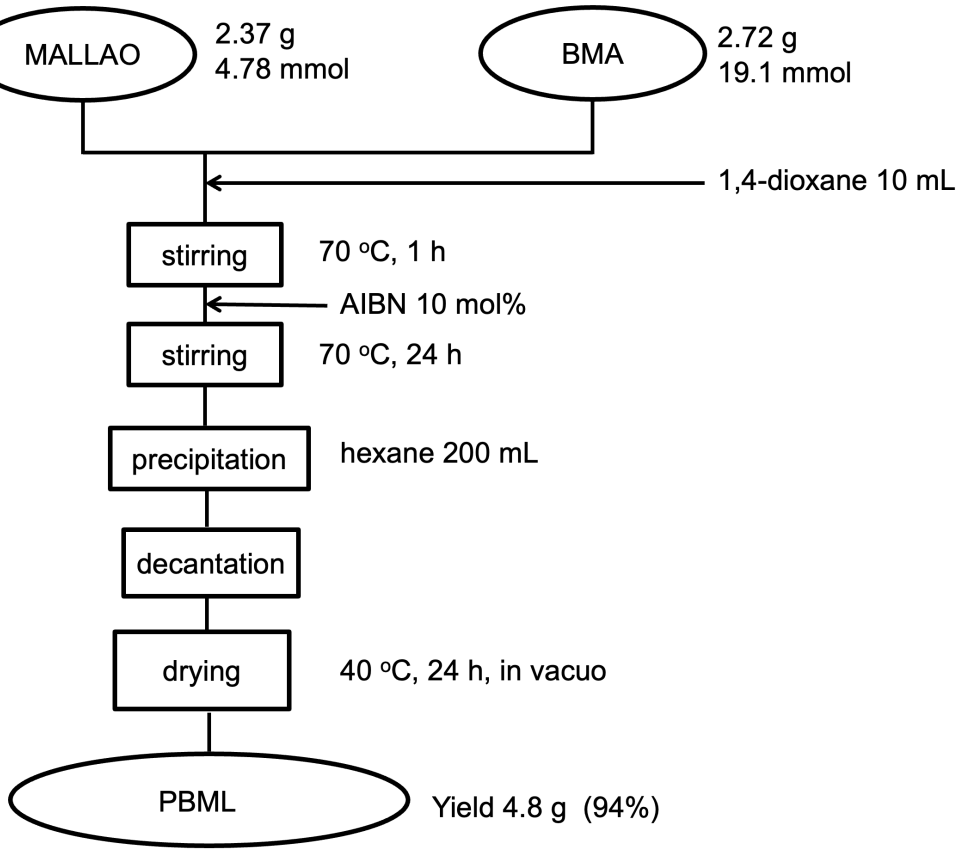

Fig.1.3. The synthesis flow chat of PBML.

1.2.5. Synthesis of PBMC

The PBMC was synthesized with the following: BMA (2.22 g, 15.6 mmol), MACLO (2.71 g, 3.90 mmol), and toluene (10 mL) were put into a nitrogen-purged three-necked flask and stirred. AIBN (0.320 g, 1.95 mmol, 10 mol% of monomers) was added to the flask after the mixture was heated to 60 °C. The molar ratio of BMA/ MACLO was fixed to 8/2. The resulting mixture was stirred for 24 hours at 60°C in an atmosphere of nitrogen. Next, the cooled reaction mixture was added to 150 mL of hexane with stirring. Finally, the supernatant hexane phase was decanted, and the separated viscous liquid phase was repeatedly washed with hexane and dried at 40 °C in a vacuum to produce PBML as a viscous liquid (4.6 g, 93%). The number and weight-averaged molecular weights (M_n and M_w) of PBMC measured by the GPC method were 7,800 and 29,800, respectively. The synthesis flow chat of PBMC is shown in Fig.1.4.

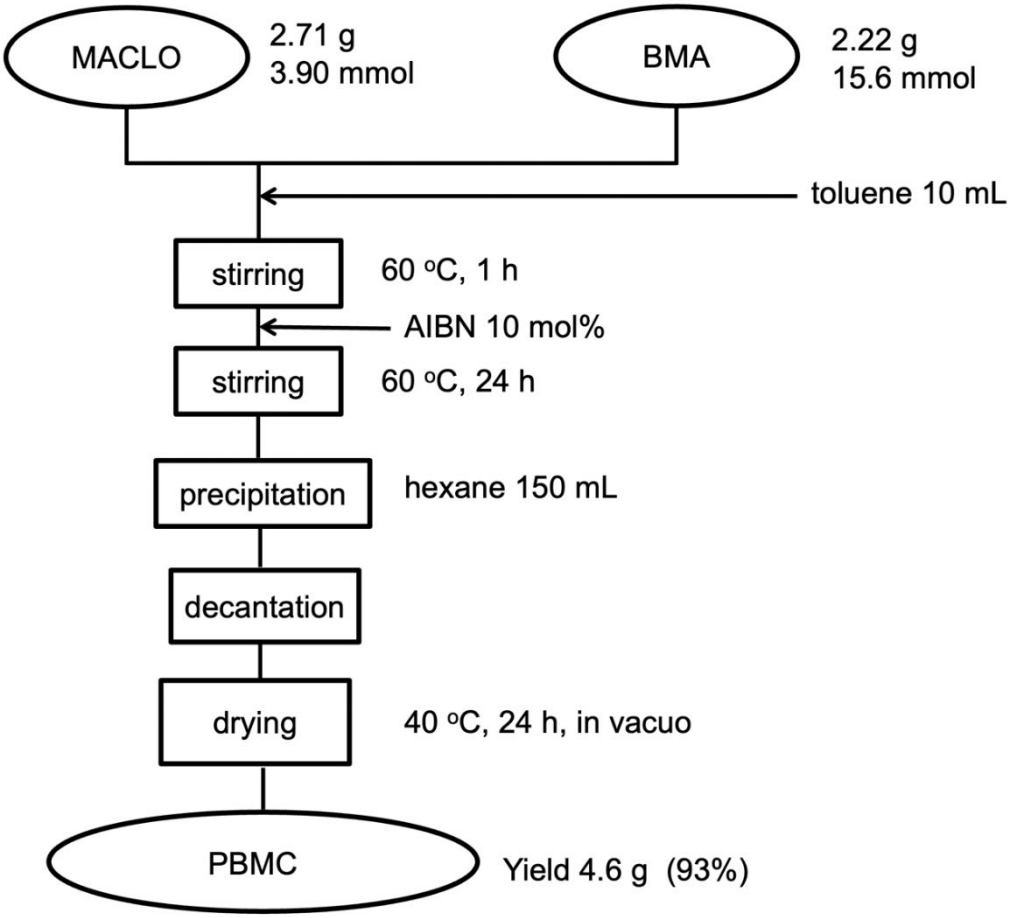

Fig1.4. The synthesis flow chat of PBMC.

1.2.6. Synthesis of PBML/Cs

PBML/Cs (100/0, 75/25, 50/50, 25/75, and 0/100) were generated by PBML, PBMC, and HDI reactions. A typical synthetic procedure for PBML/C 50/50 is shown below. A solution of PBML (1.85 g, 1.75 mmol-OH), PBMC (1.85 g, 1.52 mmol-OH), and HDI (0.330 g, 3.92 mmol-NCO) in DCE (50 mL) was poured into a polystyrene petri dish (100 mm in diameter) with a diameter of 100 mm (tetrafluoroethylene).The molar ratio of OH/NCO in (PBML + PBMC)/HDI was fixed to 1/1.2. The mixture was dried at 60 °C for 24 h and then at 130 °C for 4 h in an electric oven. First, the PBML/C 50/50 film (thickness: approximately 0.5 mm) was removed from the petri dish. Next, 100/0, 50/50, and 0/100 PBML/C films were prepared similarly. The feed amount of PBML, PBMC, and HDI was shown in Table 1 and the synthesis flow chat of PBML/Cs was shown in Fig.1.5.

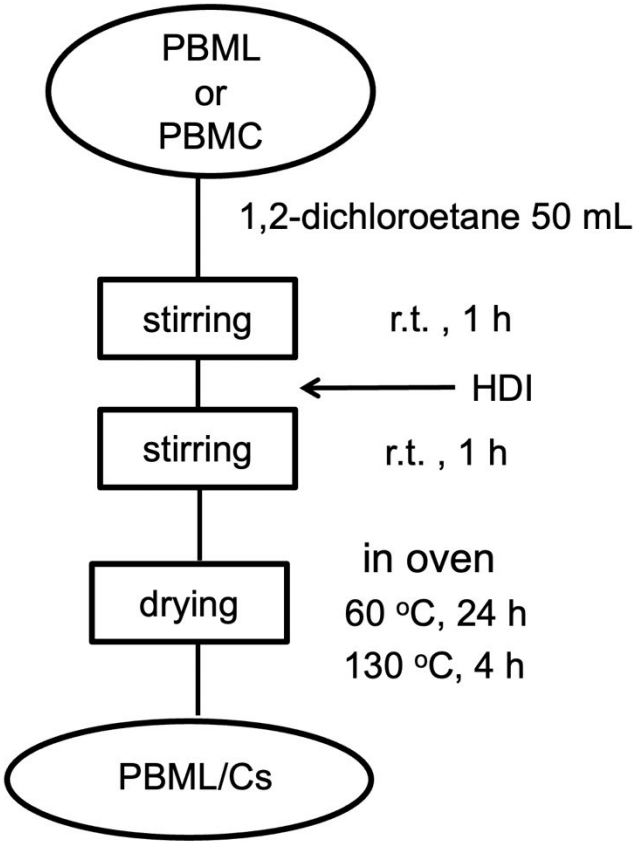

Fig.1.5. Synthesis flow chart of PBML/Cs

Table 1. The feed amounts of PBML, PBMC, and HDI for the synthesis of PBML/Cs

PBML/Cs	PBML		PBMC		Total-OH	HDI	
	g	mmol-OH	g	mmol-OH	mmol	g	mmol-NCO
100/0	3.68	3.47	-	-	3.47	0.349	4.16
75/25	2.77	2.60	0.920	0.760	3.66	0.340	4.03
50/50	1.85	1.75	1.85	1.52	3.27	0.330	3.92
25/75	0.930	0.87	2.78	2.30	3.17	0.320	3.80
0/100	-	-	3.72	3.07	3.07	0.310	3.68

1.2.7. Measurements

a. Proton nuclear magnetic resonance (^{1}H NMR)

Proton nuclear magnetic resonance (^{1}H-NMR) spectra were recorded on a JEOL JNM-ECA500 (500MHz) using $CDCl_3$ and tetra-methylsilane as a solvent and an internal standard.

b. Fourier transform infrared (FT-IR)

Fourier transform infrared (FT-IR) spectra were recorded at room temperature in the range from 4000 to 600 cm^{-1} on a Shimadzu (Kyoto, Japan) IRAffinity-1S by the attenuated total reflectance (ATR) method. The IR spectra were acquired using 50 scans at a resolution of 4 cm^{-1}.

c. Gel Permeation Chromatography (GPC)

Averaged molecular weights (M_n and M_w) were measured on a Shimadzu LC9A gel permeation chromatography (GPC) apparatus equipped with two OHpak SB-806M HQ GPC columns (Showa Denko) and a refractive index (RI) detector at 40 °C. N,N-Dimethylformamide (DMF) was used as an eluent at a flow rate of 0.5 mL min^{-1}. Polystyrene standards with a narrow distribution of molecular weights (M_w: 580–377,400) were used for molecular weight calibrations.

d. Degree of swelling (D_s) and Gel fraction

Degree of swelling (D_s) measurements were performed by dipping a film (10 × 10 × 0.5 mm3) in chloroform or DMF at room temperature for 48 h according to the following equation: D_s (%) = $100(w_1–w_0)/w_0$; where w_0 is the initial weight of the film and w_1 is the weight of the swollen film after dipping.

Gel fraction measurements were carried out by the following procedure: A film (10 × 10 × 0.5 mm^3) was dipped in chloroform at room temperature for 48 h, subsequently the film which was taken out was dried at 40 °C in a vacuum oven for 24 h. The gel fraction was calculated by the equation: Gel fraction (%) = 100 w_2/w_0; where w_0 and w_2 are the weights of original and dried films, respectively.

e. Differential scanning calorimetry (DSC)

Differential scanning calorimetry (DSC) analysis was performed on a PerkinElmer (Waltham, MA) Diamond DSC in a nitrogen atmosphere. A sample (8～12 mg) was heated from −100 °C to 200 °C at a heating rate of 20 °C min^{-1}, held at the temperature for 3 min to eliminate a thermal history of the sample, and then cooled to −100 °C at a cooling rate of 100 °C min^{-1}. After held at −100 °C for 3 min, the second heating scan was monitored at a heating rate of 20 °C min^{-1}. Glass transition temperature (T_g) was determined from the second heating curves.

f. Dynamic mechanical analysis (DMA)

Dynamic mechanical analysis (DMA) of the rectangular plate (40 × 8 × 1.0～0.6 mm^3) was performed on a Rheolograph Solid instrument (Toyo Seiki Co., Ltd, Tokyo, Japan) under an atmosphere of air with a chuck distance of 20 mm, a frequency of 1 Hz and a heating rate of 2 °C min^{-1}, based on ISO 6721–4:1994 (Plastics-Determination of dynamic mechanical properties, Part 4: Tensile vibration−Non-resonance method).

g. Thermogravimetric analysis (TGA)

Thermogravimetric analysis (TGA) was performed on a Shimadzu TGA-50 thermogravimetric analyzer using a sample of ca. 5 mg at a heating rate of 20 °C min^{-1} in a nitrogen atmosphere. The temperature at which 5% weight loss occurred ($T_{d5\%}$) was calculated from the TGA curve.

h. Field Emission-Scanning Electron Microscopy (FE-SEM)

Morphology of fractured surfaces of samples was observed by field emission-scanning electron microscopy (FE-SEM), using a Hitachi S-4700 machine (Hitachi High-Technologies Corporation, Tokyo, Japan). All samples were fractured after immersion in liquid nitrogen for about 5 min. The fracture surfaces were sputter coated with gold to provide enhanced conductivity.

i. Tensile test

Tensile tests of rectangular specimens (40 × 5 × 1.0～0.6 mm^3) were performed at the room temperature at around 25 °C using a Shimadzu Autograph AG-1. Span length and testing speed were 25 mm and 5 mm min^{-1}, respectively. Five specimens were tested for each set of samples, and the mean value and the standard deviation were calculated.

1.3. Results and Discussion

1.3.1. Characterization of MALLAO and MACLO

1.3.1.1 ^{1}H-NMR

a. MALLAO

The ring-opening polymerization of L-LA and CL initiated by HEMA produced MALLAO and MACLO with polymerization degrees (*l* values) of 5.08 and 4.95, respectively [26, 29, 30], which were then copolymerized with BMA at molar ratios of BMA/MALLAO and BMA/MACLO of 8/2 to generate PBML and PBMC (Scheme 1). Also, MALLAO and MACLO were synthesized with an *l* value higher than 5. However, radical copolymerization of these macromonomers with BMA frequently produced gelatinous products that are difficult to crosslink with HDI. Fig.2.1. illustrates the ^{1}H-NMR spectra of HEMA, L-LA, and MALLAO in $CDCl_3$. Also, Table 2.3 shows chemical shifts of the ^{1}H-signals of MALLAO. The methine group peak ^{1}H-signal (H-f) in the repeating units of MALLAO was observed at 5.26 ppm, which was in a lower magnetic field than the corresponding ^{1}H-signal (H-h) observed at 5.45 ppm for L-LA. In addition, MALLAO displayed the ^{1}H-signal (H-f',d,e) of the terminal methine group and the ethylenedioxy groups at 4.25～4.45 ppm. The methyl ^{1}H-signals of the repeating and terminal lactate units were observed of 1.58 and 1.45 ppm, respectively. From the integral ratios of repeating methine protons [(*l*-1)H, H-f] and the summation of a terminal methine proton (1H, H-f') and O*C*H_2*C*H_2*O* protons (4H, H-d, e) in the ^{1}H-NMR spectrum of MALLAO, the degree of polymerization (*l*) of the poly(lactic acid) chain was calculated to be 5.08. The observed *l* value (5.08) was slightly higher than the theoretical *l* value (4.18).

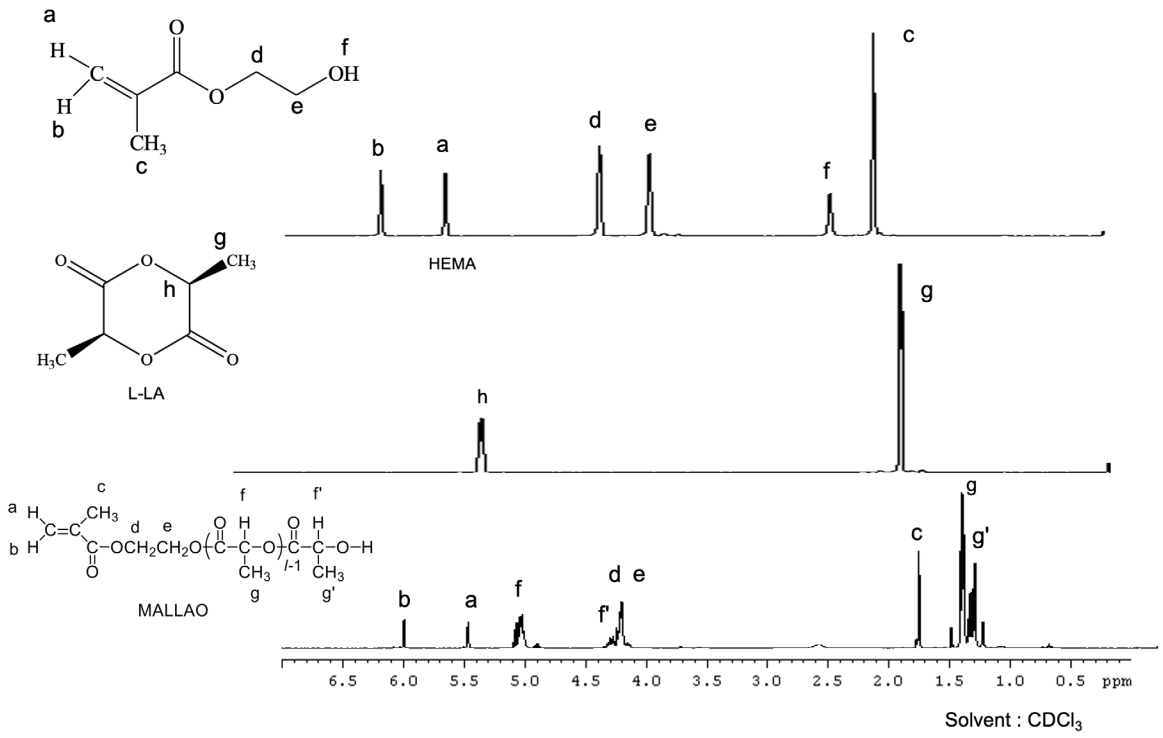

Fig 2.1. ^{1}H-NMR spectra of HEMA, L-LA, and MALLAO in $CDCl_3$

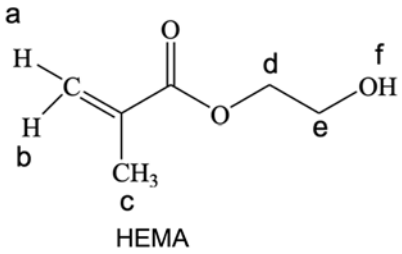

Table 2.1. ^{1}H-NMR chemical shifts of HEMA

Signal	Chemical shift (ppm)	Measured integral value	Theoretical integral value
c	1.98	1.299	3.00
f	2.35	0.422	1.00
e	3.88	0.848	2.00
d	4.31	0.859	2.00
a	5.62	0.425	1.00
b	6.17	0.425	1.00

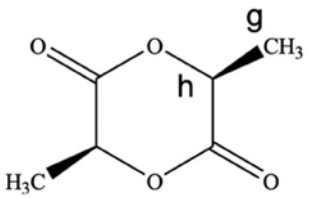

L-LA

Table 2.2. ^{1}H-NMR chemical shifts of L-LA

Signal	Chemical shift (ppm)	Measured integral value	Theoretical integral value
g	1.45	49.912	3.00
h	5.45	15.874	1.00

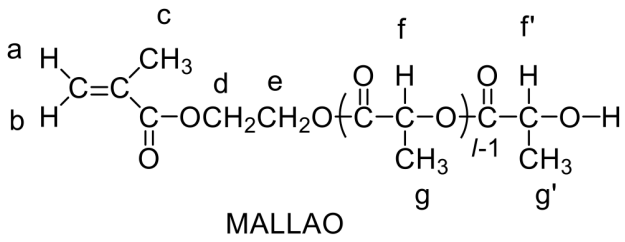

MALLAO

Table 2.3 ^{1}H-NMR chemical shifts of MALLAO

Signal	Chemical shift (ppm)	Measured integral value	Theoretical integral value
g, g’	1.49-1.58	150.15	15.00
c	1.92	24.33	3.00
d, e ,f’	4.25-4.45	47.02	5.00
f	5.26	38.36	4.00
a	5.56	8.14	1.00
b	6.08	8.28	1.00

b. MACLO

Fig.2.2 shows ^{1}H-NMR spectra of HEMA, CL, and MACLO in $CDCl_3$ and Table 2.5 shows the chemical shifts of ^{1}H-signals of MACLO. In the ^{1}H-NMR spectrum of MACLO, the ^{1}H-signals of the repeating oxyhexanoate units were observed at 4.04 ppm (H-j), 2.29 ppm (H-f), 1.20～1.70 ppm (H-g,h,i), which were in a higher magnetic field than those (4.04, 2.61, 1.55～1.77 ppm) of CL. In addition, a new methine ^{1}H-signal (H-j') at 3.64 ppm of the terminal oxyhexanoate was observed. From the integral ratio of repeating C*H*$_2$OC=O protons [2(*l*-1)H, H-j and a corresponding terminal methylene proton (2H, H- j') in the ^{1}H-NMR spectrum of MACLO, the degree of polymerization (*l*) of the polycaprolactone was calculated to be 4.95. The observed *l* value (4.95) was slightly higher than the theoretical *l* value (4.49).

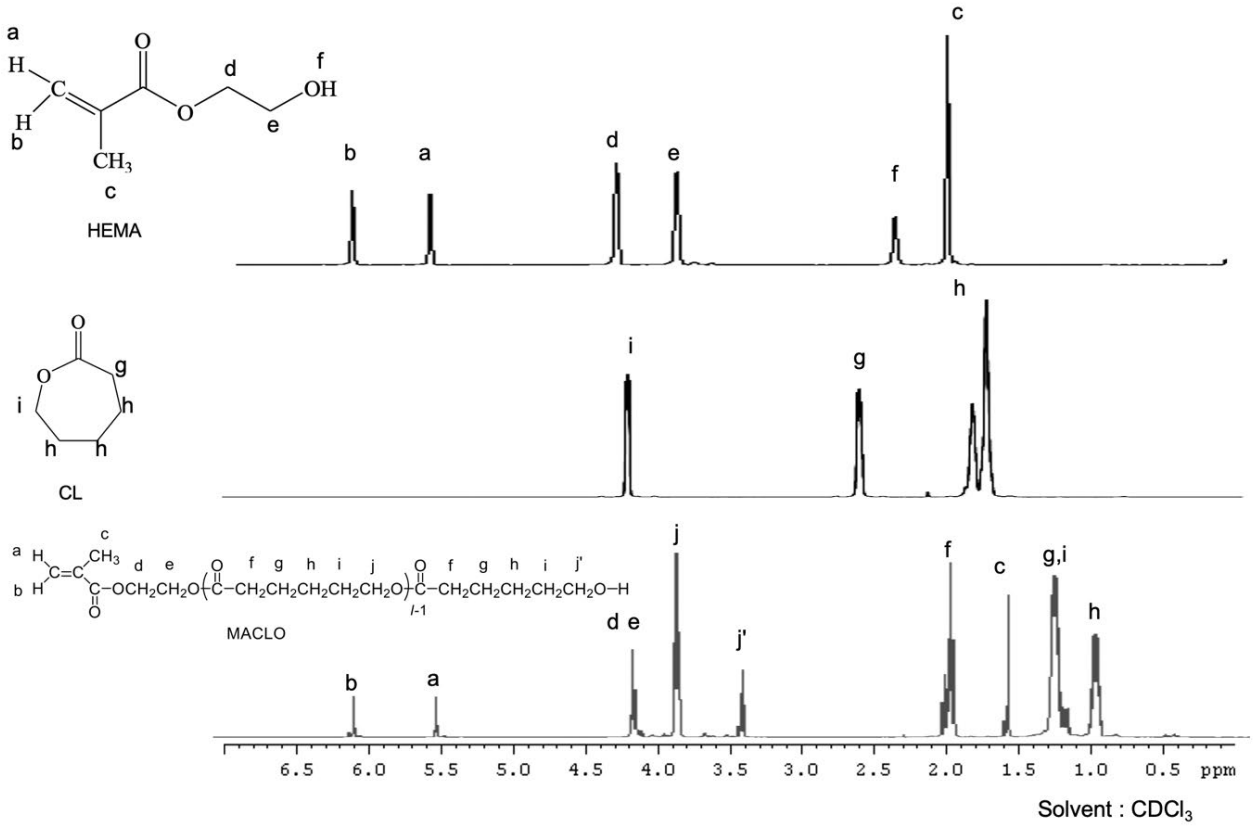

Fig.2.2. ^{1}H-NMR spectra of HEMA, CL, and MACLO in $CDCl_3$.

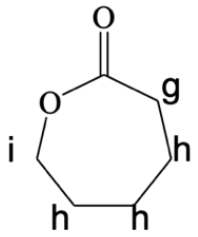

CL

Table 2.4. ^{1}H-NMR chemical shifts of CL

Signal	Chemical shift (ppm)	Measured integral value	Theoretical integral value
h	1.55-1.77	6.10	6.00
g	2.61	2.00	2.00
i	4.21	2.00	2.00

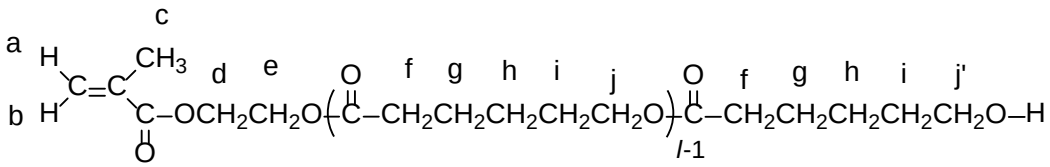

MACLO

Table 2.5. The chemical shift of MACLO.

Signal	Chemical shift (ppm)	Measured integral value	Theoretical integral value
h	1.20	43.24	10.00
g, i	1.70	90.22	20.00
c	1.90	12.53	3.00
f	2.29	31.17	8.00
j’	3.64	6.13	6.00
j	4.04	25.20	8.00
d, e	4.23-4.34	15.96	4.00
a	5.58	4.22	2.00
b	6.11	4.20	2.00

1.3.2. Characterization of PBML and PBMC

1.3.2.1 ^{1}H-NMR

Fig.2.4 shows the ^{1}H-NMR spectra of PBML and PBMC in $CDCl_3$. The chemical shift of PBML and PBMC were shown in Table 2.7 and 2.8. From the integral ratio of H-c (2H, OCH_2) of the BMA unit and H-i,j,k' (5H, OCH_2CH_2, and terminal methine) of the MALLAO unit in the PBML spectrum, the incorporated BMA/MALLAO molar ratio was calculated to be 79.8/20.2, in agreement with the feed ratio of 8/2. Furthermore, according to a report [29] the reaction time dependence of monomer conversion during radical copolymerization of BMA and MALLAO strongly supported the formation of random copolymers. It is assumed that the synthesized PBML in this study has a random structure. From the integral ratio of H-c (2H, OCH_2) of the BMA unit and H-o' (2H, terminal methylene) of the MACLO unit in the PBMC spectrum, the incorporated BMA/MACLO molar ratio was calculated to be 76.6/23.4, that was slightly lower than the feed ratio of 8/2. Therefore, this result suggests that the radical polymerizable of MACLO is presumed to be slightly higher than that of BMA.

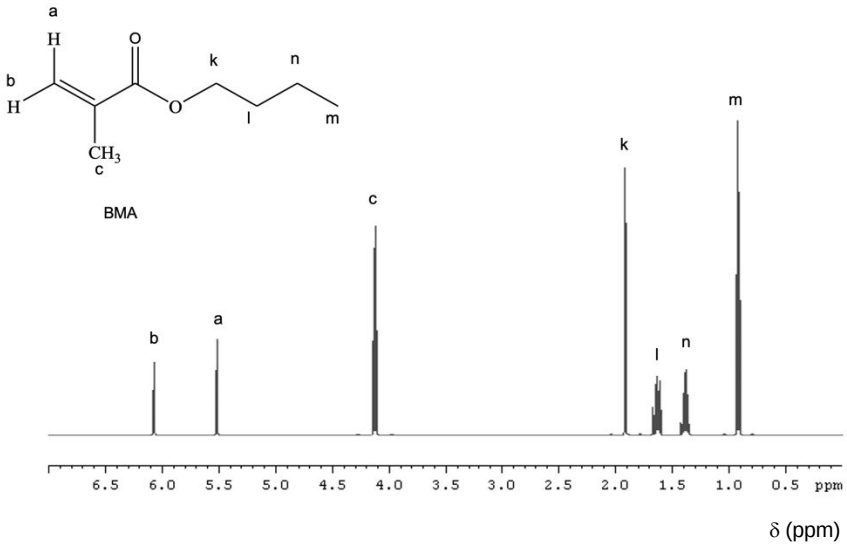

Fig.2.3. ^{1}H-NMR spectra of BMA in $CDCl_3$

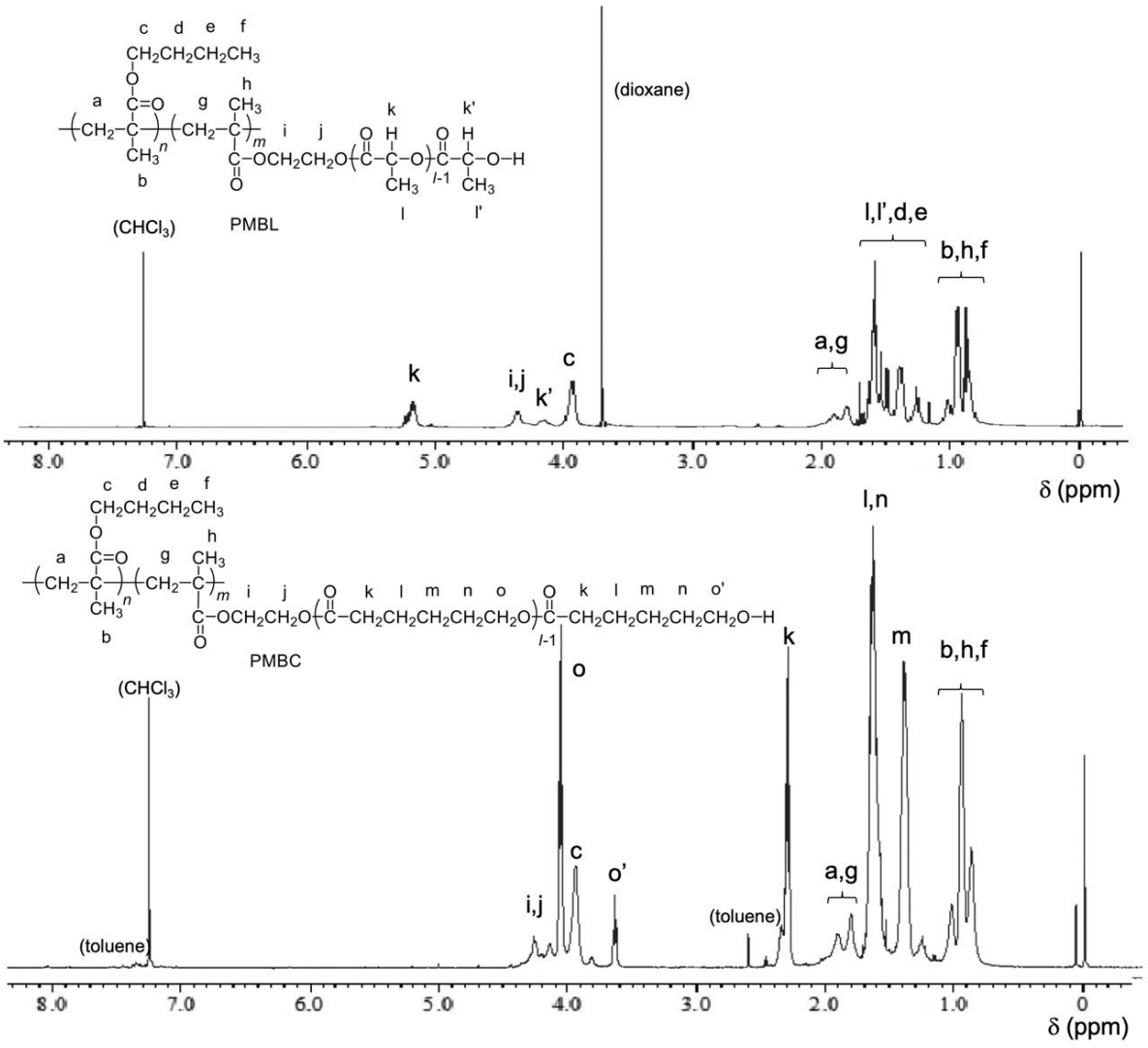

Fig.2.4. ^{1}H-NMR spectra of PBML and PBMC in $CDCl_3$

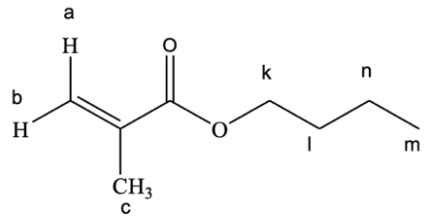

BMA

Table 2.6. ^{1}H-NMR chemical shifts of BMA

Signal	Chemical shift (ppm)	Measured integral value	Theoretical integral value
m	0.92	53.15	3.00
n	1.40	35.52	2.00
l	1.65	37.75	2.00
c	1.91	53.42	3.00
k	4.13	35.71	2.00
a	5.52	17.78	1.00
b	6.09	17.83	1.00

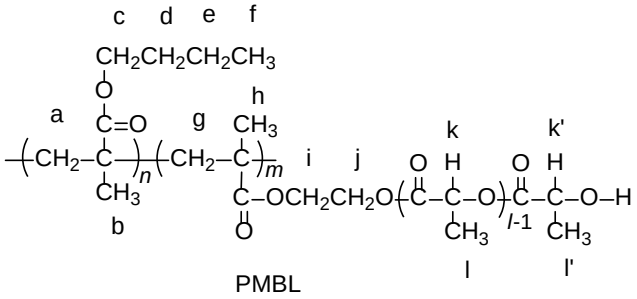

PMBL

Table 2.7. ^{1}H-NMR chemical shifts of PBML

Signal	Chemical shift (ppm)	Measured integral value	Theoretical integral value
b,h,f	0.89-1.05	41.72	9.00
l, l’,d,e	1.40-2.08	42.35	19.00
a,g	2.20-2.35	32.20	4.00
c	3.93	18.28	2.00
k’, i,j	4.07-4.57	11.54	5.00
k	5.17	9.01	4.00

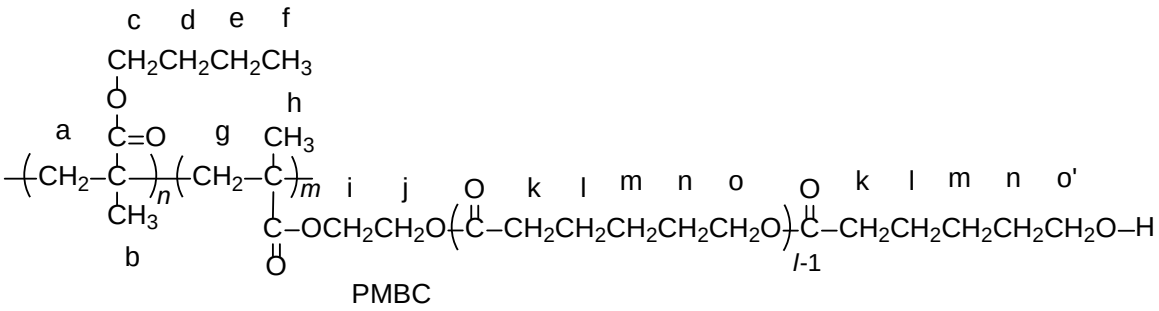

PMBC

Table 2.8. ^{1}H-NMR chemical shifts of PBMC

Signal	Chemical shift (ppm)	Measured integral value	Theoretical integral value
b,h,f	0.81-1.08	13.64	36.00
l, n,m	1.21-1.40	45.70	34.00
a,g	1.58-1.68	55.20	20.00
k	2.30	2.18	10.00
o’	3.58-3.67	33.20	2.00
c	3.94	10.12	2.00
o	4.01-4.10	1.97	10.00
i,j	4.10-4.35	29.17	4.00

1.3.2.2. FT-IR

PBML/PBMC mixtures at the weight ratios of 100/0, 75/25, 50/50, 25/75 and 0/100 were crosslinked with HDI at the OH/NCO ratio of 1/1.2 to produce PUN-BML/Cs (Scheme 2). The FT-IR spectra of PUN-BML/Cs 100/0, 75/25, 50/50, 25/75, and 0/100 are shown in Fig.3 as compared with those of PBML, PBMC, and HDI. PBML and PBMC exhibited weak absorption bands due to the O–H stretching vibration (ν_{OH}) at approximately 3510 cm^{-1}. HDI displayed a strong band due to NCO stretching vibration (ν_{NCO}) at 2249 cm^{-1}. For PUN-BML/Cs, the corresponding bands were nonexistent, and new N-H stretching and bending vibration absorption bands (ν_{NH} and δ_{NH}) appeared at 3335～3370 cm^{-1} and 1530 cm^{-1}, respectively. PBMC and PUN-BML/C 0/100 (PUN-BMC) demonstrated an absorption band due to C=O stretching vibration ($\nu_{C=O}$) at 1724 cm^{-1}, indicating that the $\nu_{C=O}$ band of PUN-BMC is attributable to ester and urethane carbonyl groups. PBML and PUN-BML/C 100/0 (PUN-BML) showed two $\nu_{C=O}$ peaks at 1755 and 1724 cm^{-1}.The C=O stretching vibration ($\nu_{C=O}$) peak at 1755 cm^{-1} corresponds to the carbonyl group of LAO segments, whereas the peak at 1724 cm^{-1} corresponds to the carbonyl group of

methacryloyl, CLO segments, and urethane groups. Furthermore, as the $\nu_{C=O}$ peaks of PUN-PBML and PUN-PBMC are superimposed according to the feed composition of PBML/PBMC, the C=O stretching vibration ($\nu_{C=O}$) peak pattern for PUN-BML/Cs changed. These results indicate that the urethane crosslinkage were formed by the reactions of hydroxy groups of PBML and PBMC with isocyanate groups of HDI.

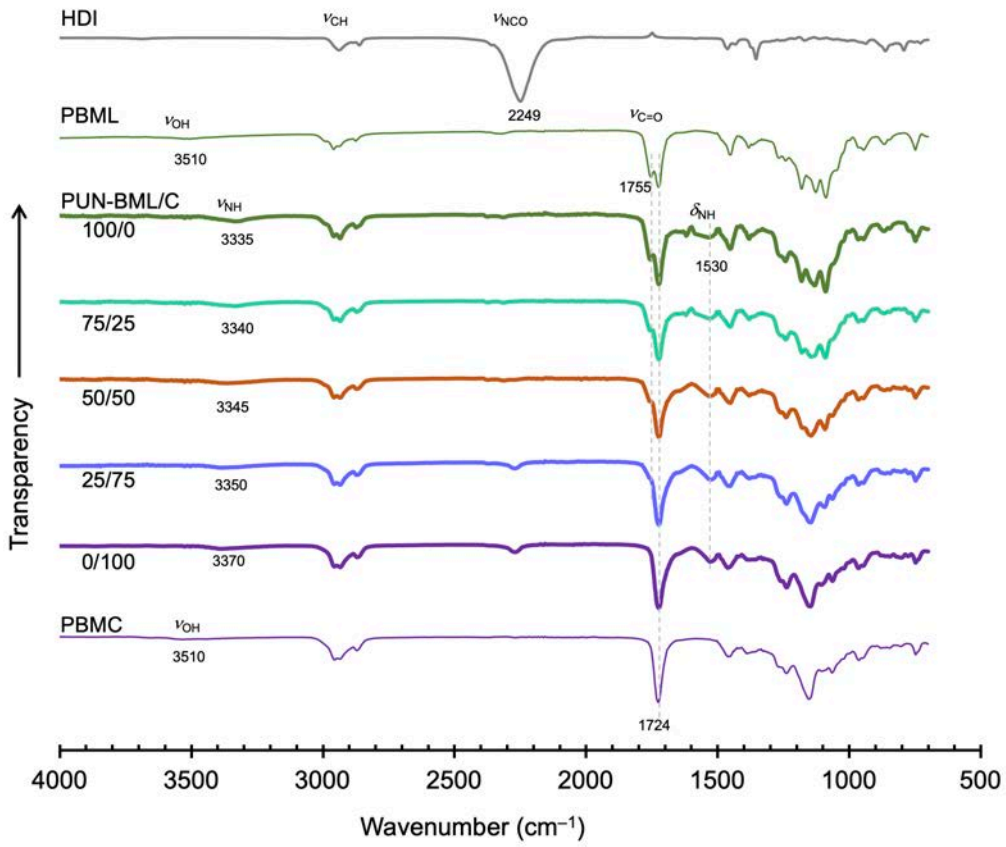

Fig.3. FT-IR spectra of PUN-BML/Cs compared with those of HDI, PBML and PBMC.

1.3.2.3. The formation of network structure and the change of crosslinking density.

Gel fractions and degrees of swelling (D_s), which are measures of the formation of network structure and the change in crosslinking density of PUN-BML/C, are shown in Fig.4. After chloroform extraction, each PUN-BML/C demonstrated a gel fraction higher than 95%, indicating that the formation of a polymer network and incorporation of most of the reactants. In addition, each PUN-BML/C exhibited a higher D_s in chloroform (ε = 4.8) than DMF (ε = 36.7), indicating that the cavity is relatively hydrophobic. Furthermore, D_s of PUN-BML/C increased with increasing feed PBMC proportion, suggesting that the crosslinking density lowed in the same order. This result is probably because the side chain of PBMC is longer than that of PBML, judging from the fact that the degrees of polymerization (l = approximately 5) of the LAO and CLO chains are practically the same, and the C–C and C–O bond numbers of lactate and CL units are 3 and 7, respectively.

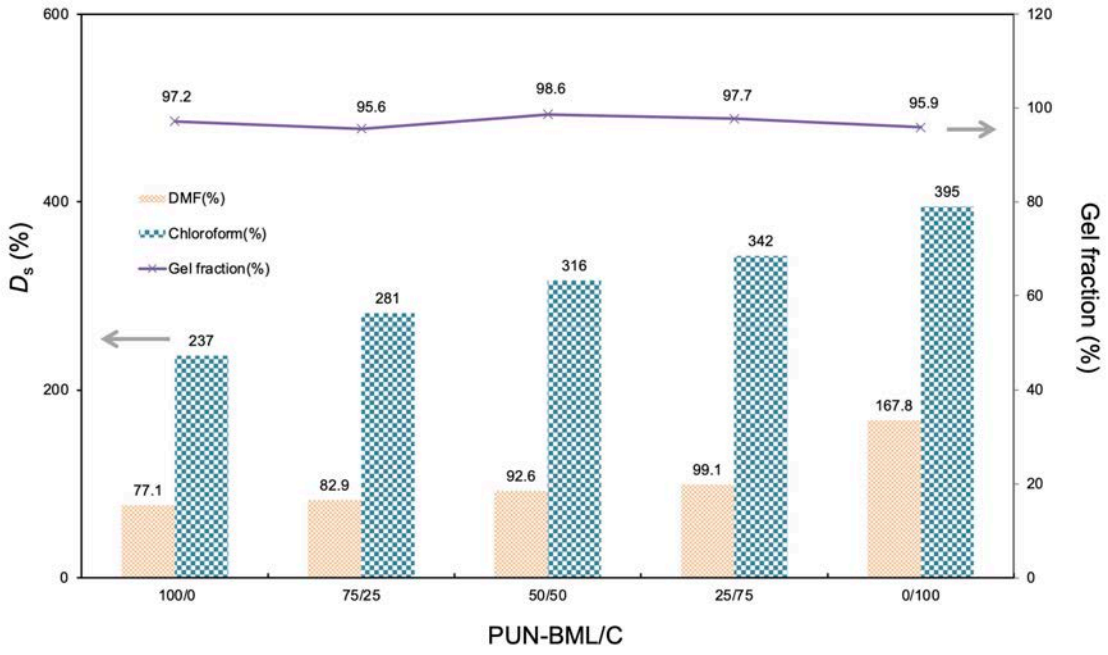

Fig.4. D_s values in chloroform and DMF and gel fractions after extraction with chloroform for PUN-BML/Cs.

1.3.3. Thermal properties and morphologies of PUN-BML/Cs

1.3.3.1. DSC

Table 3 summarizes T_g values of PBML, PBMC and PUN-BML/Cs determined by DSC measurements (Fig.5). All the samples exhibited neither an exothermal peak due to cold crystallization nor an endothermal peak due to melting, indicating that neither the LAO nor CLO segments crystallized. The T_g of MALLAO (l = 5.7), which has a slightly higher l value than MALLAO (l = 5.1) in this study, was reported to be −17 °C [29], suggesting that the T_g is due to the glass transition of grafted LAO segments in MALLAO. Also, the same authors reported that the T_g of a PBMA-*g*-PLA (BMA/MALLAO (l = 5.7) in copolymer = 82/18, M_n = 22,500, M_w = 68,900) with a similar chemical structure to PBML (BMA/MALLAO (l = 5.1) in copolymer = 82/18, M_n = 17,000, M_w = 48,300) was 25 °C [29]. The glass transition temperature (T_g) of PBML was 1.0 °C, which was slightly lower than that of PBMA-*g*-PLA due to the lower l, M_n and M_w values. The compatibilization of the grafted LAO segments with the polymethacrylate main chain is indicated by the facts that PBML and PBMA-*g*-PLA exhibited only one T_g at 0～25 °C, and no inflection point due to glass transition was observed at approximately −17 °C. It is considered that the random arrangement of BMA and MALLAO units contributes to the excellent compatibility. In the DSC curve of PBMC, a single T_g was observed at −53.7 °C, indicating that the grafted CLO segments are also compatible with the polymethacrylate main chain, given that the T_gs of poly(butyl methacrylate) [30]and poly(ε-caprolactone) [31] were reported to be 20 °C and −60 °C, respectively, that T_g of poly(alkyl methacrylate) decreases with increasing carbon number of the alkyl group (C6: −5 °C, C8: −45 °C, C10: −62 °C) [30]. PUN-BML/C 100/0 and PUN-BML/C 0/100 (PUN-BML and PUN-BMC) exhibited T_gs at 31.2 and −17.3 °C, which were much higher than those (1.0 and −53.7 °C) of PBML and PBMC, respectively. This result indicates that the formation of crosslinked structures prevents the thermal mobility of LAO and CLO segments. The T_gs of PUN-BML/Cs 75/25, 50/50, and 25/75 were 32.2, 4.6, and −10.6 °C, respectively. In addition, there was a tendency for the T_g of PUN-BML/C to decrease as the MACLO fraction of the feed increased, indicating that the LAO and CLO segments are partially compatible. However, the degree of compatibility because is not precisely evaluated from the DSC because the difference in T_g (48.5°C) between PUN-BML and PUN-BMC is relatively small, and the glass transition inflection was observed over a wide temperature range. Therefore, in the subsequent sections of DMA and FE-SEM measurements, the compatibility of PUN-BML/Cs 75/25, 50/50, and 25/75 was discussed.

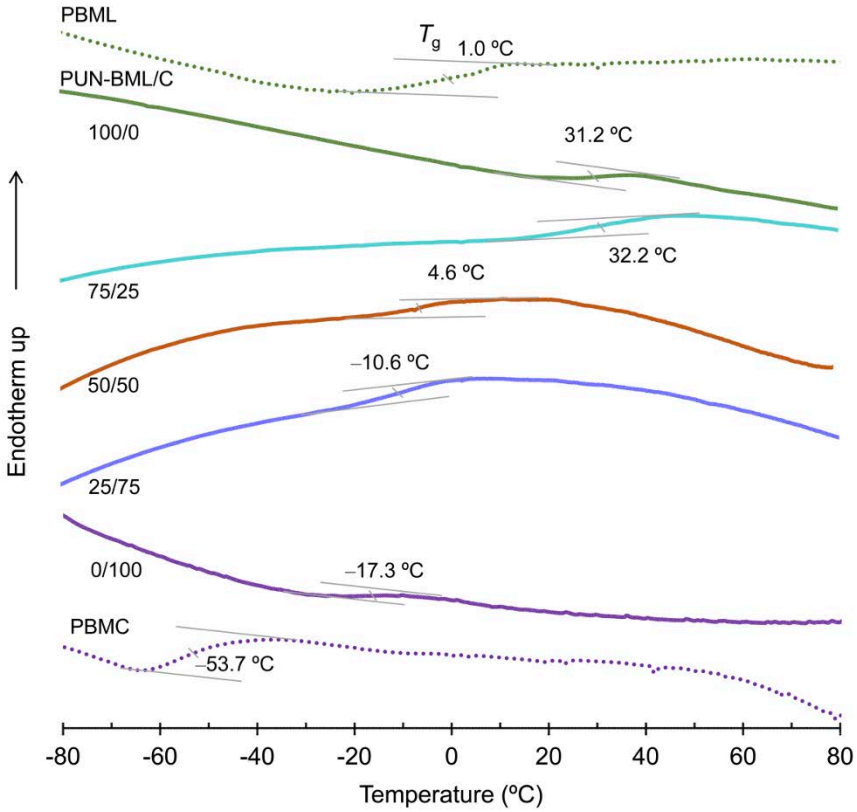

Fig.5. DSC curves of PBML, PBMC and PUN-BML/Cs.

Table 3. T_g, T_α, T_β and $T_{d5\%}$ values of PUN-BML/Cs.

Sample	T_g (°C) [a]	T_β (°C) [b]	T_α (°C) [b]	$T_{d5\%}$ (°C) [c]
PBML	1.00	-	-	232
PUN-BML/C 100/0	31.2	-	26.4	288
PUN-BML/C 75/25	32.2	3.80	21.0, 27.2	289
PUN-BML/C 50/50	4.60	−14.2	4.2, 11.3	296
PUN-BML/C 25/75	−10.6	−24.8	−8.9, 10.9	297
PUN-BML/C 0/100	−17.3	−30.4	−14.3	299
PBMC	−53.7	-	-	275

[a] The values were measured by DSC.

[b] The values were measured by DMA.

[c] The values were measured by TGA.

1.3.3.2. DMA

Fig.6. illustrates the DMA curves of PUN-PBML/Cs 100/0, 75/25, 50/50, 25/75 and 0/100. Table 3 also summarizes the tan δ peak temperatures associated with the primary and secondary transitions (T_α and T_β, respectively) of PUN-PBML/Cs. The network polymers PUN-PBML/Cs 100/0 and 75/25 exhibited a distinct plateau region of rubbery storage modulus (*E'*). However, PUN-PBML/Cs 50/50, 25/75, and 0/100 was not detected a distinct rubbery plateau region, because the DMA measurements stopped automatically at temperatures below 40 °C due to substantial softening and deformation. PUN-BML/C 100/ 0 (PUN-BML) exhibited a T_α of 26.4 °C, which corresponded to the glass transition based on the rapid decrease of storage modulus (*E'*) at approximately 10 °C. The *E'* of PUN-BML/C 0/100 (PUN-BMC) decreased slightly at approximately −50 °C and further decreased at −26 °C. Accordingly, weak T_β and strong T_α peaks were observed at −30.4 and −14.3 °C, respectively, in the tan δ curve of PUN-BMC, which are likely associated with a local motion of side butoxy carbonyl groups and a glass transition of the polymer network, respectively. In the tan δ curves of PUN-BML/Cs 25/75, 50/50, and 75/25, the T_β rose gradually with increasing feed PBML fraction, indicating that a PUN-BML/C with a higher PBML fraction suppresses local motion more effectively. Furthermore, according to the two-step *E'* drop, PUN-BML/Cs 25/75 and 75/25 exhibited two T_α peaks (8.2, 10.9°C and 21.0, 27.2°C, respectively), indicating that CLO-based and LAO-based networks are phase-separated. Although two distinct T_α peaks could not be distinguished for PUN-BML/C 50/50, a strong T_α peak at 11.3 °C appeared to contain a shoulder peak at 4.2 °C. Thus, CLO and LAO segments for PUN-BML/Cs 25/75, 50/50, and 75/25 are considered phase-separated. As shown in Table 3 in the tan δ curves of PUN-BML/Cs 25/75, 50/50, and 75/25, a low-temperature side T_α associated with the crosslinked CLO segments increased gradually with increasing feed PBML fraction, and a high-temperature side T_α associated with the crosslinked LAO segments decreased gradually with decreasing feed PBMC fraction. These results indicate that the LAO and CLO segments are not miscible but compatible to some degree. Recently, we reported the synthesis and properties of conetworks prepared by the crosslinking reaction of hydroxy-terminated 4-armed star-shaped L-lactide and ε-caprolactone oligomers (H4LLAO and H4CLO) with the degree of polymerization per arm of approximately 5 with 4,4'-methylenebis(ε-caprolactone) (phenyl isocyanate). The paper discovered that the star-shaped polymer-based conetworks (PUN-starL/Cs) exhibited a single T_αs that changes with LAO/CLO composition [24]. This result is very different from the PUN-BML/Cs DMA result. The factor is discussed in the FE-SEM section

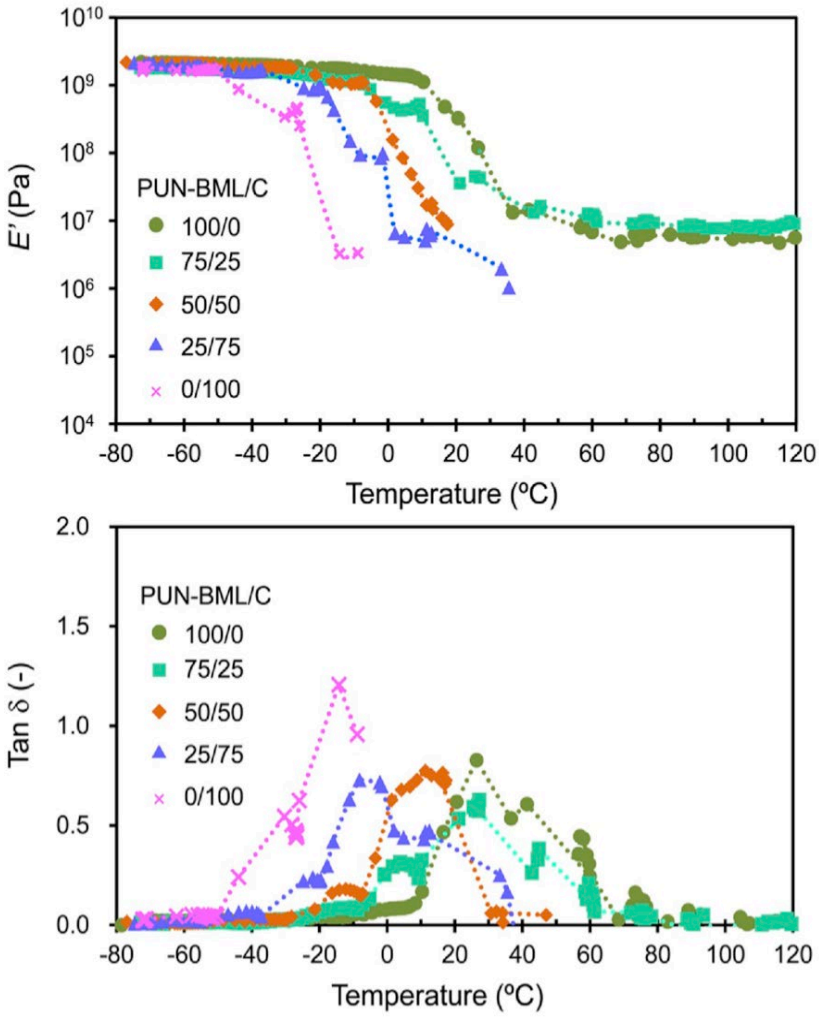

Fig.6. DMA curves of PUN-BML/Cs 100/0, 75/25, 50/50, 25/75 and 0/100.

1.3.3.3. TGA

Fig.7. shows the TGA curves for PUN-BML/Cs and $T_{d5\%}$ value of PUN-BML/Cs. The $T_{d5\%}$ values (288 and 299 °C) of PUN-BML/C 100/0 and PUN-BML/C 0/100 were higher than those (232 and 275 °C) of PBML and PBMC, indicating that the formation of a crosslinked structure improves the heat resistance. In addition, the $T_{d5\%}$ between 288～292 °C of PUN-BML/C slightly increased as the feed PBMC fraction increased. In contrast, the $T_{d5\%}$ at 262～335 °C of PUN-starL/C increased significantly with increasing feed H4CLO fraction [24], which is consistent with the fact that the $T_{d5\%}$ at 402 °C of PCL is significantly higher than that 370 °C of poly(L- lactide) (PLLA) [32]. The $T_{d5\%}$s of poly(butyl methacrylate) [33] and poly(methyl methacrylate) [34] were reported to be approximately 210～220 °C and 252 °C, respectively. Therefore, the fact that there was a slight difference in the $T_{d5\%}$s of PUN-BML/Cs may be because the thermal decomposition of polymethacrylate segments occurred during the initial stage of degradation

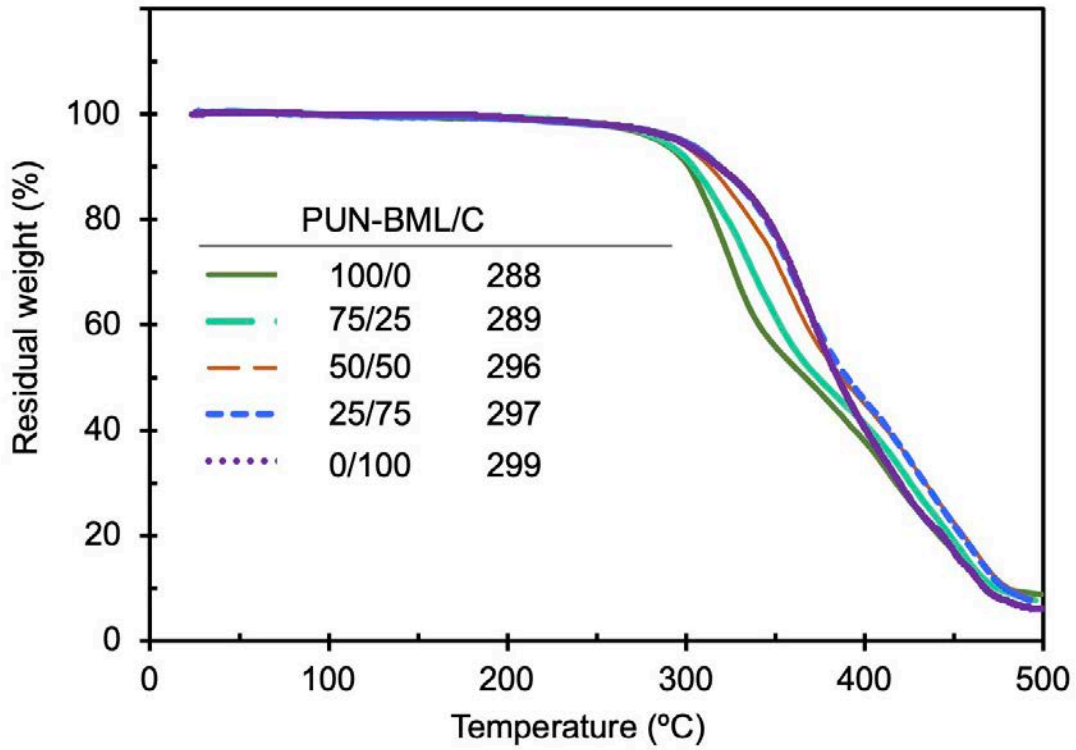

Fig.7. TGA curves of PBML. PBMC and PUN-BML/Cs.

1.3.3.4. FE-SEM

Fig.8. shows FE-SEM micrographs of fractured PUN-BML/Cs surfaces. The smooth and homogeneous fractured surfaces of PUN-BML/Cs 100/0 and 0/100 (PUN-BML and PUN-BMC) indicate that the MALLAO/BMA and MACLO/BMA units are miscible. In addition, the 75/25, 50/50, and 25/75 conetworks of PUN-BML/Cs exhibited microphase-separated morphology, accordant with the DMA results. On the other hand, based on FE-SEM measurements, the previously reported PUN-starL/Cs exhibited excellent compatibility between the LAO and CLO segments [24]. The difference in compatibility between PUN-BML/C and PUN-starL/C may be attributable to the following factors:

1) PUN-starL/C has a regular tetrahedral network composed of randomly arranged 4-armed star-shaped L-lactide and ε-caprolactone oligomers, and it is difficult for LAO or CLO segments to aggregate.

2) PUN-BML/Cs possesses an irregular network composed of comb-shaped polymer grafted with LAO and CLO segments, and the grafted LAO or CLO segments readily aggregate.

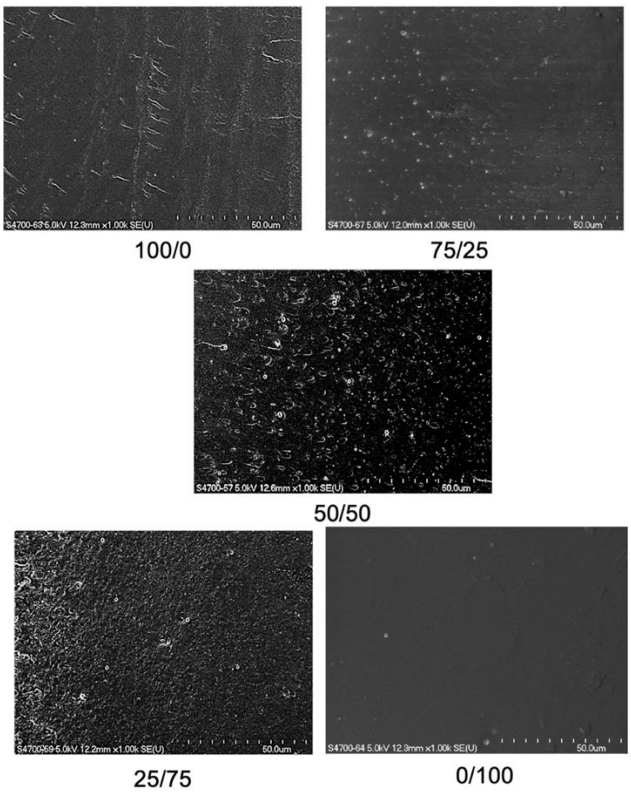

Fig.8. FE-SEM images of the fractured surfaces of PUN-BML/Cs 100/0, 75/25, 50/50, 25/75 and 0/100.

1.3.4. Mechanical properties

Fig.9. illustrates the stress-strain curves of PUN-BML/Cs. As expected, the maximum stress (tensile strength) of PUN-BML/C decreased with increasing PBMC fraction, as PCL (20 MPa) has a significantly lower tensile strength than PLLA (51 MPa) [33]. Although PCL has a significantly higher strain (elongation) at break (780%) than PLLA (4%), PUN-BML/C 75/25 had the highest strain at break among the PUN-BML/Cs. As toughness is defined as the energy needed to break a sample of unit area and unit length (J m−3), it is given by the area under the stress-strain curve. The stress-strain curves in Fig.9 reveal that the toughness of PUN-BML/C 75/25 is significantly higher than that of PUN-BML/Cs 0/100, 25/75, and 50/50.The tensile properties obtained from the stress-strain curves of all the samples are summarized in Fig.10. As can be expected based on the tensile properties of PLLA and PCL [33], the tensile strength and modulus of PUN-BML/C increased with increasing feed PBML fraction, except for the 25/75 sample, whose modulus was comparable to that of the 0/100 sample. PUN-BML/C 75/25 unexpectedly showed the highest elongation at break (82%) and tensile toughness (2.8 MJ m^{-3}), which were higher than the 100/0 and 0/100 samples (18%, 1.6 MJ m^{-3}, and 28%, 0.12 MJ m^{-3}, respectively).As a similar trend, we had previously reported that PUN-starL/C 50/50 exhibited the highest elongation at break (186%) and tensile toughness (8.6 MJ m^{-3}), which were higher than those of the 100/0 and 0/100 samples (4.3%, 0.29 MJ m^{-3}, and 152%, 2.5 MJ m^{-3}, respectively) [24]. Although it is unknown why a synergistic effect was observed between elongation at break and tensile toughness, it is considered that the compatibility system (partial compatibility) forms a particular microphase-separated structure not observed in the homogeneous system and that the entangled flexible and rigid components contribute to the strong interfacial adhesion strength. The entanglement of the flexible caprolactone and rigid lactic acid components also contribute significantly to the tensile toughness and elongation at break of the PUN-BML/C 75/25 conetwork because the different phases absorb energy and deform without fracturing, thereby preventing crack propagation and premature failure. The T_{α}s value due to the glass transition of PUN-BML/C 75/25 and PUN-starL/C 50/50 in DMA analysis was observed at approximately 30 ℃.This reveals that the glass transition occurs precisely at the tensile test temperature. In addition, at the glass transition, tan δ (*E"*/*E'*) reaches its maximum value. Namely, the loss elastic modulus (*E"*) indicates a high value, which may contribute to the release of tensile stress as thermal energy.

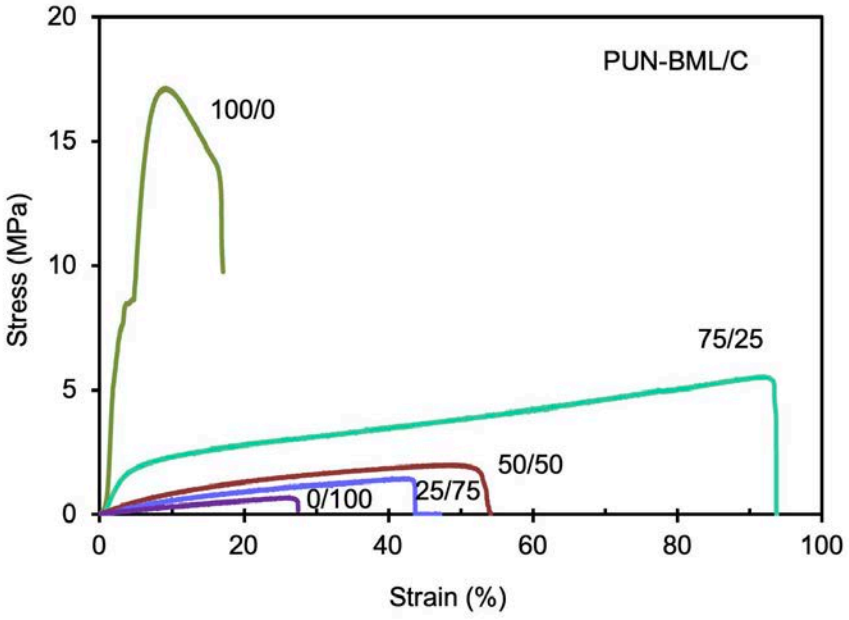

Fig.9. Stress-strain curves of PUN-BML/Cs.

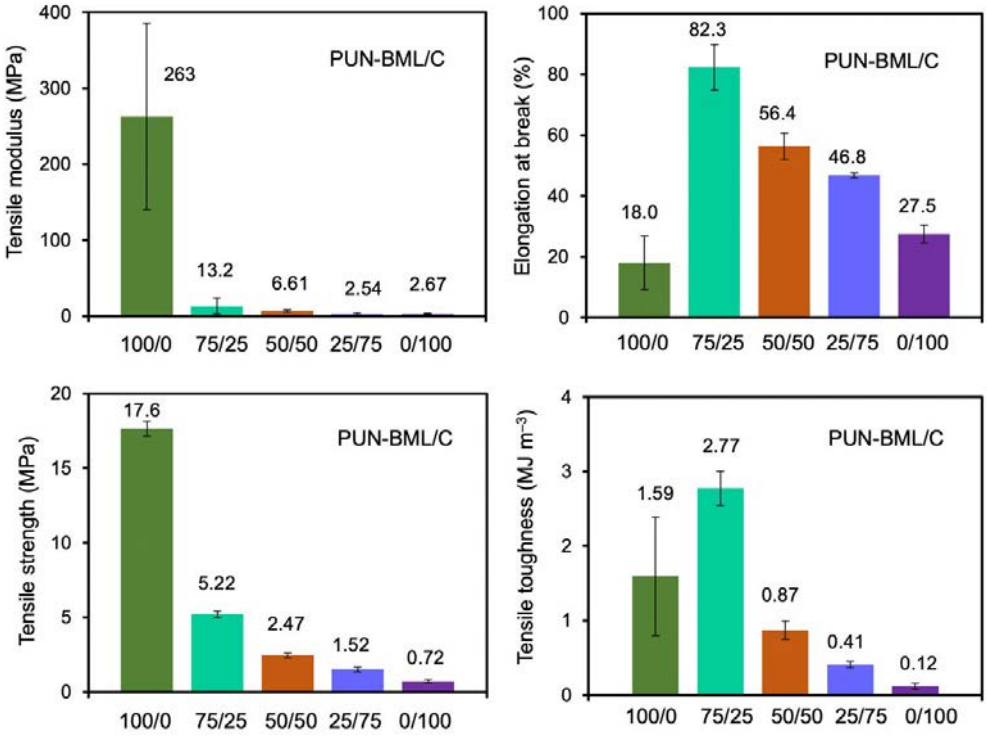

Fig.10. Tensile properties of PUN-BML/Cs 100/0, 75/25, 50/50, 25/75 and 0/100.

1.4. Conclusions

PUN-BML/Cs 100/0, 75/25, 50/50, 25/75, and 0/100 were synthesized by reacting HDI with PBML and PBMC, and their morphologies, thermal and mechanical properties were compared to those of PBML, PBMC, and the previously reported PUN-starL/Cs. Analyses of FT-IR spectra and gel fractions demonstrated that HDI certainly reacted with PBML and PBMC to generate polyurethane networks. The swelling test revealed that the crosslinking density decreased as the fraction of PBMC in the feed increased. According to the DSC analysis, the T_gs and T_{d5} values of PUN-BML/C 100/0 and PUN-BML/C 0/100 were significantly higher than those of PBML and PBMC, respectively. The DMA and FE-SEM analyses demonstrated that the LAO and CLO segments of PUN-BML/Cs 75/25, 50/50, and 25/75 are not fully miscible but are partially compatible. This result was in marked contrast to that of PUN-starL/Cs, where the LAO and CLO segments were almost miscible, reflecting the difference between the comb-shaped and star-shaped structures. Since PBML and PBMC are viscous liquids, it was not possible to measure their tensile properties at room temperature. However, the HDI-crosslinked PUN-BML/C films were relatively tough. The tensile strength and modulus of PUN- BML/C increased as the feed PBML content increased. Interestingly, PUN-BML/C 75/25 demonstrated a higher elongation at break and tensile toughness than the samples 100/0 and 0/100. Crosslinking of terminal functional groups of grafted side chains in comb-shaped polymers is an effective method for enhancing the thermal and mechanical properties of the original comb-shaped polymers.

1.5. References

[1] F.-L. Jin, R.-R. Hu, S.-J. Park, Improvement of thermal behaviors of biodegradable poly(lactic acid) polymer: A review, Compos. B. Eng. 164 (2019) 287–296. https://doi.org/10.1016/j.compositesb.2018.10.078.

[2] S. Farah, D.G. Anderson, R. Langer, Physical and mechanical properties of PLA, and their functions in widespread applications — A comprehensive review, Adv. Drug Deliv. Rev. 107 (2016) 367–392. https://doi.org/10.1016/j.addr.2016.06.012.

[3] B. Tyler, D. Gullotti, A. Mangraviti, T. Utsuki, H. Brem, Polylactic acid (PLA) controlled delivery carriers for biomedical applications, Adv. Drug Deliv. Rev. 107 (2016) 163–175. https://doi.org/10.1016/j.addr.2016.06.018.

[4] H. Liu, J. Zhang, Research progress in toughening modification of poly(lactic acid), J. Polym. Sci. B Polym. Phys. 49 (2011) 1051–1083. https://doi.org/10.1002/polb.22283.

[5] R.M. Rasal, A.V. Janorkar, D.E. Hirt, Poly(lactic acid) modifications, Prog. Polym. Sci. 35 (2010) 338–356. https://doi.org/10.1016/j.progpolymsci.2009.12.003.

[6] A.L. Sisson, D. Ekinci, A. Lendlein, The contemporary role of ε-caprolactone chemistry to create advanced polymer architectures, Polymer. 54 (2013) 4333–4350. https://doi.org/10.1016/j.polymer.2013.04.045.

[7] M.A. Woodruff, D.W. Hutmacher, The return of a forgotten polymer—Polycaprolactone in the 21st century, Prog. Polym. Sci. 35 (2010) 1217–1256. https://doi.org/10.1016/j.progpolymsci.2010.04.002.

[8] L.S. Nair, C.T. Laurencin, Biodegradable polymers as biomaterials, Prog. Polym. Sci. 32 (2007) 762–798. https://doi.org/10.1016/j.progpolymsci.2007.05.017.

[9] R.P. Babu, K. O'connor, R. Seeram, Current progress on bio-based polymers and their future trends, Prog. Biomater. 2 (2013) 1–16.

[10] 柴田充弘, 山口達明, E-コンシャス 高分子材料, 三共出版, 2009.

[11] A. Nijenhuis, D. Grijpma, A. Pennings, Crosslinked poly (L-lactide) and poly (ε-caprolactone), Polymer. 37 (1996) 2783–2791.

[12] H.M. Younes, E. Bravo-Grimaldo, B.G. Amsden, Synthesis, characterization and in vitro degradation of a biodegradable elastomer, Biomaterials. 25 (2004) 5261–5269.

[13] R. Sabater i Serra, J.L. Escobar Ivirico, J.M. Meseguer Duenas, A.A. Balado, J.L. Gomez Ribelles, M. Salmerón Sánchez, Segmental dynamics in poly (ε-caprolactone)/poly (L-lactide) copolymer networks, J. Polym. Sci. B: Polym. Phys. 47 (2009) 183–193.

[14] Q. Liu, L. Jiang, R. Shi, L. Zhang, Synthesis, preparation, in vitro degradation, and application of novel degradable bioelastomers—A review, Prog. Polym. Sci. 37 (2012) 715–765.

[15] M. Shibata, N. Teramoto, K. Hoshino, H. Takase, A. Shibita, Thermal and mechanical properties of semi-interpenetrating polymer networks composed of diisocyanate-bridged, four-armed, star-shaped ε-caprolactone oligomers and poly(ε-caprolactone): ARTICLE, J. Appl. Polym. Sci. (2013) n/a-n/a. https://doi.org/10.1002/app.39551.

[16] A. Shibita, H. Takase, M. Shibata, Semi-interpenetrating polymer networks composed of poly(l-lactide) and diisocyanate-bridged 4-arm star-shaped ε-caprolactone oligomers, Polymer. 55 (2014) 5407–5416. https://doi.org/10.1016/j.polymer.2014.08.074.

[17] H. Takase, A. Shibita, M. Shibata, Semi-interpenetrating polymer networks composed of diisocyanate-bridged 4-arm star-shaped l-lactide oligomers and poly (ε-caprolactone), J. Polym. Sci. Part B: Polym. Phys. 52 (2014) 1420–1428. https://doi.org/10.1002/polb.23581.

[18] M. Shibata, M. Katoh, H. Takase, A. Shibita, Stereocomplex formation in stereoblock copolymer networks composed of 4-armed star-shaped lactide oligomers and a 2-armed ε-caprolactone oligomer, Polym. Chem. 6 (2015) 4123–4132. https://doi.org/10.1039/C5PY00401B.

[19] A. Shibita, S. Kawasaki, T. Shimasaki, N. Teramoto, M. Shibata, Stereocomplexation in Copolymer Networks Incorporating Enantiomeric Glycerol-Based 3-Armed Lactide Oligomers and a 2-Armed ε-Caprolactone Oligomer, Materials. 9 (2016) 591. https://doi.org/10.3390/ma9070591.

[20] A. Shibita, Y. Mizumura, M. Shibata, Stereocomplex crystallization behavior and physical properties of polyesterurethane networks incorporating diglycerol-based enantiomeric 4-armed lactide oligomers and a 1,3-propanediol-based 2-armed rac-lactide oligomer, Polym. Bull. 74 (2017) 3139–3160. https://doi.org/10.1007/s00289-016-1890-1.

[21] A. Shibita, T. Shimasaki, N. Teramoto, M. Shibata, Tough conetworks composed of 4-armed star-shaped oligomers of l-lactide, d-lactide and ε-caprolactone, Polym. Bull. 75 (2018) 2369–2390. https://doi.org/10.1007/s00289-017-2154-4.

[22] K. Sugane, H. Takahashi, T. Shimasaki, N. Teramoto, M. Shibata, Stereocomplexation, Thermal and Mechanical Properties of Conetworks Composed of Star-Shaped l-Lactide, d-Lactide and ε-Caprolactone Oligomers Utilizing Sugar Alcohols as Core Molecules, Polymers. 9 (2017) 582. https://doi.org/10.3390/polym9110582.

[23] H. Takase, K. Morita, A. Shibita, M. Shibata, Polymer networks prepared from 4-arm star-shaped L-lactide oligomers with different arm lengths and their semi-interpenetrating polymer networks containing poly (L-lactide), J. Polym. Res. (2014) 10.

[24] A. Shibita, T. Shimasaki, N. Teramoto, M. Shibata, Conetworks composed of 4-armed star-shaped l-lactide oligomer and 4-armed star-shaped ε-caprolactone oligomer, Polymer. 74 (2015) 54–62. https://doi.org/10.1016/j.polymer.2015.07.052.

[25] D.W. Lim, S.H. Choi, T.G. Park, A new class of biodegradable hydrogels stereocomplexed by enantiomeric oligo (lactide) side chains of poly (HEMA-g-OLA) s, Macromol. Rapid Commun. 21 (2000) 464–471.

[26] K. Ishimoto, M. Arimoto, H. Ohara, S. Kobayashi, M. Ishii, K. Morita, H. Yamashita, N. Yabuuchi, Biobased Polymer System: Miniemulsion of Poly(alkyl methacrylate- *graft* -lactic acid)s, Biomacromolecules. 10 (2009) 2719–2723. https://doi.org/10.1021/bm9007937.

[27] J. Bao, L. Han, G. Shan, Y. Bao, P. Pan, Preferential Stereocomplex Crystallization in Enantiomeric Blends of Cellulose Acetate- *g* -Poly(lactic acid)s with Comblike Topology, J. Phys. Chem. B. 119 (2015) 12689–12698. https://doi.org/10.1021/acs.jpcb.5b05398.

[28] R. Ferrari, Y. Yu, M. Morbidelli, R.A. Hutchinson, D. Moscatelli, ε-Caprolactone-Based Macromonomers Suitable for Biodegradable Nanoparticles Synthesis through Free Radical Polymerization, Macromolecules. 44 (2011) 9205–9212. https://doi.org/10.1021/ma201955p.

[29] K. Ishimoto, M. Arimoto, T. Okuda, S. Yamaguchi, Y. Aso, H. Ohara, S. Kobayashi, M. Ishii, K. Morita, H. Yamashita, N. Yabuuchi, Biobased Polymers: Synthesis of Graft Copolymers and Comb Polymers Using Lactic Acid Macromonomer and Properties of the Product Polymers, Biomacromolecules. 13 (2012) 3757–3768. https://doi.org/10.1021/bm301212a.

[30] Glass Transition Temperatures, (2015). http://polymerdatabase.com/polymer%20physics/Polymer%20Tg.html (accessed July 6, 2022).

[31] T. Patrício, P. Bártolo, Thermal stability of PCL/PLA blends produced by physical blending process, Procedia Eng. 59 (2013) 292–297.

[32] A. Shibita, H. Takase, M. Shibata, Semi-interpenetrating polymer networks composed of poly(l-lactide) and diisocyanate-bridged 4-arm star-shaped ε-caprolactone oligomers, Polymer. 55 (2014) 5407–5416. https://doi.org/10.1016/j.polymer.2014.08.074.

[33] S.L. Malhotra, L. Minh, L.P. Blanchard, Thermal Decomposition and Glass Transition Temperature of Poly(ethyl Methacrylate) and Poly(n-butyl Methacrylate), J. Macromol. Sci. A. 19 (1983) 559–578. https://doi.org/10.1080/10601328308056535.

[34] N.W. Elshereksi, S.H. Mohamed, A. Arifin, Z.A.M. Ishak, Thermal Characterisation of Poly(Methyl Methacrylate) Filled with Barium Titanate as Denture Base Material, J. Phys. Sci. 25 (2014) 13.

Chapter 2

Self-healing disulfide-containing polyester-urethane networks composed of 6-armed star-shaped oligolactide and oligocaprolactone segments

2.1. Introduction

Polymer networks derived from biodegradable and biocompatible polyesters such as polylactide (PLA) and poly(ε-caprolactone) (PCL) have been utilized extensively as biomaterials in the fields of tissue engineering, regenerative medicine, controlled drug delivery, etc. The compatibility, biodegradability, thermal properties, and mechanical properties of these polymers can be tailored by modifying the crosslinking density to form bio-materials with specific characteristics [1–3]. In chapter 1, we have succeeded in improving thermal and mechanical properties in addition to the compatibility of the PLA and PCL segments was investigated by changing the ratio of PLA/PCL segments of crosslinking comb-shaped polymers.

Recently, as polymer materials reduce environmental load, self-healing polymers having the ability to repair physical damage and cracks, thereby leading to the extension of their lifetime and effective use of resources, are attracting the most attention in addition to biodegradable and biobased polymers. Thermo-reversible DA and transesterification reactions have been used to develop the self-healing PLA networks [4–7]. Furthermore, The self-healing PCL networks have been studied and developed using the quadruple hydrogen bonding in 2-ureido-4[1H]-pyrimidinone (UPy) ,Disulfide metathesis, and thermos-reversible DA reaction [8–16]. In recent years, dynamic disulfide bonds have been introduced into polymer networks in order to generate self-healing polymer networks, as the exchange reaction of disulfide bonds can easily occur at a moderate temperature or under UV irradiation conditions in the absence of catalysts and initiators [17–19].However, most disulfide-containing polymer networks that are potentially healing at room temperature do not contain biodegradable (or biocompatible) polyester units.

Recently, Li et al. reported the synthesis and characteristics of disulfide-containing self-healing biodegradable PCL networks. These networks were produced at 60 °C utilizing the 1-methylimidazole-catalyzed thiol-ene reaction utilizing acrylate-terminated 3-armed PCL, bis(2-(acryloyloxy)ethyl) dithiodipropionate, bis(2-(acryloyloxy)ethyl) adipate, and pentaerythritol tetra(3-mercapto propionate) as the reactants [16]. The thermo-induced reversible disulfide bond formation (i.e., disulfide metathesis) was implemented to accomplish healing efficiencies of 68～

99.9% (yield strength) in PCL networks after 1 h of annealing at 60 °C. However, self-healing PLA networks containing disulfide bonds have not been reported.

In chapter 1, we found that the glass transition temperatures (T_gs) of the PLA-PCL conetworks are controlled by the ratios of the components (the PLA/PCL ratio). Furthermore, the crystallinities of PLA and PCL components decreased with increased crosslinking density. It is believed that the healing effectiveness (resulting from disulfide recombination) is dependent on the T_gs and crystallinity of the sample. Therefore, the healing efficiency of disulfide-containing PLA/PCL conetworks can be modulated by modifying the PLA/PCL ratio and crosslinking densities. Consequently, in chapter 2, the introduction of disulfide bonds into the conetworks consisting of 6-armed star-shaped L-lactide and ε-caprolactone oligomers was investigated to provide the self-healing properties driven by the disulfide metathesis reaction. In this study, hydroxy-terminated 6-armed star-shaped L-lactide and ε-caprolactone oligomers (H6LAO and H6CLO) were synthesized by the ring-opening polymerization reactions of LLA and CL initiated with dipentaerythritol. The disulfide-containing polyester-urethane networks (PN-LC*xy*-DS*z*, weight ratios of H6LAO/H6CLO: *x*/*y* = 1/0, 3/1, 1/1, 1/3, and 0/1, BHEDS/(H6LAO + H6CLO) molar ratios: *z* = 0, 1, and 3) were prepared by the reaction of H6LAO, H6CLO, and bis(2-hydroxyethyl) with HDI (Scheme 1 and Scheme 2).

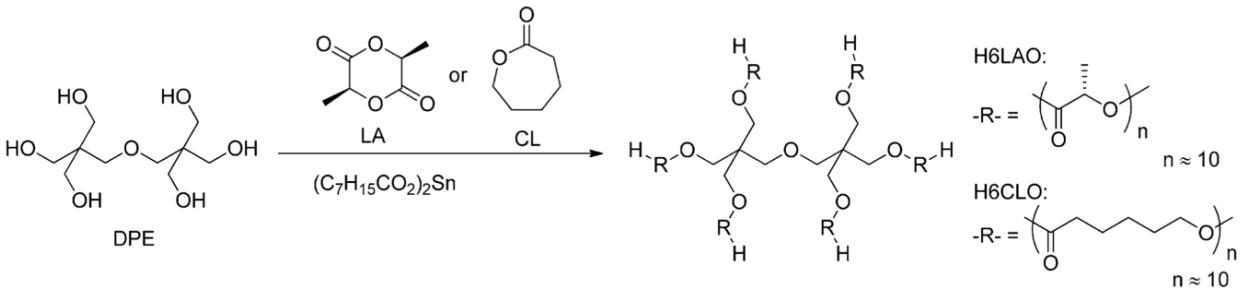

Scheme 1. Synthesis of H6LAO and H6CLO

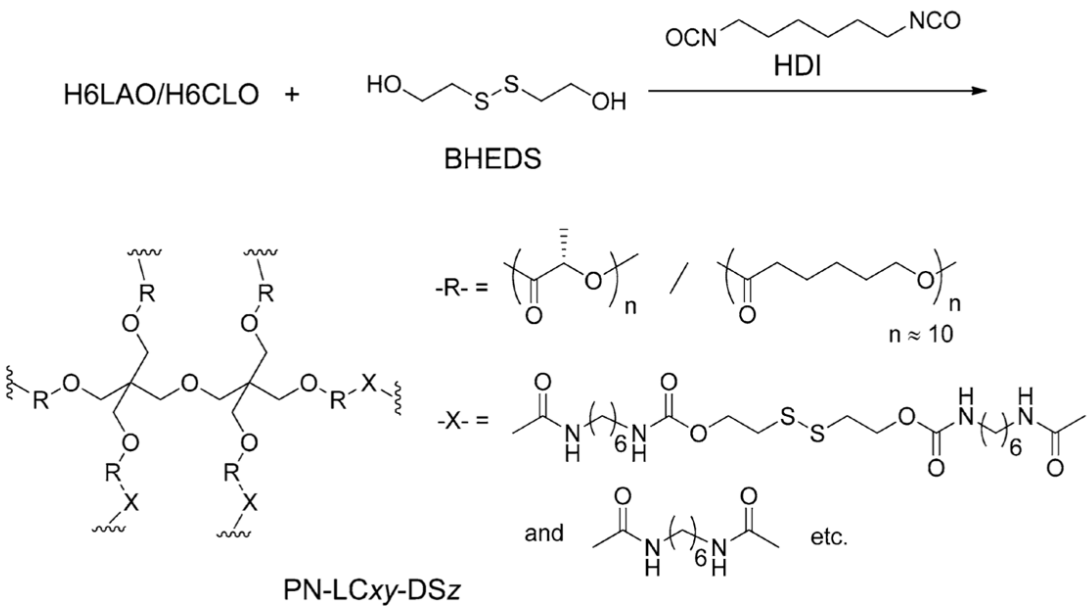

Scheme 2. Synthesis of PN-LC*xy*-DSzs.

2.2. Experimental section

2.2.1. Materials

Dipentaerythiol (DPE)

MW :254.28

m.p.: 215～218 ℃

b.p.: 356 ℃

Tokyo Chemical Industry

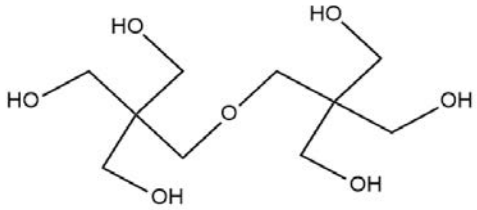

L-lactide (LLA)

MW: 144.13

m.p.: 92.0～94.0 ℃

b.p.: 255 ℃

Daiwakasei Industry Co., Ltd.

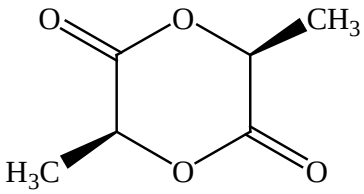

ε-caprolactone (CL)

MW: 114.14

m.p.: −1.00 ℃

b.p.: 140 ℃ (35 mmHg)

Tokyo Chemical Industry Co., Ltd.

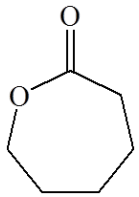

Bis(2-hydroxyethyl) disulfide (BHEDS)

MW: 154.24

m.p.: 25.0～27.0 ℃

b.p.: 158～163 ℃

Tokyo Chemical Industry

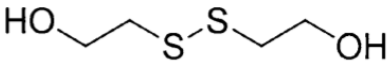

Hexamethylene diisocyanate (HDI)

MW: 168.19

m.p.: −55.0 ℃

Tokyo Chemical Industry Co., Ltd.

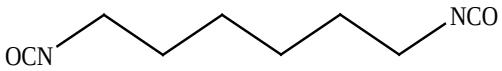

Tin (II) bis(2- ethylhexanoate) ($Sn(Oct)_2$)

MW: 405.12

b.p.: 228 ℃

Nacalai Tesque Inc.

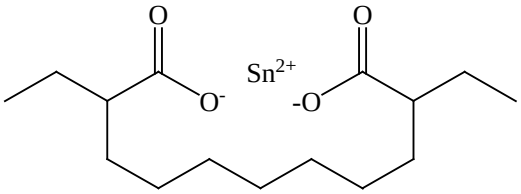

Chlorobenzene

MW: 112.56

m.p.: −45.0 ℃

FUJIFILM Wako Pure Chemical Corporation.

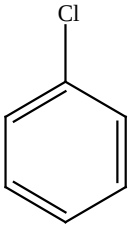

n-hexane

MW: 86.18

m.p.: −95.3℃

b.p.: 68.7℃

FUJIFILM Wako Pure Chemical Corporation.

1,2-dichloroethane (DCE)

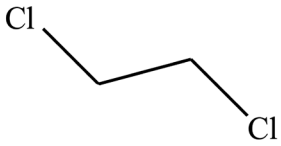

MW: 98.96

m.p.: −35.0 ℃

b.p.: 83.0～84.0 ℃

Kanto Chemical Co. Inc.

2.2.2. Synthesis of hydroxy-terminated 6-armed star-shaped L-lactide (H6LAO) and *ε*-caprolactone oligomers (H6CLO)

H6LAO and H6CLO were synthesized according to protocols previously reported for synthesizing 4-armed star-shaped lactide and ***ε***-caprolactone oligomers (H4LAO and H4CLO) [20,21]. During the synthesis of 6-armed star-shaped H6LAO and H6CLO, in this study, the synthetic route is modified by substituting DPE for pentaerythritol (Scheme 1). The LLA/DPE and CL/DPE ratios (feed molar ratios) were set at 30/1 and 60/1.

Fig.1.1. shows a flow chart of the synthesis of H6LAO. First, 30 mL of chlorobenzene was added to 1.67 g (6.55 mmol) of DPE and 28.3 g (197 mmol) of L-Lactide, which was then stirred at 150 °C for 1 h in a nitrogen atmosphere (N_2), followed by the addition of 1 phr of $(Oct)_2Sn$. Next, the mixture was stirred for 24 hours at 150 °C. 200 mL of hexane was then added to the reaction mixture. The formed precipitates were filtered, and dried at 60 °C for 24 h to produce H6LAO as a white solid in 96% yield. For analysis, ^{1}H-NMR and FT-IR measurements were performed.

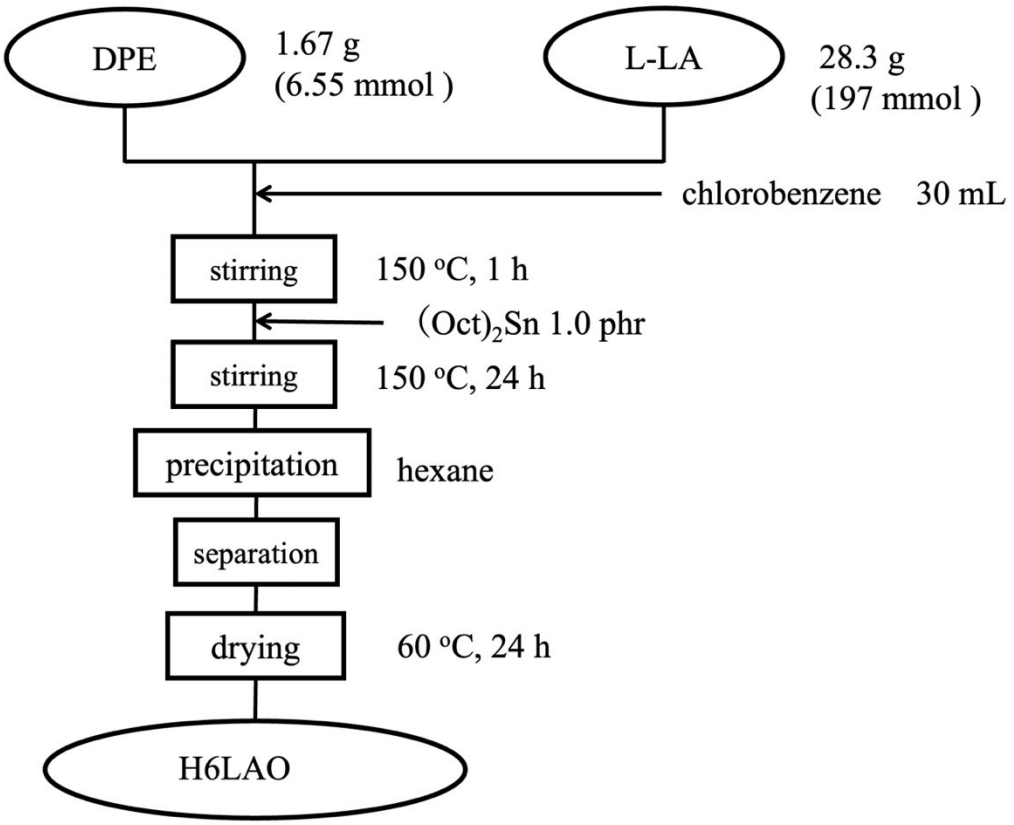

Fig.1.1. The synthesis of H6LAO flow chart.

Fig.1.2. shows the synthetic flowchart of H6CLO. First,1.07 g (4.22 mmol) of DPE and 28.9 g (253 mmol) of ε-caprolactone (CL) were added and stirred at 150 °C for 1 h in a nitrogen atmosphere (N_2), Next 1 phr of $(Oct)_2Sn$ was added, then the reaction was continued for 24 h at 150 °C. The product was then precipitated with 200 mL of hexane, separated, and dried at 60 °C for 24 hours to produce solid white H6CLO in 90% yield. For analysis, ^{1}H-NMR and FT-IR measurements were performed.

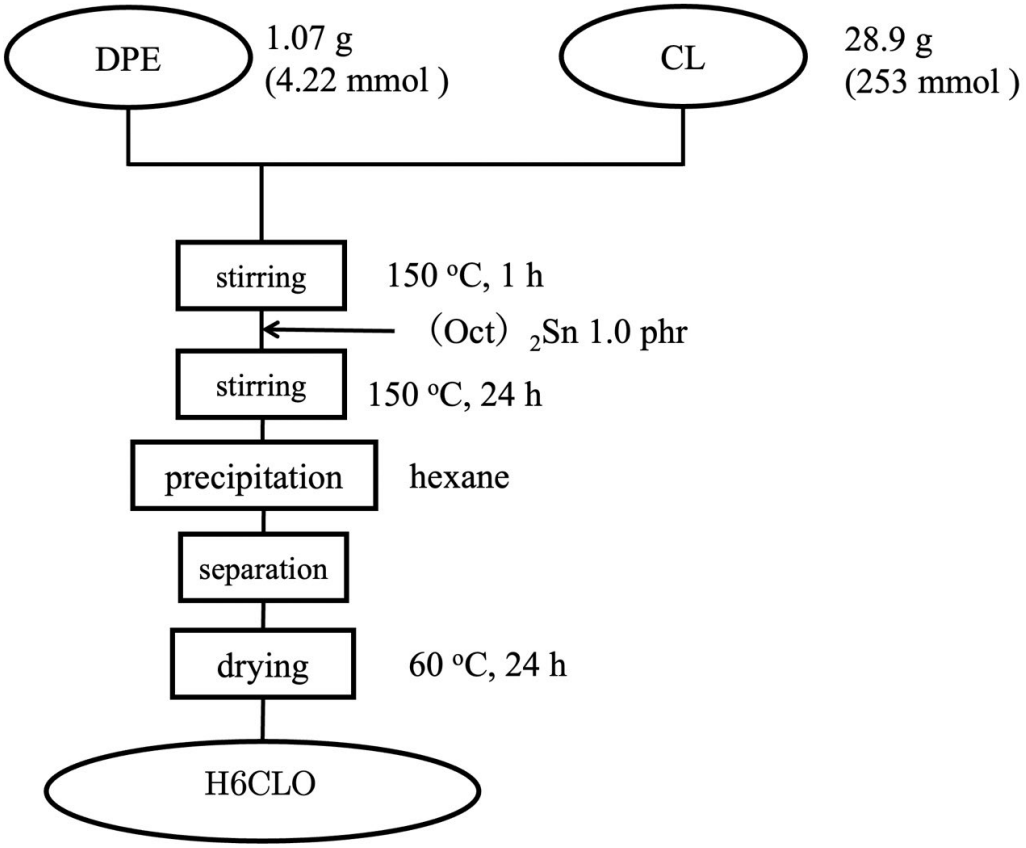

Fig.1.2. The synthesis of H6CLO flow chart.

2.2.3. Synthesis of disulfide-containing polymer networks (PN-LCxy-DSzs)

The PN-LC*xy*-DS*z* networks (H6LAO/H6CLO weight ratios: *x*/*y* = 1/0, 3/1, 1/1, 1/3, and 0/1; molar ratios of (H6LAO + H6CLO)/BHEDS: *z* = 0, 1, and 3) were prepared with the reagents H6LAO, H6CLO, BHEDS, and HDI. For example, in the preparation of the PN-LC11-DS1 film, a solution 2.18 g (0.458 mmol, 2.75 mmol-OH) of H6LAO, 2.18 g (0.306 mmol, 1.83 mmol-OH) of H6CLO, 0.118 g (0.765 mmol, 1.53 mmol-OH) of BHEDS, and 0.514 g (3.06 mmol, 6.11 mmol) of HDI was poured into a petri dish (diameter: 100 mm) made of poly(tetrafluoroethylene).The mixture was dried in a 60 °C electric oven for 24 h. Then, the obtained PN-LC11-DS1 film (thickness: 0.6 mm) was removed from the petri dish by peeling. All other PN-LC*xy*-DS*z* films were produced using a similar method. Nonetheless, the PN-LC10-DS1 film was prepared in a glass petri dish. The molar ratio of OH/NCO during film preparation was fixed at 1/1. During PN-LC10-DS1 film preparation, the OH/NCO ratio was set to 1/1.2. When

the PN-LC10-DS1 film was prepared (OH/NCO = 1/1), a approximately circular film of petri dish dimensions was not obtained. This may be because the steric hindrance caused by the side-chain methyl group of the lactate unit lowers the reactivity of a hydroxy-terminated lactate unit toward an isocyanate group compared to a hydroxy-terminated CL unit. Table 1 summarizes the feed monomer compositions of all PN-LC*xy*-DS*z*s and the preparation of PN-LC*xy*-DS*z*s flow chat shown in Fig.1.3.

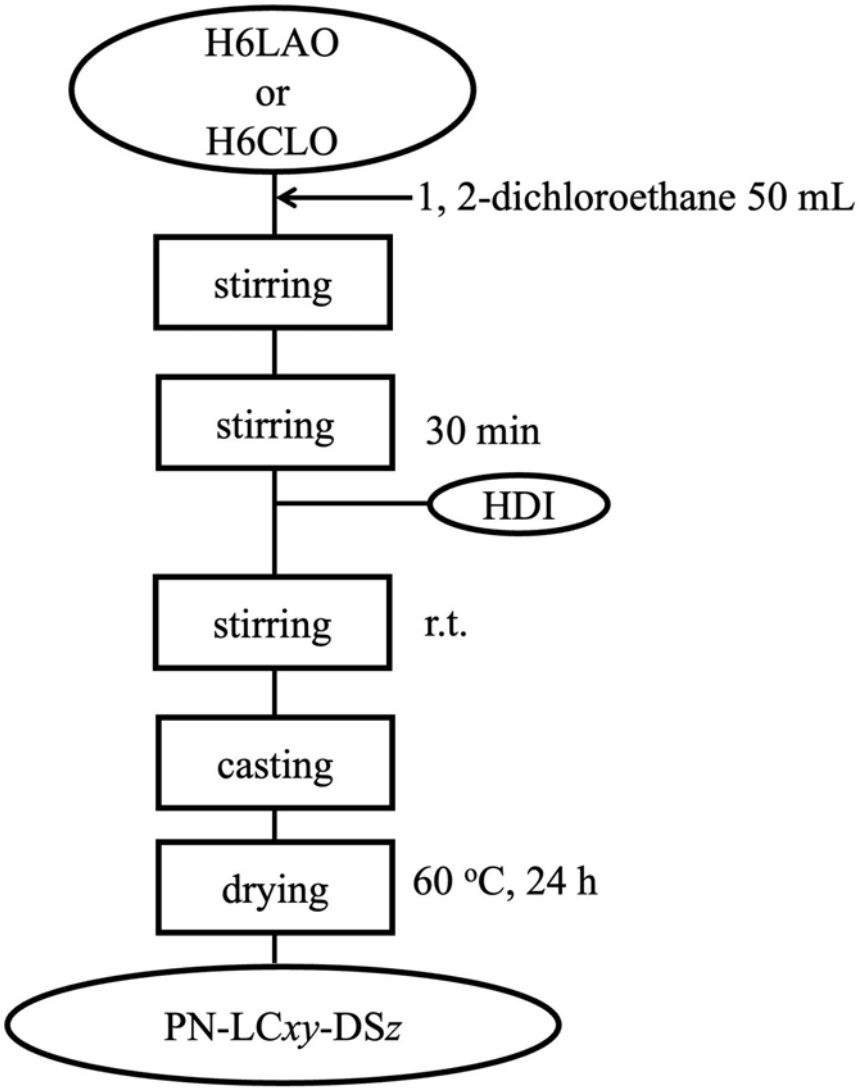

Fig.1.3. The preparation of PN-LC*xy*-DS*z*s flow chart.

Table 1. Feed amounts of H6LAO, H6CLO, BHEDS and HDI for the preparation of PN-LC*xy*-DSzs

Sample	H6LAO [a] (g) (mmol) (mmol-OH)	H6CLO [b] (g) (mmol) (mmol-OH)	BHEDS [c] (g) (mmol) (mmol-OH)	Total OH (mmol-OH)	HDI [d] (g) (mmol) (mmol-NCO)	OH/NCO molar ratio
PN-LC10-DS0	4.44 0.931 5.59	0 0 0	0 0 0	5.59	0.564 3.55 6.70	1/1.2
PN-LC10-DS1	4.16 0.873 5.24	0 0 0	0.135 0.873 1.746	6.99	0.705 4.19 8.38	1/1.2
PN-LC31-DS1	3.23 0.678 4.07	1.08 0.151 0.909	0.128 0.830 1.66	6.64	0.559 3.32 6.64	1/1
PN-LC11-DS1	2.18 0.458 2.75	2.18 0.306 1.83	0.118 0.765 1.53	6.11	0.514 3.06 6.11	1/1
PN-LC13-DS1	1.11 0.233 1.40	3.32 0.466 2.79	0.108 0.700 1.40	5.59	0.469 2.79 5.58	1/1
PN-LC01-DS1		4.48 0.628 3.77	0.0969 0.628 1.26	5.03	0.423 2.51 5.02	1/1
PN-LC01-DS3		4.14 0.581 3.48	0.269 1.74 3.49	6.97	0.587 3.49 6.98	1/1
PN-LC01-DS0	0 0 0	4.67 0.655 3.93	0 0 0	3.93	0.331 1.965 3.93	1/1

[a] The molecular weight of H6LAO was calculated to be 4764.11, based on the degree of polymerization per arm, $n = 10.4$.

[b] The molecular weight of H6CLO was calculated to be 7129.47, based on the degree of polymerization per arm, $n = 10.0$.

[c] The molecular weight of BHEDS is 154.24.

[d] The molecular weight of HDI is 168.20.

2.2.4. Self-healing procedure

Healing process I: PN-LC*xy*-DS*z* film (length: 50 mm, width: 10 mm, thickness: 0.4～0.6 mm). A 5 mm long slit in the longitudinal direction (through the center) of a PN-LC*xy*-DS*z* film was provided using a razor blade with a thickness of 0.1 mm. The self-healing sample was produced by allowing the damaged specimen to heal at room temperature for 24 hours. Of all the PN-LC*xy*-DSzs (z = 1 and 3) films, only the PN-LC01-DS3 film did not follow the healing mechanism mentioned above.

Healing process II: The damaged PN-LC01-DS3 film was healed following a different pathway. The PN-LC01-DS3 film (length 50 mm, width 5 mm, thick-ness 0.4～0.6 mm) was cut

into two halves. The two pieces were superposed with the length of contact being 5 mm. The superposed pair was kept sandwiched between two sheets of poly(tetrafluoroethylene) and were allowed to heal at 60 °C for 24 h to produce the adhered sample. The adhered sample was hot-pressed at 60 °C under a pressure of 0.8 MPa for 1 h to produce a sample of uniform thickness. The dimensions of the specimen were adjusted to 45 mm × 10 mm × 0.4∼0.6 mm to produce the healed PN-LC01-DS3 film. The healing process I and II is shown in Scheme 3.

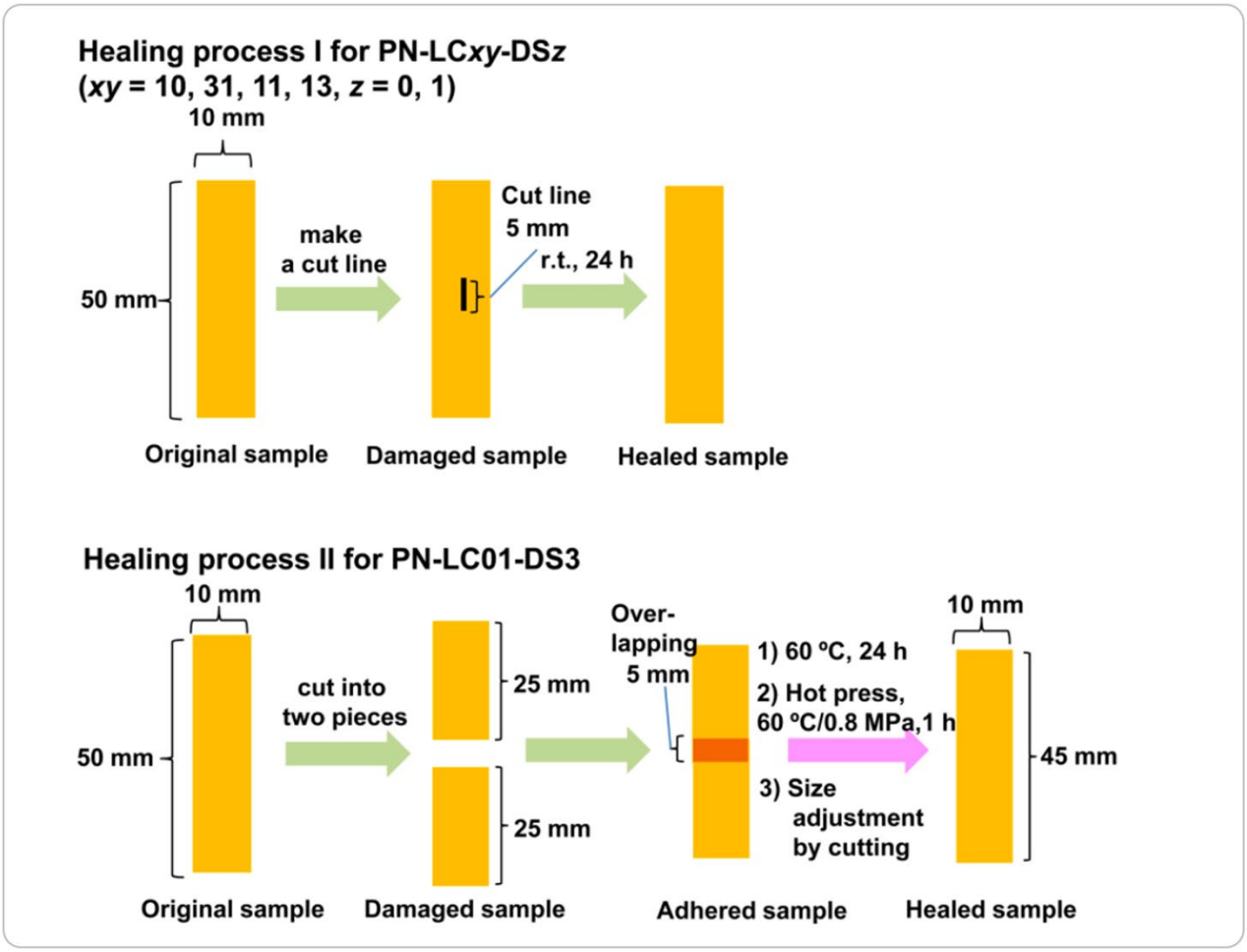

Scheme 3. Healing processes of PN-LC*xy*-DSzs.

2.2.5. Measurements

a. Proton nuclear magnetic resonance (^{1}H-NMR)

Proton nuclear magnetic resonance (^{1}H-NMR) spectra were recorded on a Bruker Ascend 400 (400 MHz) (Madison, WI, USA) using d6-DMSO or $CDCl_3$ as a solvent.

b. Fourier transform infrared (FT- IR)

Fourier transform infrared (FT- IR) spectra were recorded at room temperature in the range from 4000 to 600 (or 500) cm^{-1} on a Shimadzu (Kyoto, Japan) IRAffinity-1S by the attenuated total reflectance (ATR) method. The IR spectra were acquired using 50 scans at a resolution of 4 cm^{-1}.

c. Gel fraction

To estimate the gel fractions of the polymers, the films (10 mm × 10 mm × 0.4～0.6 mm) were kept dipped in chloroform for 24 h at room temperature. subsequently the film which was taken out was dried at 40 °C in a vacuum oven for 24 h. The gel fraction was calculated by the equation: Gel fraction (%) = 100 w_2/w_0; where w_0 and w_2 are the weights of original and dried films, respectively.

d. Differential scanning calorimetry (DSC)

Differential scanning calorimetry (DSC) analysis was performed on a PerkinElmer (Waltham, MA) Diamond DSC in a nitrogen atmosphere. A sample (8～12 mg) was heated from −100 °C to 200 °C at a heating rate of 20 °C min^{-1}, held at the temperature for 3 min to eliminate a thermal history of the sample, and then cooled to −100 °C at a cooling rate of 100 °C min^{-1}. After held at −100 °C for 3 min, the second heating scan was monitored at a heating rate of 20 °C min^{-1}. Glass transition temperature (T_g) was determined from the second heating curves.

e. Dynamic mechanical analysis (DMA)

Dynamic mechanical analysis (DMA) of the rectangular specimen (length 25 mm, width 5 mm, thickness 0.8～1.0 mm) was performed on RSA3 Dynamic Mechanical Analyzer (TA Instruments, Delaware, USA) with a chuck distance of 10 mm, a frequency of 1 Hz, a stain of 0.2-0.4 % and a heating rate of 3 °C min^{-1}.

f. Thermogravimetric analysis (TGA)

Thermogravimetric analysis (TGA) was performed on a Shimadzu TGA-50 thermogravimetric analyzer using a sample of ca. 5 mg at a heating rate of 20 °C min^{-1} in a nitrogen atmosphere. The temperature at which 5% weight loss occurred ($T_{d5\%}$) was calculated from the TGA curve.

g. Field Emission-Scanning Electron Microscopy (FE-SEM)

Morphology of fractured surfaces of samples was observed by field emission-scanning electron microscopy (FE-SEM), using a Hitachi S-4700 machine (Hitachi High-Technologies Corporation, Tokyo, Japan). All samples were fractured after immersion in liquid nitrogen for about 5 min. The fracture surfaces were sputter coated with gold to provide enhanced conductivity.

h. Tensile tests

Tensile tests of rectangular specimens (40 × 5 × 1.0～0.6 mm^3) were performed at the room temperature at around 25 °C using a Shimadzu Autograph AG-1. Span length and testing speed were 25 mm and 5 $mmmin^{-1}$, respectively. Five specimens were tested for each set of samples, and the mean value and the standard deviation were calculated.

i. Optical microscopic measurement

Optical microscopic measurement was carried out using an Olympus BXP microscope equipped with a Sony CCD-IRIS color video camera. The specimen was put on a glass plate and directly visualized using the microscope.

2.3. Results and Discussion

2.3.1. Synthesis and characterization of PN-LC*xy*-DSz*s*

H6LAO and H6CLO (degrees of polymerization (*n*) per arm of 10.4 and 10.0, respectively) were synthesized by ring-opening polymerization reactions of LA and CL using DPE ([LA]0/[OH]0 = 5.0 and [CL]0/ [OH]0 = 10.0, Scheme 1). The oligomers with $n \approx 10$ were chosen because the hydroxy-terminated oligomers' reactivity with HDI decreased as *n* increased (when $n > 10$). When $n < 10$, the curing shrinkage made it very difficult to prepare the flat films. Therefore, H6LAO, H6CLO, and BHEDS were combined in various proportions (H6LAO/H6CLO weight ratios: x/y = 1/0, 3/1, 1/1, 1/3, and 0/1; molar ratios of BHEDS/(H6LAO + H6CLO): z = 0, 1, and

3) and reacted with HDI to produce films (Scheme 2). Since BHEDS contains two hydroxy groups, this study utilized hydroxy-terminated 6-armed oligomers (H6LAO and H6CLO) to produce polymer networks with high gel fractions.

2.3.1.1. ^{1}H-NMR

a. H6LAO

Fig.2.1 shows ^{1}H-NMR spectra of DPE, L-LA, and H6LAO.The chemical shifts of DPE, L-LA, and H6LAO is shown in Table 2.1, 2.2, and 2.3, respectively. In the ^{1}H-NMR spectra of H6LAO, repeating unit and terminal methine ^{1}H-signals (H-a,a') of the lactic acid oligomer (LAO) chain were observed at 4.98～5.29 ppm and 4.25～4.43 ppm, respectively, while those of methyl groups (H-b,b') were observed at 1.35～1.80 ppm and 1.35 ppm, respectively. Additionally, the methylene protons (H-c,d) of the DPE unit of H6LAO were measured at 4.13 ppm and 3.35 ppm, respectively. Thus, it was confirmed that H6LAO had an objective chemical structure. Using the integrated values of H-a and H-a', the degree of polymerization *n* was calculated to be 10.4.

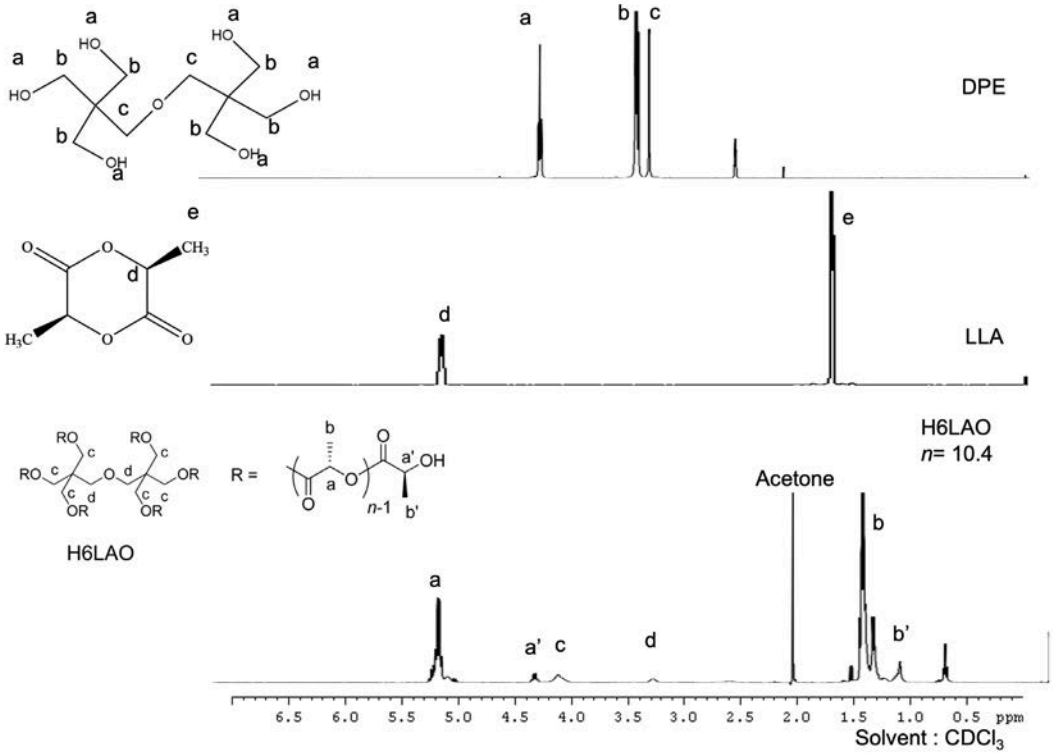

Fig.2.1 ^{1}H-NMR spectra of DPE, LLA and H6LAO in $CDCl_3$

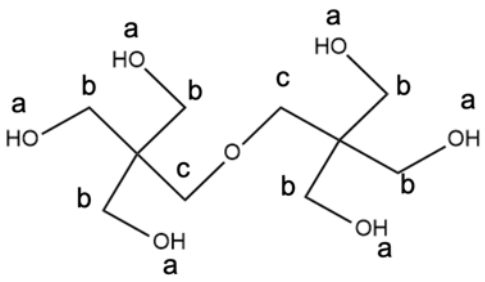

Table 2.1 ^{1}H-NMR chemical shifts of DPE

Signal	Chemical shift (ppm)	Measured integral value	Theoretical integral value
c	2.50	0.30	4.00
b	3.24-3.40	3.23	12.00
a	4.18	1.00	6.00

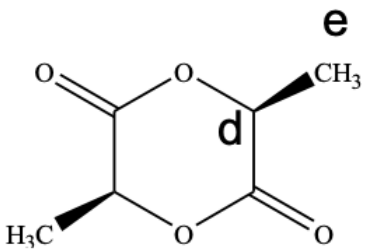

Table 2.2 ^{1}H-NMR chemical shifts of L-LA

Signal	Chemical shift (ppm)	Measured integral value	Theoretical integral value
e	1.45	49.912	3.00
d	5.45	15.874	1.00

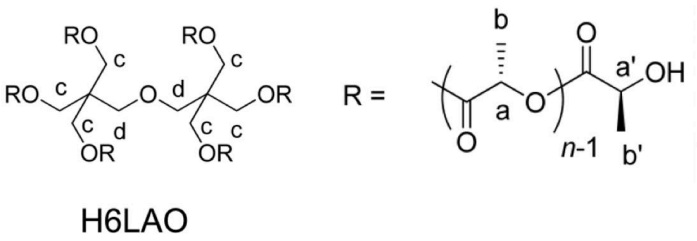

H6LAO

Table 2.3 ^{1}H-NMR chemical shifts of H6LAO

Signal	Chemical shift (ppm)	Measured integral value	Theoretical integral value
b’	1.28	29.84	3.00
b	1.35-1.80	328.14	27.00
d	3.35	7.64	4.00
c	4.13	20.17	12.00
a’	4.25-4.43	10.68	1.00
a	4.98-5.29	100.00	9.00

b. H6CLO

Fig.2.2 shows ^{1}H-NMR spectra of DPE, CL, and H6CLO. The chemical shifts of DPE, CL, and H6CLO are shown in Table 2.4,2.5, and 2.6, respectively. In the ^{1}H-NMR spectrum of H6CLO, the methylene ^{1}H-signals H-a, H-b,d, and H-c of oxyhexanoate units were mainly observed at 2.31 ppm, 1.55～1.74 ppm, and 1.38 ppm, respectively. In addition, the methylene ^{1}H-signals (H-f,e and H-e’) of repeating and terminal oxyhexanoate units were observed at 4.01～4.17 ppm and 3.48 ～3.72 ppm, respectively. The ^{1}H-signal (H-g) of the DPE unit was observed at 3.38 ppm. The ^{1}H-signals of H-f and H-e were conjointly observed at 4.01～4.17 ppm. Thus, it was confirmed that H6CLO has an objective chemical structure. Furthermore, the degree of polymerization *n* was determined to be 10.0 based on the integrated values of H-f,e and H-e’.

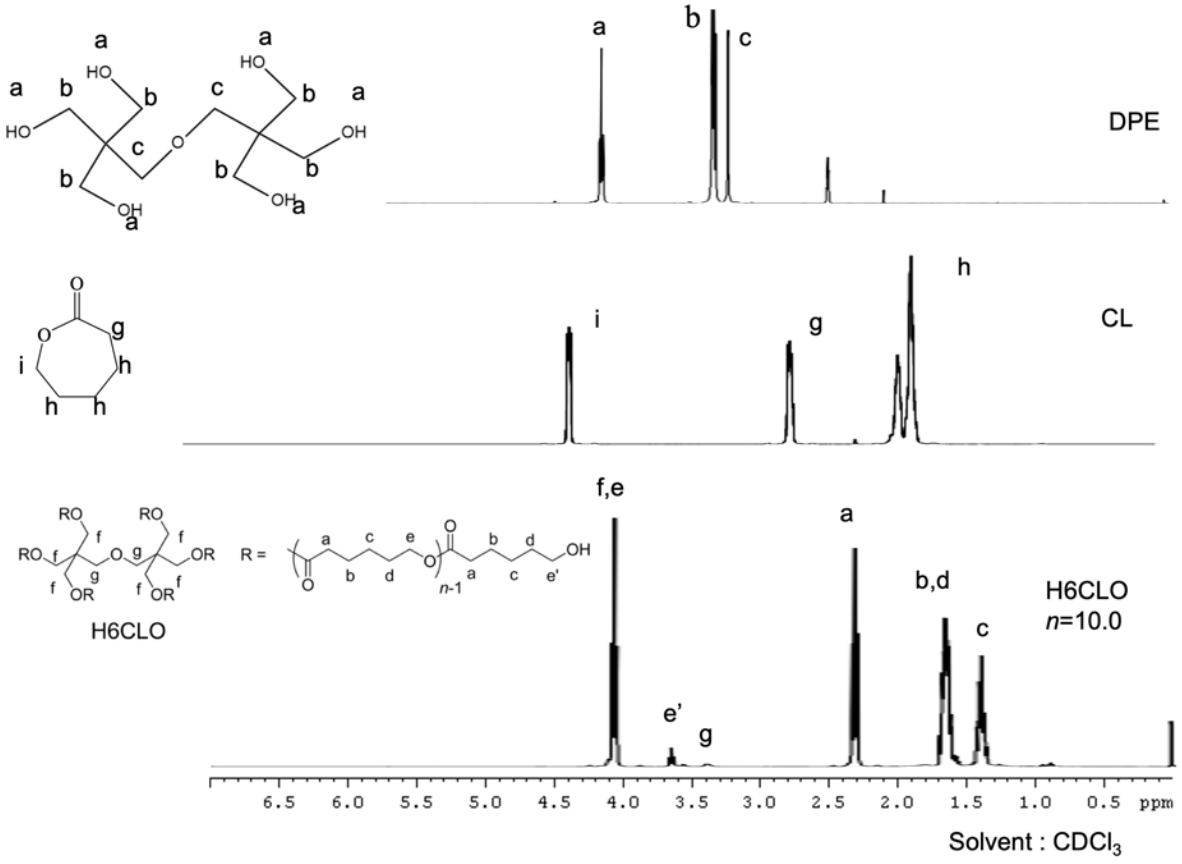

Fig.2.2. ^{1}H-NMR spectra of DPE, CL and H6CLO in $CDCl_3$

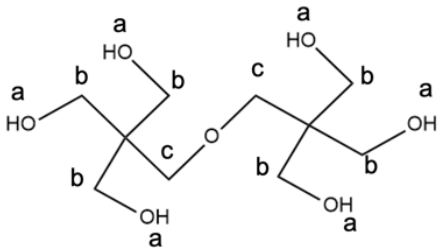

Table 2.4 ^{1}H-NMR chemical shifts of DPE

Signal	Chemical shift (ppm)	Measured integral value	Theoretical integral value
c	2.50	0.30	4.00
a	3.24-3.40	3.23	12.00
b	4.18	1.00	6.00

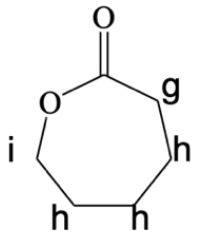

CL

Table 2.5 ^{1}H-NMR chemical shifts of CL

Signal	Chemical shift (ppm)	Measured integral value	Theoretical integral value
h	1.55-1.77	6.10	6.00
g	2.61	2.00	2.00
i	4.21	2.00	2.00

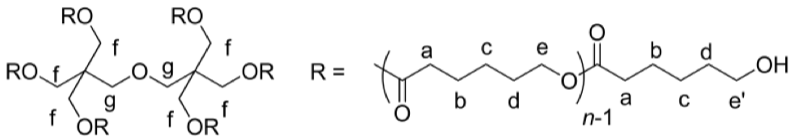

H6CLO

Table 2.6 ^{1}H-NMR chemical shifts of H6CLO

Signal	Chemical shift (ppm)	Measured integral value	Theoretical integral value
c	1.38	109.43	20.00
b,d	1.55-1.74	217.57	40.00
a	2.31	106.87	20.00
g	3.38	3.37	4.00
e’	3.48-3.72	9.97	2.00
f,e	4.01-4.17	100.00	30.00

2.3.1.2. FT-IR

Fig.3. compares the FT-IR spectral profiles of different PN-LCxy-DSzs, HDI, BHEDS, H6LAO, and H6CLO. HDI exhibited an absorption band at 2251 cm^{-1} corresponding to the NCO-stretching vibration (ν_{NCO}). The absorption band at approximately 3500 cm^{-1} in the FT-IR spectrum of H6LAO was attributed to the OH-stretching vibration (ν_{OH}). BHEDS showed an intense ν_{OH} band at 3300 cm^{-1}. On the other hand, the NCO and OH bands were nonexistent in the FT-IR spectral profiles of PN-LC*xy*-DSzs. New peaks corresponding to the NH-stretching (ν_{NH}) and NH-bending (δ_{NH}) vibrations were observed at 3340 cm^{-1} and 1531 cm^{-1}, respectively [21,22]. The distinct absorption band corresponding to the urethane C=O stretching vibration ($\nu_{C=O)}$ was not detectable in the spectral profile because it overlapped with the ester C=O bands (of the LAO and CLO segments) in the 1746～1753 and 1730～1746 cm^{-1} regions. These results indicate that the reaction (using H6LAO, H6CLO, BHEDS, and HDI as reagents) proceeded smoothly to form urethane bonds.

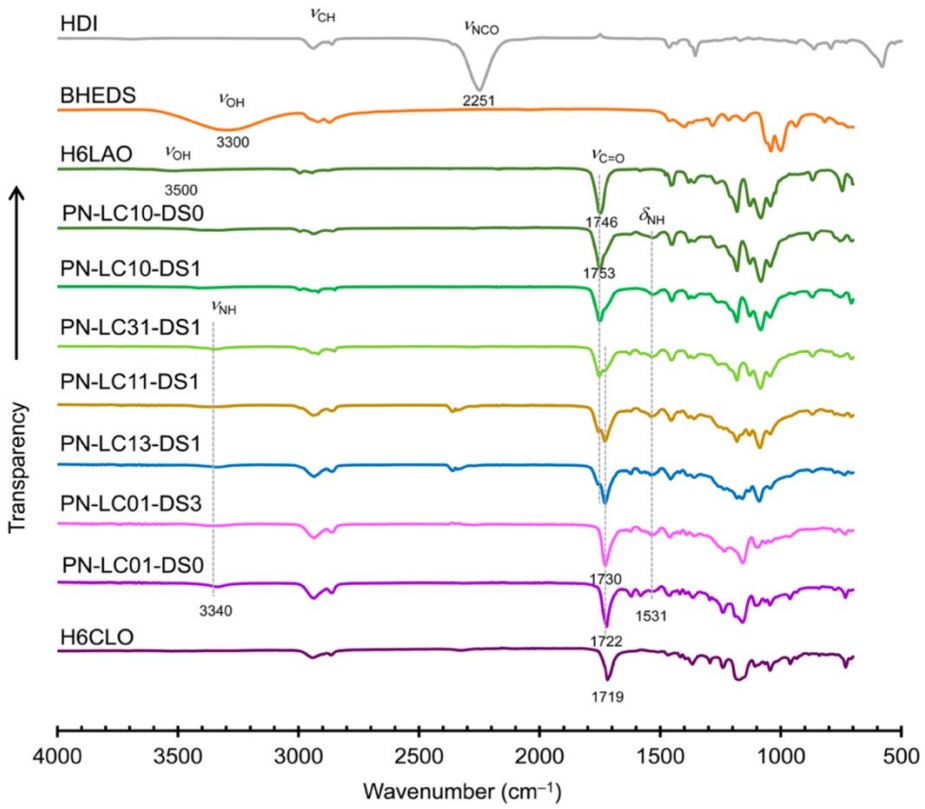

Fig.3. Comparison of the FT-IR spectral profiles of PN-LC*xy*-DSzs, HDI, BHEDS, H6LAO, and H6CLO.

2.3.1.3. Gel fraction

Fig.4. shows the results of gel fraction of the PN-LC*xy*-DS*z*. Also, Table 3 summarizes the gel fractions of the PN-LC*xy*-DS*z* films. The gel fractions of the PN-LC*xy*-DS1 (*xy* = 10, 31, 11, and 13) films were higher than 97%, indicating that the polymer networks were successfully formed. However, the gel fraction of the PN-LC01-DS3 film was significantly lower than that of the other films (75.0%), indicating the partial formation of polymer networks due to the use of a higher feed fraction of BHEDS.

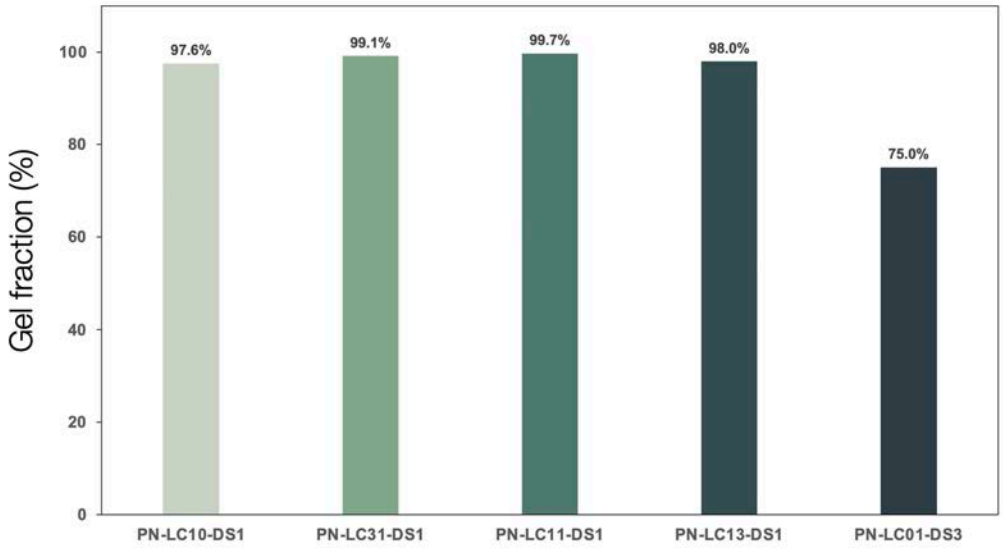

Fig.4.Gel fractions of PN-LC10-DS1, PN-LC31-DS1, PN-LC11-DS1, PN-LC13-DS1, and PN-LC01-DS3

Table 3. Gel fractions of the PN-LC*xy*-DS*z* films.

Sample	Gel fraction (%)
PN-LC10-DS1	97.6
PN-LC31-DS1	99.1
PN-LC11-DS1	99.7
PN-LC13-DS1	98.0
PN-LC01-DS3	75.0

2.3.2. Thermal properties of PBSI-LPs and PBSI-EDT crosslinked films

2.3.2.1. DSC

Fig.5.1. shows the second-heating DSC curves corresponding to H6LAO, H6CLO, and PN-LC*xy*-DSzs. Particular regions of the DSC curves have been zoomed in and shown in Fig.5.2, 5.3, and 5.4. The glass transition temperatures (T_gs) of the PN-LC10-DS0 and PN-LC01-DS0 films (55.9 °C and −46.0 °C, respectively) were significantly higher than those of H6LAO and H6CLO (24.0 °C and −53.9 °C, respectively), indicating that the formation of the polyurethane networks increased the T_gs. On the other hand, the glass transition temperature (T_g) of the PN-LC10-DS1 film was lower than that of the PN-LC10-DS0 film, indicating that the incorporation of flexible disulfide bonds decreased the glass transition temperature (T_g). Even though the T_g of the PN-LC01-DS3 film (−46.3 °C) was lower than those of the previously reported disulfide-containing thiol-ene PCL networks (from −15.6 to −18.0 °C) [16], the T_g of the PN-LC10-DS1 film was significantly higher, since the T_g of the PLA network was significantly higher than that of the PCL network [22]. Although H6CLO, PN-LC01-DS0, and PN-LC01-DS3 exhibited melting temperatures of CLO segments ($T_{m,CLO}$s), whereas H6LAO, PN-LC10-DS0, and PN-LC10-DS1 did not exhibit melting temperatures of LAO segments ($T_{m,LAO}$s), indicating that the former samples were semi-crystalline, whereas the latter samples were amorphous. The absence of $T_{m,CLO}$, and $T_{m,LAO}$ in the PN-LC31-DS1 film indicates its amorphous nature. In contrast, the crystalline CLO segments of PN-LC13-DS1 resulted in a weak melting peak. A very weak melting endothermic peak (Fig.5.3) indicates that the PN-LC11-DS1 film had fewer crystalline CLO segments. The $T_{g,CLO}$ of the PN-LC11-DS1 film (−22.7 °C) was significantly higher than those of the PN-LC13-DS1 and PN-LC01-DS3 films (−41.9 °C and −46.3 °C, respectively), indicating the compatibility of the CLO and LAO segments of the PN-LC11-DS1 film. In this study, the $T_{g,LAO}$s of all conetworks were not detected by the DSC analysis.

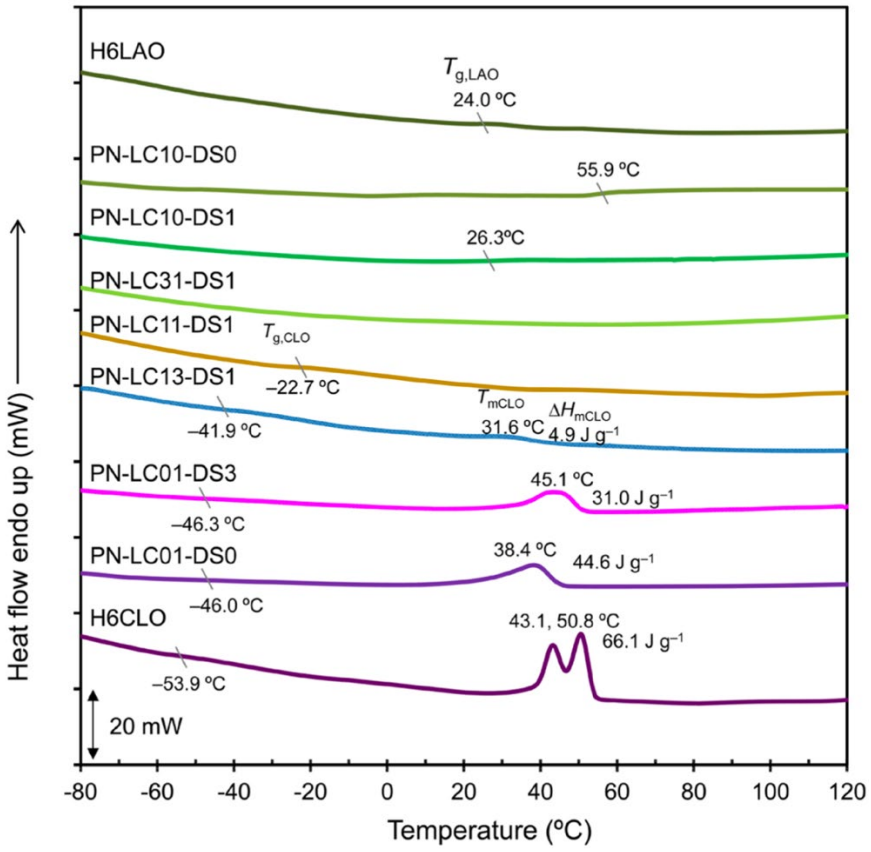

Fig.5.1. Second heating DSC curves of PN-LC*xy*-DSzs, H6LAO and H6CLO

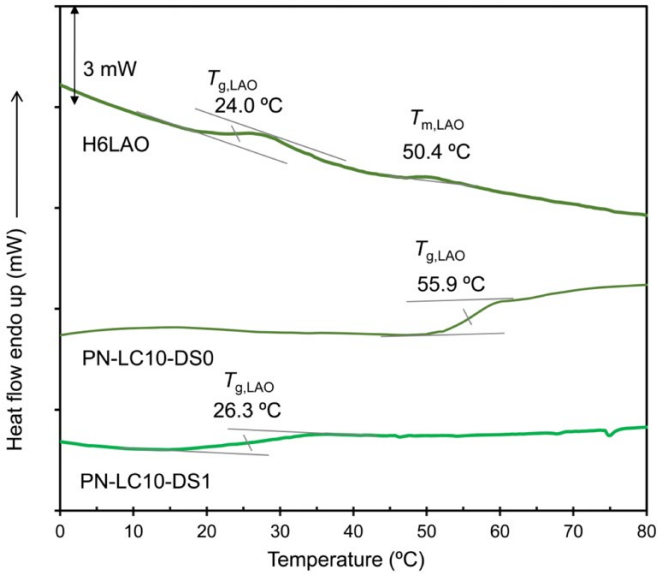

Fig.5.2. Zoomed second heating DSC curves of H6LAO, PN-LC10-DS0 and PN-LC10-DS1.

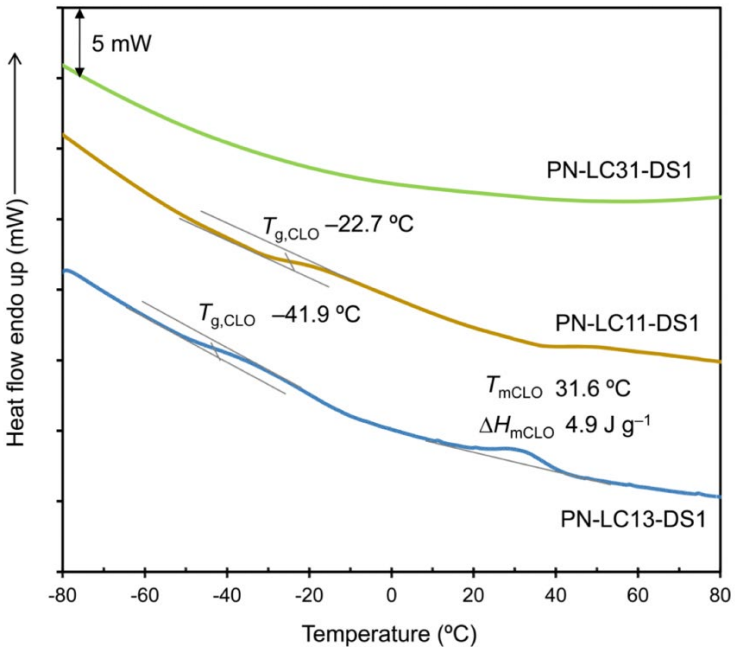

Fig.5.3. Zoomed second heating DSC curves of PN-LC31-DS1, PN-LC11-DS1 and PN-LC13-DS1.

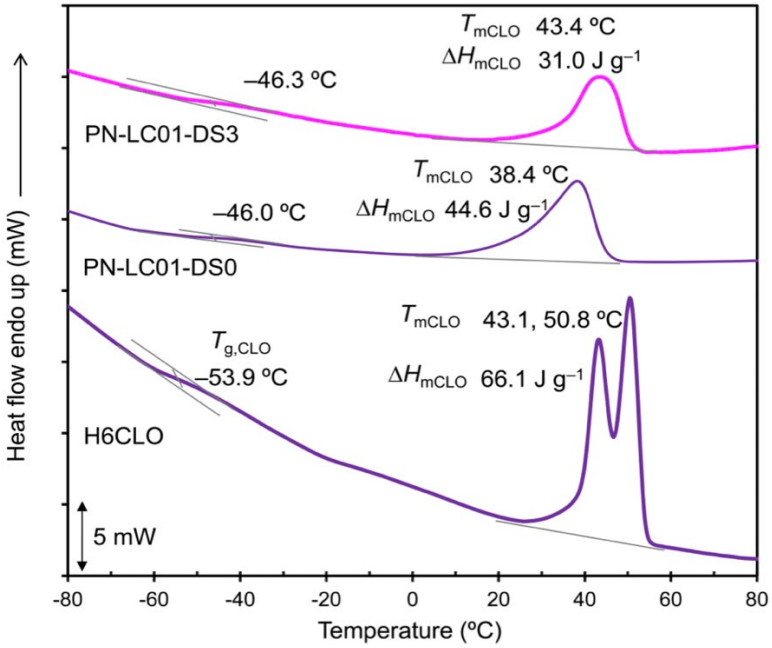

Fig.5.4. Zoomed second heating DSC curves of PN-LC01-DS3 and PN-LC01-DS0 H6CLO.

2.3.2.2. DMA

The DMA curves of the disulfide bond containing PN-LC*xy*-DSzs are shown in Fig.6. Table 4 summarizes the primary dispersion temperatures (T_αs), secondary dispersion temperatures (T_{ss}s) derived from the temperature dependence of the loss tangent (tan δ), and the temperature-dependent loss modulus (*E"*) peak temperatures.

The storage modulus (*E'*) of PN-LC10-DS1 decreased in two steps as the temperature increased (at ~30 °C and ~50 °C). When the temperature exceeded 70 °C (i.e., a rubbery plateau region was observed), the *E'* value reached a constant value (~4.6 MPa) at 30.1 °C due to the glass transition. PN-LC10-DS1 exhibited only one *E"* peak temperature. As a result, the tan δ curve of PN-LC10-DS1 film exhibited two peaks at 36.0 °C and 60.3 °C. The peak temperature of 36.0 °C was assigned to $T_{\alpha,LAO}$ (attributed to the glass transition of the LAO segments).The temperature was slightly higher than the T_g (28.3 °C) estimated by the DSC method. It was believed that the recombination of the dynamic disulfide bonds was responsible for the tan δ peak temperature at 60.3 °C (expressed as T_{ss}) and the drop in the *E'* value at ~50 °C. Guo et al. reported a similar drop in *E'*, over two steps, in a disulfide bond-containing polyurea network [19]. The PN-LC01-DS3 film showed a two-step *E'* drop at approximately −50 °C and 45 °C. The $T_{\alpha,CLO}$ and T_{ss} temperatures were estimated to be −39.5 °C and 54.3 °C, respectively. The drop in *E'* value at ~45 °C may have been caused by the melting of crystalline CLO segments. The disulfide exchange reaction caused a gradual drop in *E'* value at temperatures above 50 °C. The PN-LC31-DS1 network exhibited only a single T_α at 33.0 °C. The *E"* peak temperature of 14.9 °C due to the glass transition indicates that the LAO and CLO segments were completely miscible. Furthermore, the T_{ss}, which originated from the disulfide exchange reaction, was not observed for the PN-LC31-DS1 network, indicating that the disulfide exchange reaction occurred close to T_α. Although the T_αs of PN-LC10-DS1 (36.0 °C) and PN-LC31-DS1 networks (33.0 °C) were comparable, PN-LC10-DS1 exhibited T_{ss} at 60.3 °C (due to the disulfide recombination reaction). On the other hand, the T_{ss} and T_α of PN-LC31-DS1 were 33.0 °C. Since the *E'* values of PN-LC10-DS1 (60 °C) and PN-LC31-DS1 (33 °C) were comparable, it is believed that the temperature at which disulfide bond recombination occurs is dependent on the softness of the sample. Each of the PN-LC11-DS1 and PN-LC13-DS1 films showed two tan δ peaks (at −33.4, 48.1 °C, and −39.3, 51.2 °C, respectively). The tan δ peaks at −33.4 and −39.3 °C are caused by the glass transition (i.e., T_α) of the CLO segments. The fact that the T_α of the PN-LC11-DS1 network (−33.4 °C) was higher than that of the PN-LC13-DS1 network (−39.3 °C) indicates that the CLO and LAO segments were compatible to some extent. Furthermore, the tan δ peaks at 48.1 °C and 51.2 °C originate primarily

from the disulfide exchange (i.e., T_{ss}), since the temperatures are higher than the T_{α} of PN-LC10-DS1 (36.0 °C). The distinct T_{α}s and *E"* peak temperatures for the LAO segments of the PN-LC11-DS1 and PN-LC13-DS1 films were not detected in this study. These results may be caused by the proximity of the temperatures at which the disulfide exchange, glass transition of LAO segments, and melting of CLO segments. This factor is in good agreement with the fact that the $T_{g,LAO}$s were not observed. In addition, *E"* curves did not exhibit maximal peaks, whereas tan δ curves did during the disulfide recombination reaction. This can be explained by the fact that *E"* values did not change, whereas *E'* values decreased during disulfide bond recombination.

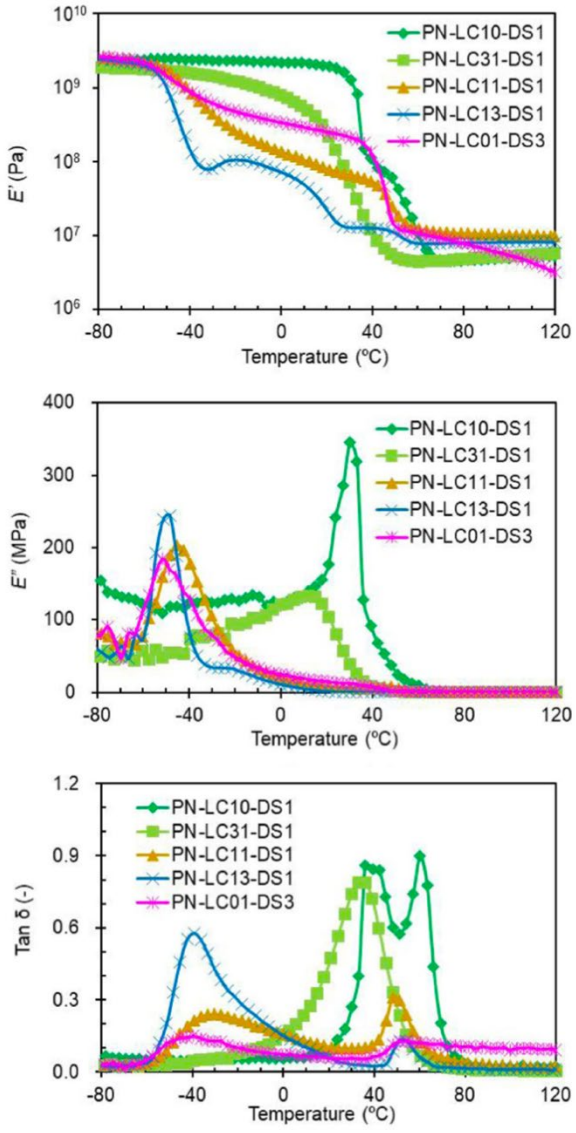

Fig.6. DMA curves of PN-LC*xy*-DS*z*s (*z* = 1 and 3)

Table 4. DMA results of PN-LC*xy*-DS*z*s (*z* =1 and 3)

Sample	T_{α} (°C) [a]	T_{ss} (°C) [b]	*E"* peak temperature(°C)
PN-LC10-DS1	36.0	60.3	30.1
PN-LC31-DS1	33.0	-	14.9
PN-LC11-DS1	−33.4	48.1	−45.4
PN-LC13-DS1	−39.3	51.2	−48.4
PN-LC01-DS3	−39.5	54.3	−51.1

[a] Tan δ peak temperatures at primary dispersion due to glass transition

[b] Tan δ peak temperature at secondary dispersion due to the recombination of disulfide bonds

2.3.2.3. TGA

Fig.7. illustrates the TGA curves of PN-LC*xy*-DS*z*s. The *x*% weight loss temperatures ($T_{dx\%}$, *x* = 5, 10 and 50) of H6LAO, H6CLO, and PN-LC*xy*-DS*z*s are summarized in Table 5. $T_{dx\%}$s (*x* = 5, 10, and 50) values of PN-LC10-DS1 films were higher than those of H6LAO, indicating that the formation of crosslinked structures enhanced the heat resistance. However, the $T_{d5\%}$ and $T_{d10\%}$ values of the PN-LC01-DS0 films were slightly lower than those of H6CLO, indicating that the thermal degradation temperature of the urethane linkages was lower than that of the PCL segments. $T_{dx\%}$s (*x* = 5, 10, and 50) of the PN-LC13-DS1, PN-LC11-DS1, and PN-LC31-DS1 conetworks increased as the H6CLO feed fraction increased. $T_{dx\%}$s (*x* = 5, 10, and 50) values for H6CLO were significantly higher than those for H6LAO. The diisocyanate-crosslinked conetworks of the 4-armed star-shaped LAO and CLO oligomers (H4LAO and H4CLO) exhibited a similar trend [21].

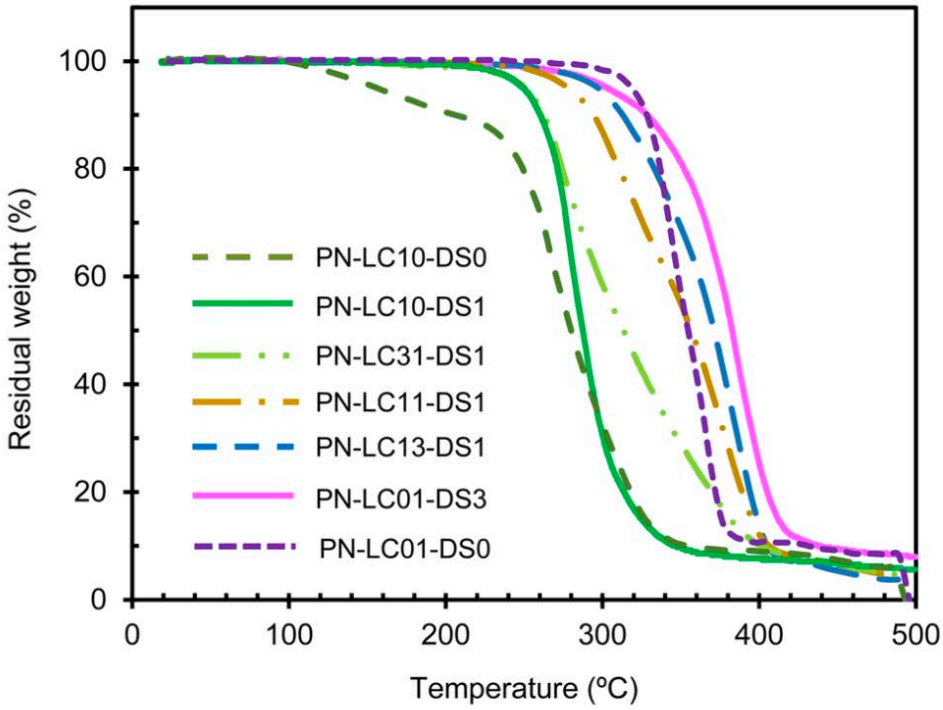

Fig.7. TGA curves of PN-LC*xy*-DSzs

Table 5. Thermal degradation temperatures of PN-LC*xy*-DSzs, H6LAO, and H6CLO

Sample	$T_{d5\%}$ **(°C)**	$T_{d10\%}$ **(°C)**	$T_{d50\%}$ **(°C)**
H6LAO	227	236	278
PN-LC10-DS0	246	254	294
PN-LC10-DS1	251	261	288
PN-LC31-DS1	254	264	314
PN-LC11-DS1	282	296	358
PN-LC13-DS1	303	316	373
PN-LC01-DS1	305	329	383
PN-LC01-DS0	327	332	357
H6CLO	332	342	373

2.3.2.4. FE-SEM

Fig.8. shows the FE-SEM images of the cryo-fractured surfaces of PN-LCxy-DSzs. The patterns in the FE-SEM images of PN-LC10-DS1, PN-LC01-DS3, and PN-LC31-DS1 are not phase-separation structures but rather patterns created by the cryo-fracture process. On the other hand, according to the DSC and DMA experiments results, the PN-LC31-DS1 network is amorphous, and its LAO and CLO segments are miscible. Consequently, some of the patterns on the surface of PN-LC31-DS1 should be caused during the cryo-fracture process. The PN-LC11-DS1 network's finely dispersed and rough surface may be caused by the fine phase-separation and/or crystallization of the CLO segments. This assumption can be made based on the findings of DSC and DMA experiments, which revealed that PN-LC11-DS1 exhibited weak crystallinity and poor compatibility. Several CLO-rich particles (the size of ～10 μm) on the surface of PN-LC13-DS1 were dispersed in the LAO-rich matrix, which is a typical of phase-separated binary system.

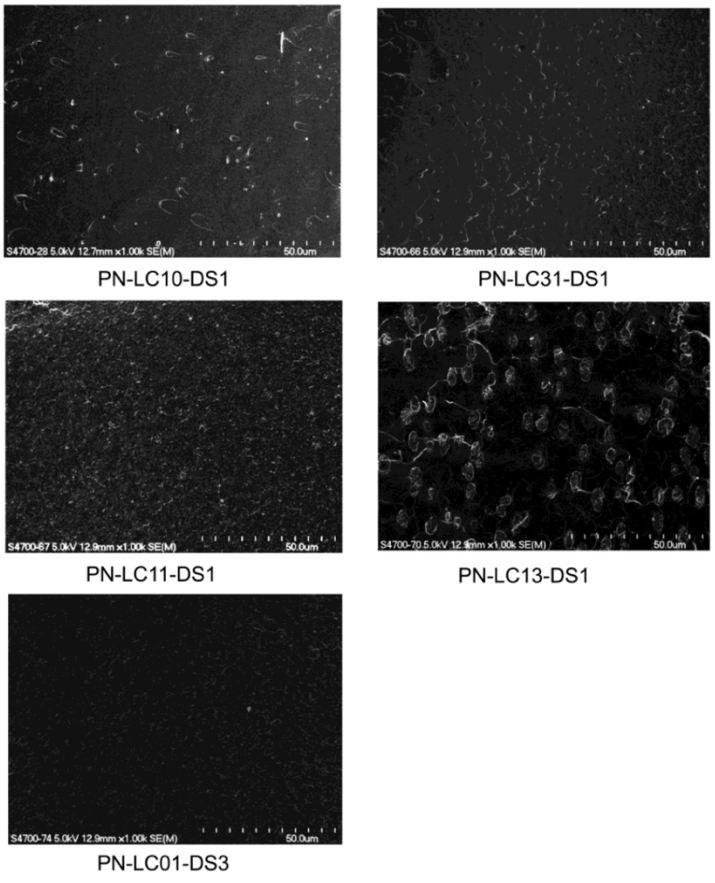

Fig.8. FE-SEM images of cryo-fractured surfaces of PN-LC*xy*-DS*z*s.

2.3.3. Self-healing properties of PN-LCxy-DSzs

To generate self-healing samples, PN-LC10-DS1, PN-LC31-DS1, PN-LC11-DS1, and PN-LC13-DS1 films were cut in the middle and allowed to heal at room temperature. Fig.9. shows images of damaged and healed PN-LC31-DS1, PN-LC10-DS0, and PN-LC01-DS0 films. The cut produced by PN-LC31-DS1 nearly disappeared after 24 hours at room temperature. It was observed that the PN-LC10-DS1, PN-LC11-DS1, and PN-LC13-DS1 films exhibited comparable healing characteristics. The wounds caused by PN-LC10-DS0 and PN-LC01-DS0 films devoid of disulfide bonds did not heal. Because PN-LC10-DS0 was stiffer than PN-LC01-DS0, a razor blade cut in PN-LC10-DS0 film was bolder than in PN-LC01-DS0 film. Also, PN-LC01-DS*z* (*z* = 1 and 3) films were not healed by the same healing procedure. When a PN-LC01-DS3 film, containing three times more feed BHEDS than PN-LC01-DS1, was cut into two pieces, overlapped, and treated at 60 °C, the overlapped films merged to form a single unit. However, when the overlapped films of PN-LC01-DS3 were kept at room temperature, the films did not adhere.

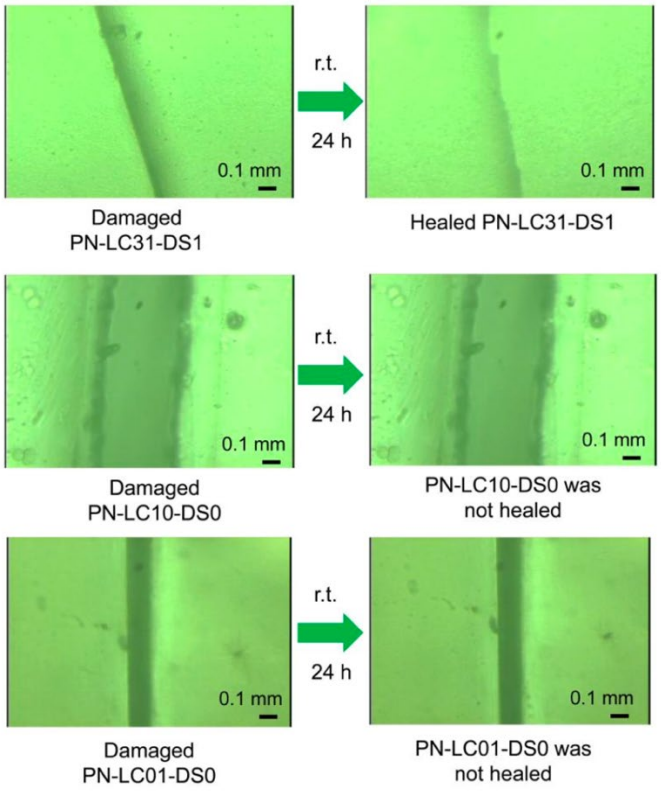

Fig.9. Microscopic images of damaged and healed PN-LC31-DS1, PN-LC10-DS0, and PN-LC01-DS0 films.

Fig.10.1 shows the tensile properties of the original, damaged, and healed PN-LC*xy*-DS*z* films. The typical stress–strain curves and the zoomed-in graphs showing the tensile moduli of all the samples are shown in Fig.10.2 and Fig. 10.3, respectively. Although the stress in the PN-LC10-DS0 film decreased due to necking (beyond the yield point), the stress in the PN-LC10-DS1 film gradually increased due to stress hardening (beyond the yield point), resulting in its failure (Fig.10.2). The tensile strength and modulus of the original PN-LC10-DS0 specimen were considerably higher than those of the original PN-LC01-DS0 specimen. The PN-LC10-DS0 film had a lower elongation at break than the PN-LC01-DS0 film. This result reflects the tensile characteristics of PLA and PCL [22]. Tensile strengths and moduli of the PN-LC10-DS1 and PN-LC01-DS3 films were significantly lower than those of the PN-LC10-DS0 and PN-LC01-DS0 films, indicating that the disulfide bonds were successfully incorporated, resulting in softer polymer networks. Because of the presence of flexible disulfide bonds, the PN-LC10-DS1 film exhibited higher elongation at break than the PN-LC10-DS0 film. However, the elongation at break of PN-LC01-DS3 was lower than that of PN-LC01-DS0. It is considered that the incorporation of disulfide bonds modified the entanglement between the crystalline and amorphous regions of CLO segments. The tensile strengths and elongations at break of the PN-LC31-DS1, PN-LC11-DS1, and PN-LC13-DS1 conetworks decreased with increasing CLO fraction. The tensile moduli of the samples were comparable to each other. The semi-crystalline PCL had a lower tensile strength, modulus, and a higher break elongation than the semi-crystalline PLA [22]. The CLO segments of the conetworks crystallized, while the LAO segments did not, as confirmed by the DSC experiments.

Since PN-LC01-DS3 was cut in the center (Healing process II), the tensile strength, tensile modulus, and elongation at break of the damaged sample were considered to be zero. Other samples damaged by the healing process I exhibited lower tensile strength and modulus by providing cut lines, while some of their elongations at break were higher than those of the original samples. The cut lines of the damaged PN-LC10-DS0 and PN-LC01-DS0 specimens did not heal, when left to stand at room temperature for 24 h. Therefore, their treated specimens had nearly the same tensile strength and modulus as their damaged counterparts, considering the error bars. In contrast, the tensile strengths, and moduli of healed PN-LC*xy*-DS1 (*xy* = 10, 31, 11, and 13) specimens were higher through the healing process I than those of damaged specimens

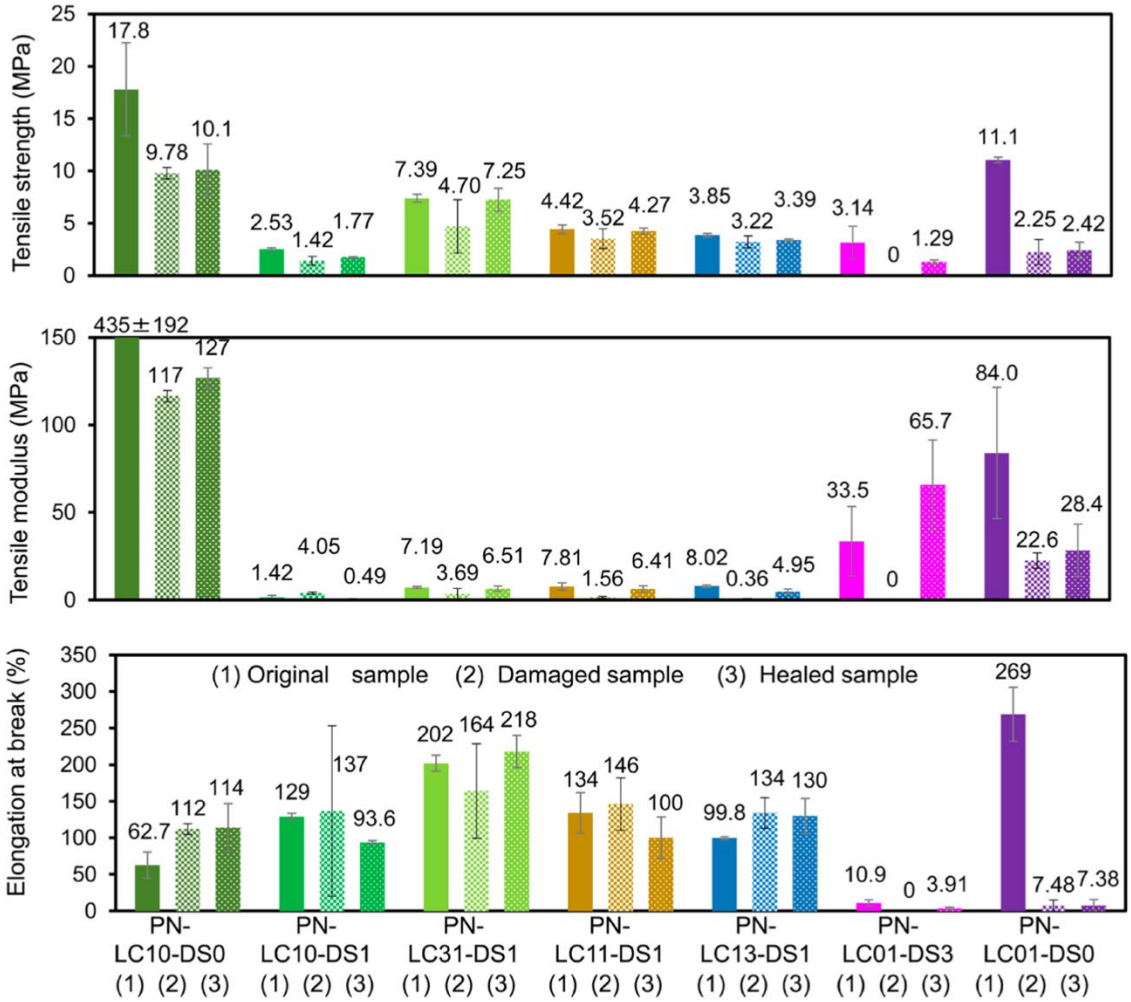

Fig.10.1 Tensile properties of the original, damaged, and healed PN-LC*xy*-DS*z* films. PN-LC10-DS0 and PN-LC01-DS0 did not heal. The tensile properties of the healed samples represent the values obtained for the samples annealed at room temperature for 24 h.

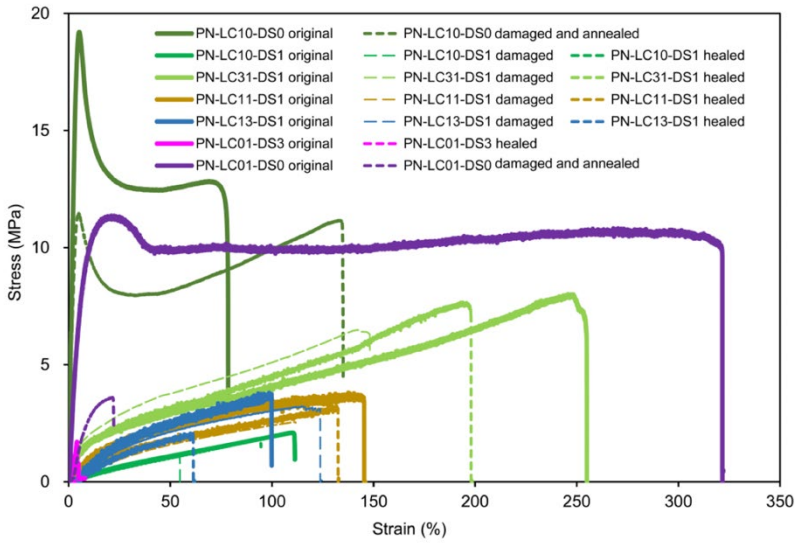

Fig.10.2 Stress-strain curves of original, damaged, and healed PN-LC*xy*-DS*z* films.

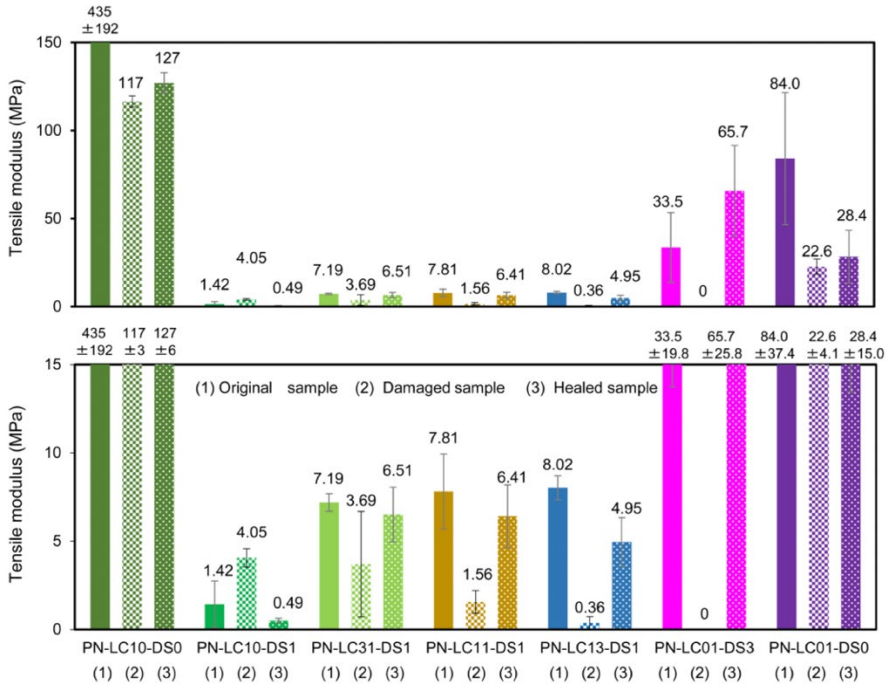

Fig.10.3. Tensile moduli of original, damaged, and healed PN-LC*xy*-DS*z* films. As PN-LC10-DS0 and PN-LC01-DS0 were not healed, the tensile properties of (3) were the values after damaged and annealed at room temperature for 24 h.

Fig.11. illustrates the effect of healing efficiencies on tensile strength as calculated by the equation: healing efficiencies on tensile strength = 100 × (tensile strength of a healed specimen)/ (tensile strength of its original specimen). As the cut inflicted on the PN-LC10-DS0 and PN-LC01-DS0 films did not heal, the healing efficiency were significantly lower than the healing efficiencies of the PN-LC*xy*-DS1 (*xy* = 10, 31, 11, and 13) films. Despite the fact that the PN-LC01-DS3 film could only be healed via healing process II, its healing efficiency was the lowest among the PN-LC*xy*-DS*z* (*xy* = 10, 31, 11, 13, and 01, *z* = 1 and 3) films. This is due to the fact that the crystallization of CLO segments produced the highest tensile modulus (as observed in the PN-LC01-DS3 film). The healing efficiencies of samples containing-disulfide decreased as follows: PN-LC31-DS1 > PN-LC11-DS1 > PN-LC13-DS1 > PN-LC10-DS1 > PN-LC01-DS3. In addition, the DMA experiments revealed that PN-LC31-DS1 possessed the highest healing efficiency. The *E'* values of the film PN-LC31-DS1 (in which the LAO and CLO segments were compatible) dropped at room temperature. The glass transition and recombination of disulfide bonds both occurred simultaneously at room temperature. Previously reported disulfide-containing PCL networks healed treatment at 60°C [16], which is higher than their T_ms (in the range 42.6 to 51.0°C). It is noted that both PN-LC31-DS1 and PN-P11-DS1 demonstrated healing efficiencies higher than 95% when kept at room temperature. The fact that PN-LC01-DS3 displayed the lowest healing efficiency should be related to the following DMA result: The value of *E'* of PN-LC01-DS3 dropped to some extent at −50 °C, but the presence of CLO crystalline phase gently reduced the *E'*, and then the value of *E'* rapidly dropped at around 40 °C due to the melting of the crystalline phase, and then disulfide rearrangement occurred as is obvious from the fact that T_β was 54.3 °C. The fact that PN-LC10-DS1 had the second-lowest healing efficiency should be correlated with the DMA result that the *E'* dropped at approximately 30 °C due to the glass transition, and then the recombination of disulfide bonds occurred, as evidenced by the T_β of 60.3 °C.

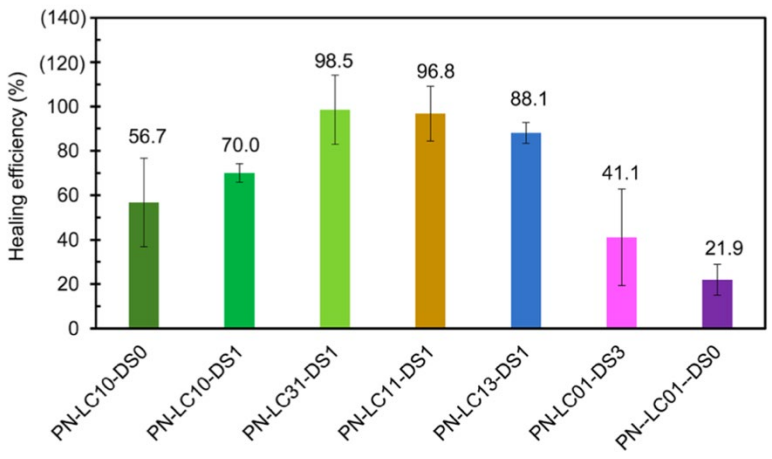

Fig.11. Effect of healing efficiency on the tensile strength of PN-LC*xy*-DS*z* films. As the PN-LC10-DS0 and PN-LC01- DS0 films did not heal, the healing efficiencies represent retention rates of tensile properties of the samples with cut lines annealed at room temperature for 24 h.

2.4. Conclusions

The thermal, mechanical, and self-healing characteristics of disulfide-incorporated polyester-urethane homo- and co-networks composed of LAO and/or CLO segments (PN-LC*xy*-DS1: *xy* = 10, 31, 11, 13, and PN-LC01-DS3) were compared to those of polyester-urethane homo-networks without of disulfide bonds (PN-LC10-DS0 and PN-LC01-DS0). Considering the compatibility of the networks, the LAO and CLO segments of PN-LC31-DS1 are totally compatible, and the compatibility of networks deteriorates as the CLO fraction increases. The CLO segments of all PN-LC*xy*-DS*z* networks are crystallized, although LAO segments are not. It is remarkable that PN-LC31-DS1 had only a single tan δ peak associated with the glass transition and recombination of disulfide bonds. $T_{dx\%}$s (*x* = 5, 10, and 50) of PN-LC*xy*-DS1 (*xy* = 31, 11, and 13) increased when feed H6CLO fraction increased. In terms of tensile parameters, PN-LC31-DS1 exhibited the highest tensile strength and elongation at break among the polymer networks containing disulfides. The cut lines on PN-LC*xy*-DS1 (*xy* = 10, 31, 11, and 13) films self-healed after 24 h at room temperature. In addition, PN-LC31-DS1 had the highest tensile strength healing efficiency in particular (98.5%). In contrast, the cut lines provided to PN-LC10-DS0 and PN-LC01-DS0 without disulfide bonds were not healed at all. Hence, the introduction of disulfide bonds and the construction of conetworks incorporating LAO and CLO segments were highly effective in providing superior mechanical properties and self-healing capabilities.

2.5. References

[1] L.S. Nair, C.T. Laurencin, Biodegradable polymers as biomaterials, Prog. Polym. Sci. 32 (2007) 762–798. https://doi.org/10.1016/j.progpolymsci.2007.05.017.

[2] L. Sartore, N. Inverardi, S. Pandini, F. Bignotti, F. Chiellini, PLA/PCL-based foams as scaffolds for tissue engineering applications, Mater. Today. 7 (2019) 410–417. https://doi.org/10.1016/j.matpr.2018.11.103.

[3] M. Shahrezaee, M. Salehi, S. Keshtkari, A. Oryan, A. Kamali, B. Shekarchi, In vitro and in vivo investigation of PLA/PCL scaffold coated with metformin-loaded gelatin nanocarriers in regeneration of critical-sized bone defects, Nanomed.: Nanotechnol. Biol. Med. 14 (2018) 2061–2073.

[4] J.P. Brutman, P.A. Delgado, M.A. Hillmyer, Polylactide Vitrimers, ACS Macro Lett. 3 (2014) 607–610. https://doi.org/10.1021/mz500269w.

[5] K. Sugane, N. Kumai, Y. Yoshioka, A. Shibita, M. Shibata, Thermo-responsive alternating conetworks by the Diels-Alder reaction of furan-terminated 4-armed star-shaped ε-caprolactone oligomers and maleimide-terminated 4-armed star-shaped l-lactide oligomers, Polymer. 124 (2017) 20–29. https://doi.org/10.1016/j.polymer.2017.07.038.

[6] S. Cai, Z. Qiang, C. Zeng, J. Ren, Multifunctional poly (lactic acid) copolymers with room temperature self-healing and rewritable shape memory properties via Diels-Alder reaction, Mater. Res. Express. 6 (2019) 045701.

[7] Z. Wang, H. Yang, B.D. Fairbanks, H. Liang, J. Ke, C. Zhu, Fast self-healing engineered by UV-curable polyurethane contained Diels-Alder structure, Prog. Org. Coat. 131 (2019) 131–136.

[8] H. Mallek, C. Jegat, N. Mignard, M. Abid, S. Abid, M. Taha, Reversibly crosslinked self-healing PCL-based networks, J. Appl. Polym. Sci. 129 (2013) 954–964. https://doi.org/10.1002/app.38595.

[9] M. Wei, M. Zhan, D. Yu, H. Xie, M. He, K. Yang, Y. Wang, Novel poly (tetramethylene ether) glycol and poly (ε-caprolactone) based dynamic network via quadruple hydrogen bonding with triple-shape effect and self-healing capacity, ACS Appl. Mater. Interfaces. 7 (2015) 2585–2596.

[10] L.-T.T. Nguyen, T.T. Truong, H.T. Nguyen, L. Le, V.Q. Nguyen, T. Van Le, A.T. Luu, Healable shape memory (thio) urethane thermosets, Polym. Chem. 6 (2015) 3143–3154.

[11] Cs. Lakatos, K. Czifrak, R. Papp, J. Karger-Kocsis, M. Zsuga, S. Keki, Segmented linear shape memory polyurethanes with thermoreversible Diels-Alder coupling: Effects of polycaprolactone molecular weight and diisocyanate type, Express Polym. Lett. 10 (2016) 324–336. https://doi.org/10.3144/expresspolymlett.2016.30.

[12] W. Chen, Y. Zhou, Y. Li, J. Sun, X. Pan, Q. Yu, N. Zhou, Z. Zhang, X. Zhu, Shape-memory and self-healing polyurethanes based on cyclic poly (ε-caprolactone), Polym. Chem. 7 (2016) 6789–6797.

[13] J. Zhao, R. Xu, G. Luo, J. Wu, H. Xia, Self-healing poly (siloxane-urethane) elastomers with remoldability, shape memory and biocompatibility, Polym. Chem. 7 (2016) 7278–7286.

[14] M. Invernizzi, S. Turri, M. Levi, R. Suriano, 4D printed thermally activated self-healing and shape memory polycaprolactone-based polymers, Eur. Polym. J. 101 (2018) 169–176. https://doi.org/10.1016/j.eurpolymj.2018.02.023.

[15] K. Sugane, Y. Yoshioka, T. Shimasaki, N. Teramoto, M. Shibata, Self-healing 8-armed star-shaped ε-caprolactone oligomers dually crosslinked by the Diels-Alder and urethanization reactions, Polymer. 144 (2018) 92–102. https://doi.org/10.1016/j.polymer.2018.04.045.

[16] L. Zhang, T. Qiu, Z. Zhu, L. Guo, X. Li, Self-Healing Polycaprolactone Networks through Thermo-Induced Reversible Disulfide Bond Formation, Macromol. Rapid Commun. 39 (2018) 1800121. https://doi.org/10.1002/marc.201800121.

[17] M. Yarmohammadi, M. Shahidzadeh, Evaluation of disulfide chain extender effect on the mechanical properties of unsaturated polyurethane-urea networks, J. Appl. Polym. Sci. 135 (2018) 46309. https://doi.org/10.1002/app.46309.

[18] K. Chang, H. Jia, S.-Y. Gu, A transparent, highly stretchable, self-healing polyurethane based on disulfide bonds, Eur. Polym. J. 112 (2019) 822–831. https://doi.org/10.1016/j.eurpolymj.2018.11.005.

[19] T. Li, Z. Xie, J. Xu, Y. Weng, B.-H. Guo, Design of a self-healing cross-linked polyurea with dynamic cross-links based on disulfide bonds and hydrogen bonding, Eur. Polym. J. 107 (2018) 249–257. https://doi.org/10.1016/j.eurpolymj.2018.08.005.

[20] A. Shibita, H. Takase, M. Shibata, Semi-interpenetrating polymer networks composed of poly(l-lactide) and diisocyanate-bridged 4-arm star-shaped ε-caprolactone oligomers, Polymer. 55 (2014) 5407–5416. https://doi.org/10.1016/j.polymer.2014.08.074.

[21] A. Shibita, T. Shimasaki, N. Teramoto, M. Shibata, Conetworks composed of 4-armed star-shaped l-lactide oligomer and 4-armed star-shaped ε-caprolactone oligomer, Polymer. 74 (2015) 54–62. https://doi.org/10.1016/j.polymer.2015.07.052.

[22] A. Shibita, H. Takase, M. Shibata, Semi-interpenetrating polymer networks composed of poly(l-lactide) and diisocyanate-bridged 4-arm star-shaped ε-caprolactone oligomers, Polymer. 55 (2014) 5407–5416. https://doi.org/10.1016/j.polymer.2014.08.074.

Chapter 3

Self-healing polyester networks prepared from poly(butylene succinate-*co*-butylene itaconate) and thiol-terminated polyether containing disulfide linkages

3.1. Introduction

Biobased and biodegradable polyesters, such as poly(butylene succinate) (PBS) and poly(lactic acid) (PLA), are being developed to overcome the depletion of petroleum resources and the increase in plastic pollution [1], [2]. From the perspective of efficient resource utilization and extended service life of polymers, it is essential for polymers to have self-healing properties, even if bio-based and biodegradable polymer. The biodegradable/biobased PBS has intermediate thermal and mechanical properties of PLA and PCL. It is considered that PBS-based network polymers could possess self-healing ability.

For self-healing PLA networks, the transesterification and thermo-reversible DA reactions have been reported [3]–[6]. In addition, self-healing PLA networks containing disulfide bonds were developed in chapter 2 via the urethanization reaction of a 6-armed star-shaped lactide oligomer and 2-hydroxyethyl disulfide with hexamethylene diisocyanate (HDI) and exhibited self-healing properties. Regarding self-healing PBS networks, the crosslinked PBS networks generated by the DA reaction of P(FS-*co*-BS) and bismaleimide showed self-healing properties [7]. However, self-healing PBS networks involving disulfide metathesis reactions have not yet been reported.

Previously, poly(butylene succinate-co-butylene itaconate) (PBSI) was produced by polycondensing BD, SA, and IA (Scheme 1) [8]. In chapter 3, the nucleophilic thiol-ene reaction of poly(butylene succinate-*co*-butylene itaconate) (PBSI) and a thiol-terminated polyether (LP-3) containing disulfide linkages at C=C/SH ratios of 2/1, 1/1, and 1/2 produced crosslinked polyester networks (PBSI-LPs) (Scheme 2). For comparison, a PBSI/2,2'-(ethylenedioxy) diethanethiol crosslinked polymer (PBSI-EDT-11, C=C/SH = 1/1) without disulfide bonds was prepared. This study focused on producing disulfide-containing PBS-based network polymers, and their thermal, mechanical, and self-healing properties were investigated.

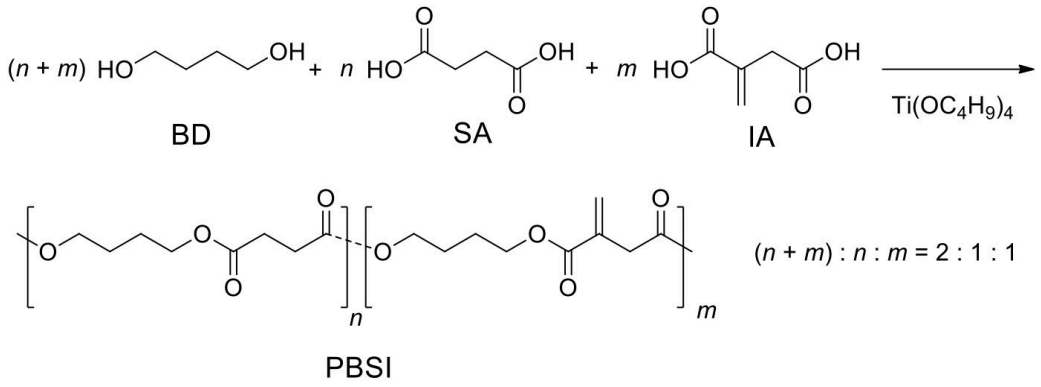

Scheme 1. Synthesis of PBSI by the polycondensation reaction of BD, SA, and IA.

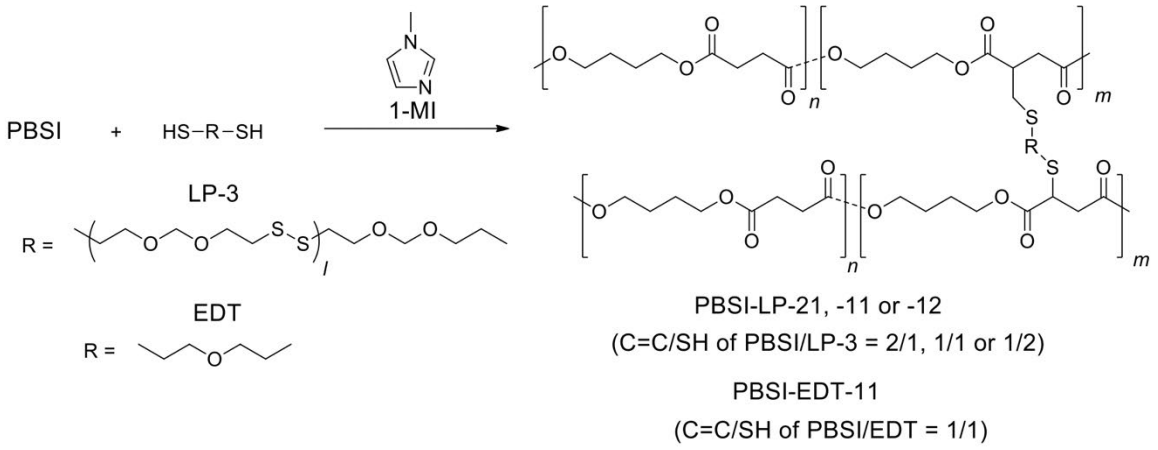

Scheme 2. Synthesis of PBSI-LPs and PBSI-EDT-11 via nucleophilic thiol-ene reactions of PBSI/LP-3 and PBSI/EDT.

3.2. Experimental section

3.2.1. Materials.

1,4-butanethiol (BD)
MW: 90.25
m.p.: −53.9 ℃
b.p.: 195.5 ℃
Kanto Chemical Co., Inc.

Itaconic acid (IA)
MW: 130.10
m.p.: 175 ℃
b.p.: 268 ℃
Tokyo Chemical Industry Co., Ltd.

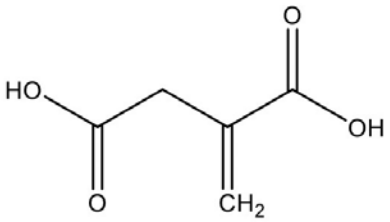

Succinic acid (SA)
MW: 118.09
m.p.: 185～190 ℃
b.p.: 235 ℃ (760 mmHg)
Wako Pure Chemical Corporation

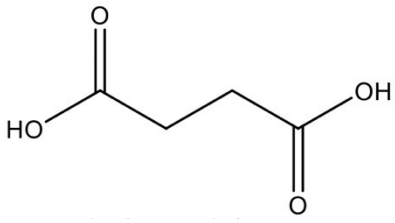

Titanium (IV) tetra-*n*-butoxide
MW: 340.32
m.p.: −55 ℃
b.p.: 260 ℃
Kanto Chemical Co., Inc.

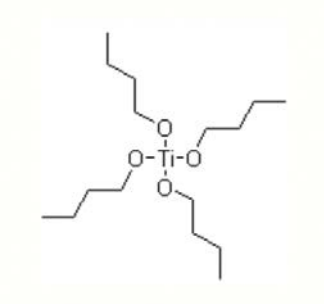

1-methylimidazole (1-MI)

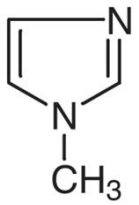

MW: 82.11

m.p.: −60 ℃

b.p.: 198 ℃

Tokyo Chemical Industry Co., Ltd.

Thiokol LP-3 (LP-3)

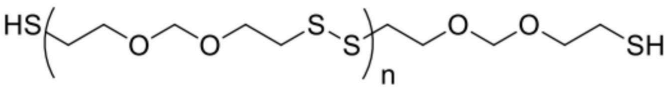

MW: 1000

mercaptan content: 6.8 wt%

crosslinking: 2.0%

Thiol equivalent 2.05 $gmol^{-1}$

Toray Fine Chemical

2,2’-(ethylenedioxy) diethanethiol (EDT)

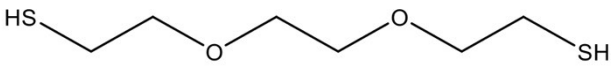

MW: 182.30

assay: 95%

b.p.: 225 ℃

Sigma-Aldrich

Methanol

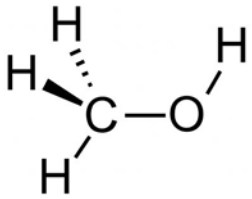

MW: 32.04

m.p.: −97.6 ℃

b.p.: 64.7 ℃ (760 mmHg)

Tokyo Chemical Industry Co., Ltd.

3.2.2. Synthesis of PBSI

In a 300 mL round-bottom flask equipped with a Dean-Stark trap, PBSI was synthesized via the bulk polymerization of BD, SA, and IA. The BD/SA/IA feed molar ratio was 2.0:1.0:1.0, respectively. The catalyst, 35 mg (0.10 mmol) of titanium (IV) tetra-n-butoxide, was added to the mixture of 29.7 g (0.330 mol) of BD, 19.5 g (0.165 mol) of SA, and 21.5 g (0.165 mol) of IA. The mixture was heated at 160 ℃ under a mildly reduced pressure of 40 Torr for 4 h, followed by 180 ℃ under the same pressure for 5 hours, while the water generated was collected in a Dean-Stark trap. The product was dissolved in chloroform (5 mL) and precipitated with methanol (1 L) after reaching room temperature. The precipitate was washed with methanol and vacuum-dried at room temperature (approximately 25 ℃) for 72 h to produce PBSI as a yellow powder with a yield of 50.5% (35.5 g). The synthetic flow chart of PBSI is shown in Fig.1.1.

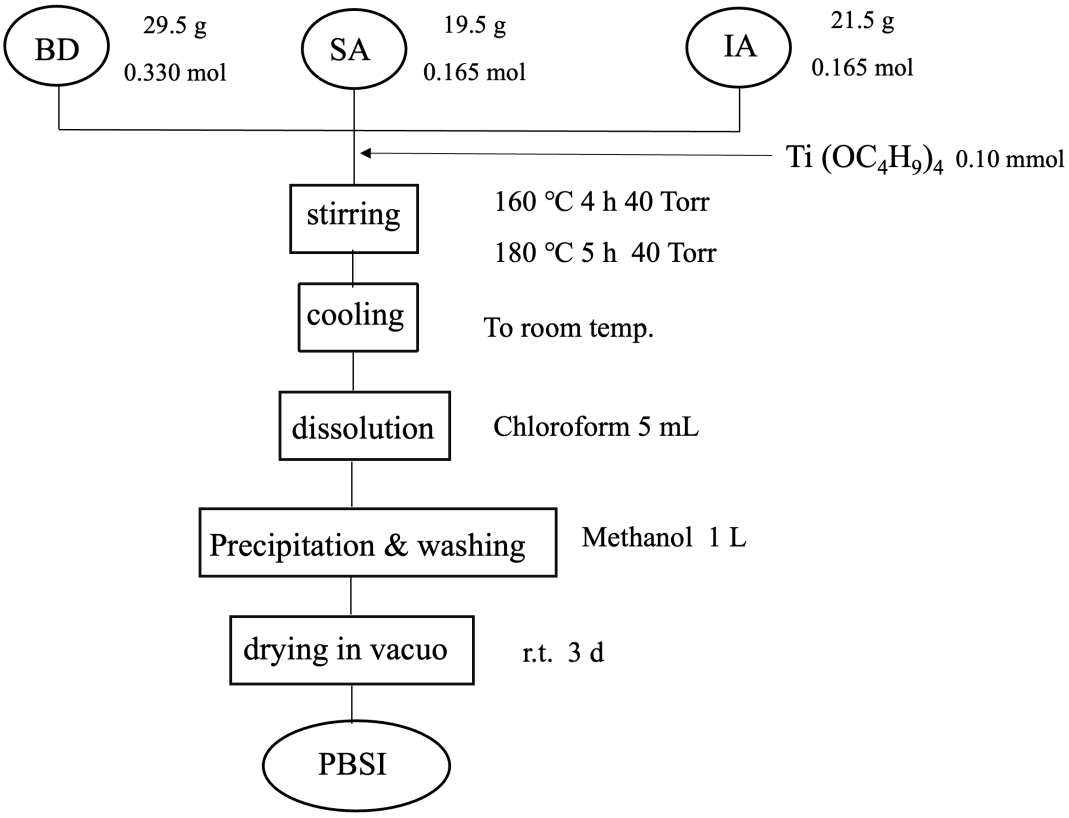

Fig.1.1. Synthesis of PBSI flow chart.

3.2.3. Preparation of crosslinked PBSI/LP-3 (PBSI-LP) and PBSI/EDT (PBSI-EDT) films.

The mixtures of PBSI/LP-3 with C=C/SH ratios of 2/1, 1/1, and 1/2 and PBSI/EDT with a C=C/SH ratio of 1/1 were thermally crosslinked using a base-catalyzed thermal thiol-ene reaction in the presence of 1-MI to produce PBSI-LP-21, 11, and 12 and PBSI-EDT-11, respectively. Typical PBSI-LP-11 preparation steps are as follows: A solution of 2.69 g (5.55 mmol-SH) of LP-3 in chloroform (5 mL) was added to a solution of 2.31 g (5.55 mmol-C=C) of PBSI in chloroform (15 mL). After 30 minutes of stirring at room temperature, 1-MI was added to the mixture (25 mg, 0.50 wt% of the total weight of PBSI and LP-3). After 1 h of stirring at room temperature, the obtained solution was poured into a 100 mm-diameter perfluoroalkoxy alkane Petri dish. The mixture was dried at room temperature for 24 h, then crosslinked at 60 ℃ for 24 h to produce a PBSI-LP-11 film with a thickness of ~0.4 mm. PBSI-LP-21, 12, and PBSI-EDT-11 films were processed similarly (Scheme 2). Fig.1.2 shows the preparation of crosslinked PBSI/LP-3 (PBSI-LP) and PBSI/EDT (PBSI-EDT) films. Table 1 summarizes the feed amounts of the reactants for all crosslinked products.

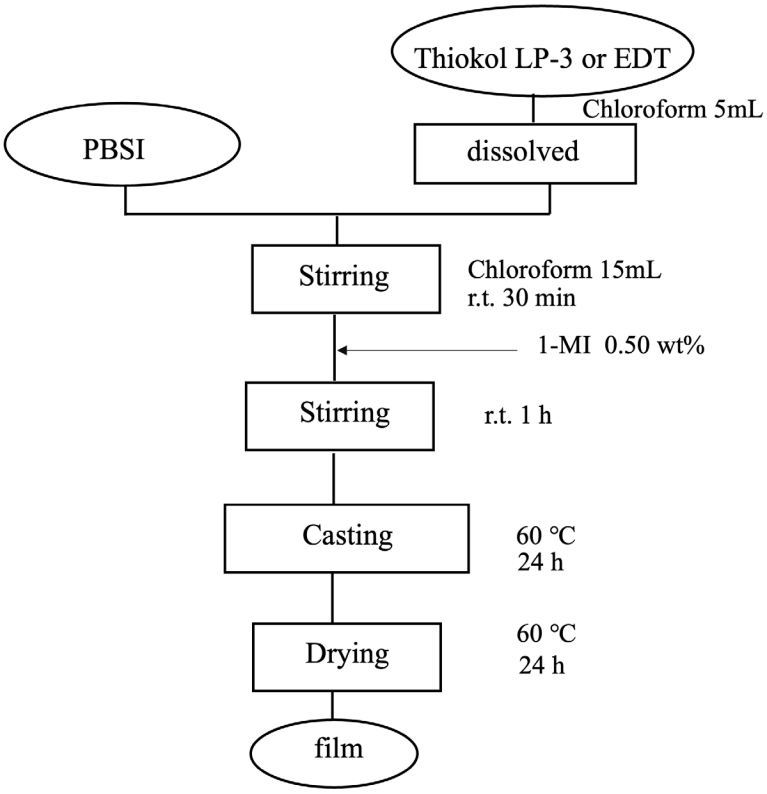

Fig.1.2. the preparation of crosslinked PBSI/LP-3 (PBSI-LP) and PBSI/EDT (PBSI-EDT) films.

Table 1. Feed amounts of reagents for the preparation of PBSI-LPs and PBSI-EDT-11.

Sample	Ratio of C=C/SH	PBSI[*1] g (mmol-C=C)	LP-3[*2] g (mmol-SH)	EDT[*3] g (mmol-SH)
PBSI-LP-21	2/1	3.15 (7.59)	1.85 (3.79)	-
PBSI-LP-11	1/1	2.31 (5.55)	2.69 (5.55)	-
PBSI-LP-12	1/2	1.50 (3.60)	3.50 (7.20)	-
PBSI-EDT-11	1/1	4.10 (9.88)	-	0.90 (9.88)

[*1] C=C equivalent = 415 g eq.$^{-1}$

[SA : IA = 1.02 : 0.76 = 1.34 : 1, 1.34 × ($C_8H_{12}O_4$)+($C_9H_{12}O_4$)= 415 g eq.$^{-1}$]

[*2] Mercaptan equivalent = 486 g eq.$^{-1}$ (Mercaptan content 6.8 wt%)

[*3] Mercaptan equivalent = 91.15 g eq.$^{-1}$ (Molecular weight = 182.30)

3.2.4. Measurements

a. Proton nuclear magnetic resonance(^{1}H-NMR)

Proton nuclear magnetic resonance(^{1}H-NMR) spectra were recorded at room temperature on a Bruker AV-400(400 Hz) using $CDCl_3$ as the solvent and tetramethyl silane (TMS) as the internal standard.

b. Gel permeation chromatography (GPC)

Averaged molecular weights (M_n and M_w) were measured on a Shimadzu LC9A gel permeation chromatography (GPC) apparatus equipped with two OHpak SB-806M HQ GPC columns (Showa Denko) and a reflective index (RI) detector at 40°C. N,N'-Dimethylformamide (DMF) was used as an eluent at a flow rate of 0.5 mLmin^{-1}. Polystyrene standard with a narrow distribution of molecular weight (M_w: 58-377,400) were used for Molecular weight calibrations.

c. Fourier transform infrared (FT-IR)

Fourier transform infrared (FT-IR) spectra were recorded at room temperature in the range from 4000 to 400 cm^{-1}on a Shimadzu (Kyoto, Japan) IR Afinity1s by the attenuated total reflectance (ATR) method. The IR spectra were acquired using 50 scans at a resolution of 4 cm^{-1}.

d. Degree of swelling (D_s) and Gel fraction.

Degree of swelling (D_s) measurements were performed by dipping a film (10 mm × 10 mm × 0.3～0.8 mm) in Acetone at room temperature for 24 h according to the following equation: D_s (%) = 100(w_1 - w_0)/w_0, where w_0 and w_1 are the weights of original and the swollen film after dipping.

To estimate the gel fraction of the network polymer, The film (10 mm × 10 mm × 0.3～0.8 mm) was dipped in Acetone for 24 h at room temperature, subsequently, the film was taken out and dried at 60 ℃ in a vacuum oven for 24 h. The gel fraction was calculated by the equation: Gel fraction (%) = 100w_2/w_0: where w_0 and w_2 are the weights of original and dried films.

e. Thermogravimetric analysis (TGA)

Thermogravimetric analysis (TGA) was performed on a Shimadzu TGA-50 thermogravimetric analyzer using a sample of approximately 5 mg at a heating rate of 20 ℃ min^{-1} in a nitrogen atmosphere. The temperature at which 5% weight loss ($T_{d5\%}$) occurred was calculated from the TGA curve respectively.

f. Differential scanning calorimetry (DSC)

Differential scanning calorimetry (DSC) analysis was performed on a PerkinElmer (Waltham MA) Diamond DSC in a nitrogen atmosphere. A sample (5～8 mg) was heated from −80 to 150 ℃ at a heating rate of 20 ℃min^{-1}, held at the temperature for 5 min to eliminate a thermal history of the sample, and then cooled to −80 ℃ at a cooling rate of 50 ℃ min^{-1}. After held at −80 ℃ for 5 min, the second heating was monitored at a heating rate 20 ℃ min^{-1} from -80 to 180 ℃. Glass transition temperature (T_g) was determined from the first heating curves.

g. Dynamic mechanical analysis (DMA)

Dynamic mechanical analysis (DMA) of the rectangular specimen (length 20 mm, width 5 mm, thickness 0.3～0.8 mm) was performed on DMA1 (Mettler-Toledo K.K.,Tokyo Japan) with a chuck distance of 10 mm, a frequency of 1 Hz, a displacement amplitude of 10 μm and a heating rate of 2 ℃ min^{-1}.

h. Tensile test

Tensile strength of the rectangular plates (length 45 mm, width 7 mm, thickness 0.3～0.8 mm) were performed at the room temperature around 25 ℃ using a Shimadzu autograph AG-1. Span length and testing speed were 25 mm and 5 mm min^{-1}, respectively. Five specimens were tested for each set of samples, and the mean value and the standard deviations were calculated.

3.3. Results and Discussion

3.3.1. Characterization of PBSI, PBSI-LP, and PBSI-EDT films

3.3.1.1. ^{1}H-MMR and GPC

The number-average molecular weight (M_n) and weight-average molecular weight (M_w) values measured by GPC for PBSI prepared at the BD/SA/IA 2.0: 1.0: 1.0 were 5,373 and 11,100, respectively. The polydispersity index (weight-average molecular weight/number-average molecular weight: M_n/M_w) was 2.07. Fig.2. shows ^{1}H-NMR spectra of BD, SA, IA, and PBSI in $CDCl_3$. The chemical shifts of the ^{1}H-signals of BD, SA, IA, and PBSI shown in Table 2.1, 2.2, 2.3, and 2.4, respectively. In the ^{1}H-NMR spectrum of PBSI, the ^{1}H-signal of butyleneoxy units were observed at 4.1 ppm (H-a) and 1.7 ppm (H-b). A weak ^{1}H-signal at 4.3 ppm was ascribed to the H-a' protons close to the exomethylene group in the butylene itaconate units. The ^{1}H-signal of succinate unit can be observed at 2.7 ppm(H-c), and aliphatic and olefinic protons of the itaconate units were observed at 3.4 ppm (H-e) and 5.8, 6.5 ppm (H-d). From the integral ratio of their ^{1}H-signals, the introduced BD/SA/IA ratio was calculated to be 2.00: 1.02: 0.76. Although the SA/IA feed molar ratio was 1.0, the introduced itaconate unit was lower than that of the succinate unit. Also, BD/(SA+IA) was 2.00: 1.78, indicating that the terminal group of PBSI was mainly a hydroxy butyl group of the BD unit. The comparatively low yield of PBSI (50.5%) may be attributable to the dissolution of unreacted IA and low-molecular-weight PBSI molecules in the methanol utilized as a precipitation solvent.

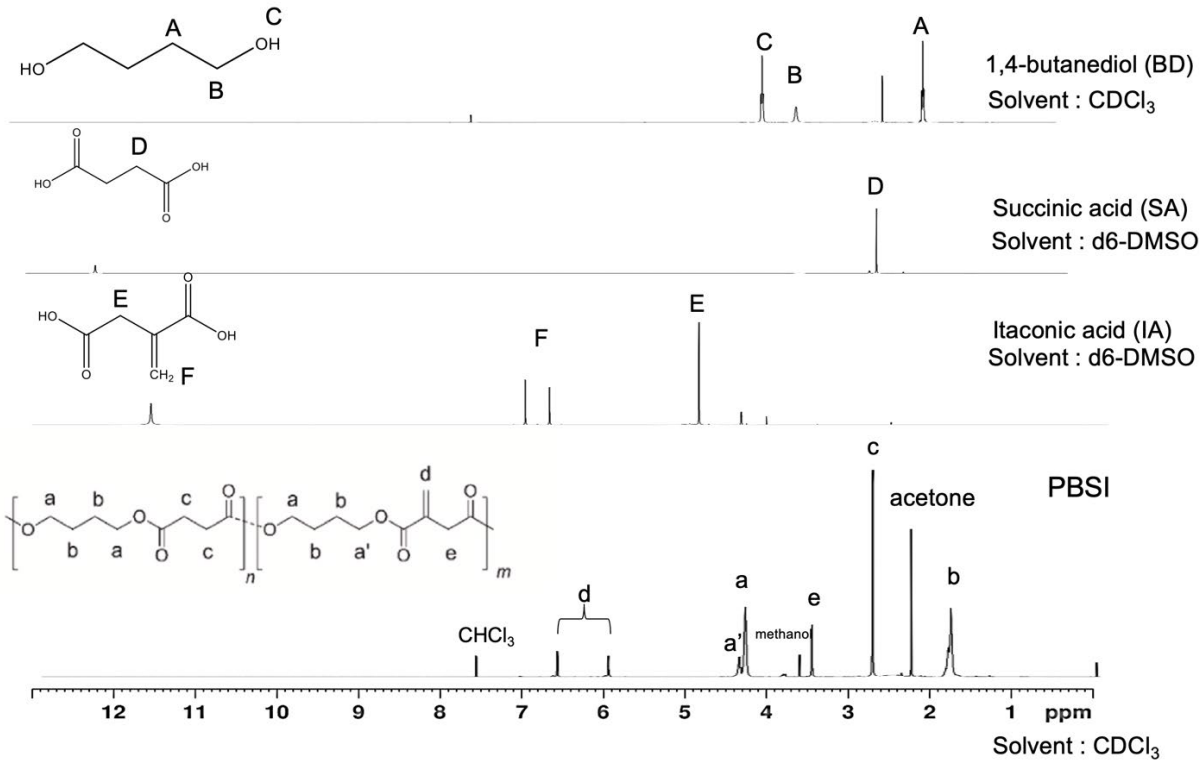

Fig.2. ^{1}H-NMR spectra of BD, SA, IA, and PBSI in $CDCl_3$.

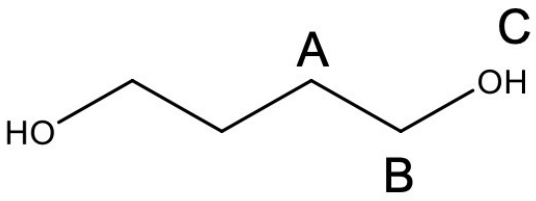

Table 2.1 The chemical shifts of 1,4-butanediol (BD).

Signal	Chemical shift (ppm)	Measured integral value	Theoretical integral value
A	1.68	1.00	2.00
B	3.25	0.46	2.00
C	3.67	0.99	1.00

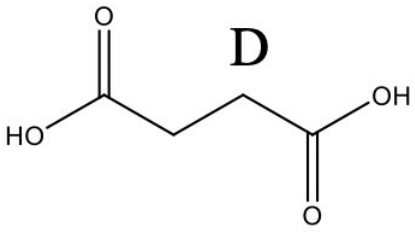

Table 2.2 The chemical shifts of Succinic acid (SA).

Signal	Chemical shift (ppm)	Measured integral value	Theoretical integral value
D	2.42	1.00	2.00

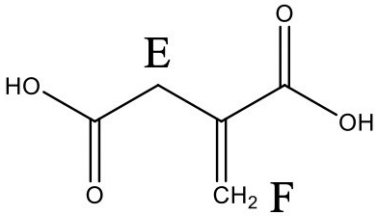

Table 2.3 The chemical shifts of Itaconic acid (IA).

Signal	Chemical shift (ppm)	Measured integral value	Theoretical integral value
E	3.21	0.30	2.00
F	5.72,6.13	0.15,0.15	2.00

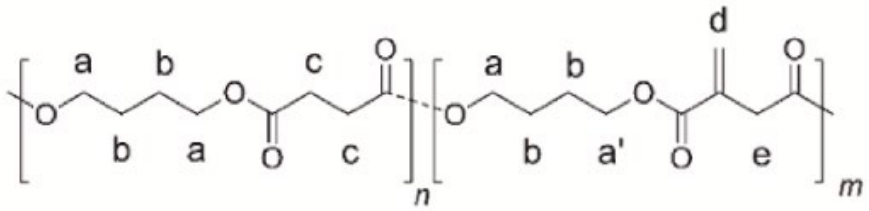

Table 2.4 The chemical shifts of PBSI.

Signal	Chemical shift (ppm)	Measured integral value	Theoretical integral value
b	1.72	1.00	8.00
c	2.73	0.51	4.00
e	3.49	0.18	2.00
a	4.18	0.755	6.00
a’	4.30	0.199	2.00
d	5.75,6.46	0.10,0.10	2.00

3.3.1.2. FT-IR

Fig.3. shows the FT-IR spectra of PBSI, LP-3, EDT, PBSI-LPs, and PBSI-EDT-11 films. LP-3 and EDT exhibit a very weak absorption band at approximately 2550 cm^{-1} due to SH stretching vibration (ν_{SH}). The ν_{SH} band at the same wavenumber could not be identified for all crosslinked films. However, the presence of the remaining thiol groups could not be determined, because the ν_{SH} bands of LP-3 and EDT were very weak. In the FT-IR spectrum of PBSI, a strong absorption band at 1712 cm^{-1} and a weak absorption band at approximately 1634 cm^{-1} were attributed to the ester C=O stretching vibration ($\nu_{C=O}$) and the C=C stretching vibration ($\nu_{C=C}$) of the itaconate unit, respectively. The fact that intensities of the $\nu_{C=C}$ bands of PBSI-LP-11, PBSI-LP-12, and PBSI-EDT-11 were lower than those of PBSI suggests that the exomethylene groups of PBSI reacted. Nonetheless, it was difficult to determine the C=C unit conversion because the $\nu_{C=C}$ band was very broad and weak.

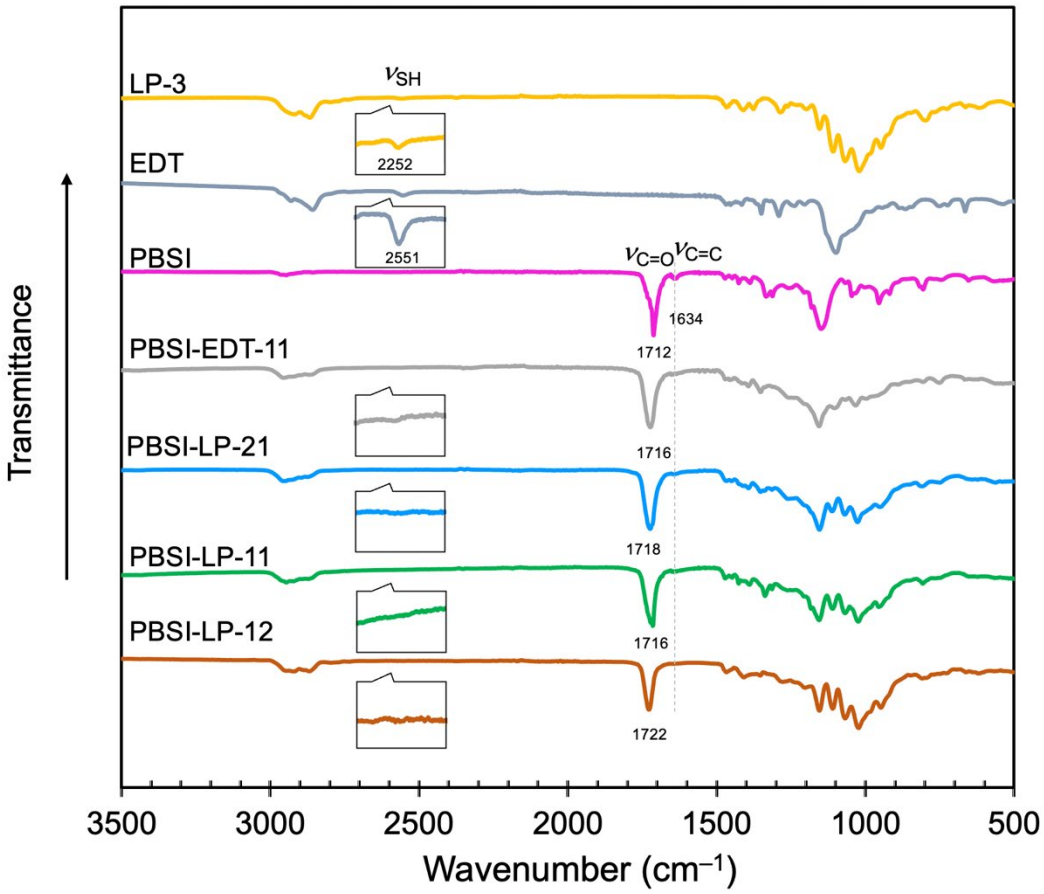

Fig.3. FT-IR spectra of LP-3, EDT, PBSI, PBSI-LPs, and PBSI-EDT-11.

3.3.1.3. The formation of the network structure and the change in cross-linking density

The formation of the network structure and the changes in cross-linking density of PBSI-LPs and PBSI-EDT-11 were studied by analyzing the gel fraction and degree of swelling in acetone, as shown in Fig.4. The degree of swelling increased as follows: PBSI-EDT-11 < PBSI-LP-21 < PBSI-LP-11 < PBSI-LP-12, indicating that the crosslinking density decreased in the same order. The fact that the degree of swelling of PBSI-EDT-11 was lower than that of PBSI-LPs could be attributed to the shorter distance between crosslinking points in PBSI-EDT-11, as a result of the lower molecular weight of EDT than that of LP-3.The difference in crosslinking densities of PBSI-LPs may be explained by the fact that the functionality (SH) of LP-3 was 2, which is significantly lower than that of PBSI (C=C, ca. 12), and the content of LP-3 with a lower functionality increases in the following order: PBSI- LP-21 < PBSI-LP-11 < PBSI-LP-12.

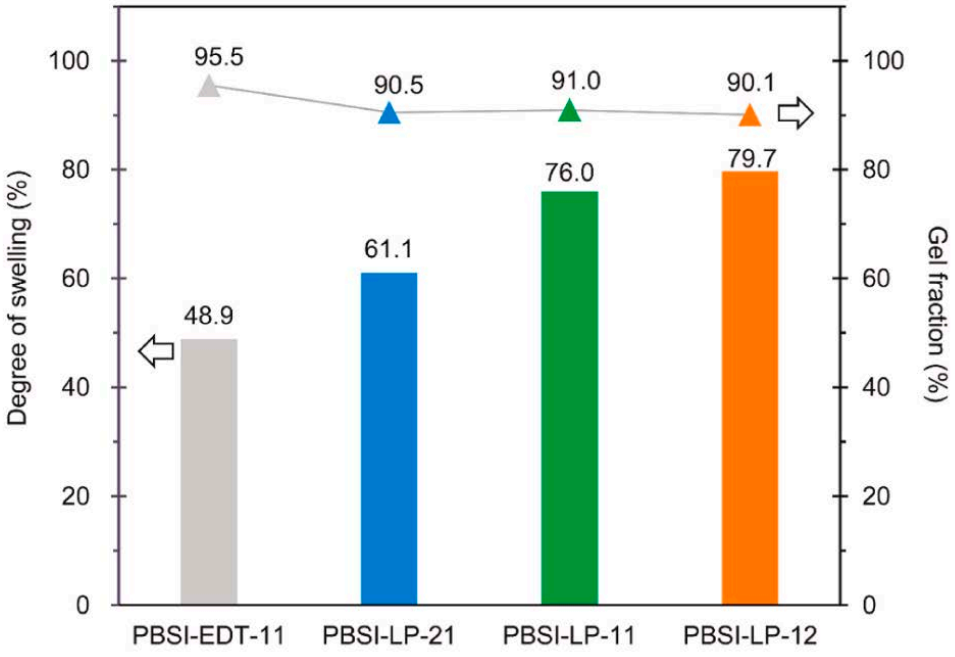

Fig.4. The gel fraction and degree of swelling of PBSI-LPs and PBSI-EDT-11.

3.3.2. Thermal properties of PBSI-LPs and PBSI-EDT crosslinked films

3.3.2.1. DSC

The first heating DSC curves of PBSI, PBSI-LPs and PBSI-EDT-11 are shown in Fig.5. The T_g of PBSI was −29.8 °C, and the two T_m of the polybutylene itaconate and polybutylene succinate units were observed at 48.7 °C and 72.9 °C, respectively. All PBSI-LPs exhibited a single T_g that decreased with increasing LP-3 content, indicating that the T_g (−63.8 ℃) of LP-3 is significantly lower than that of PBSI. This result suggests that the compatibility of the PBSI and LP-3 segments is good. In addition, the ΔH_m values of PBSI- LPs were significantly lower than those of PBSI and decreased as the LP-3 fraction increased. This is due to the formation of a crosslinked structure and the compatibilization of the PBSI and LP-3 segments. The T_g of PBSI-EDT-11 (−27.4 ℃) was higher than that of PBSI-LP-11 (−40.4 ℃), indicating that the distance between the crosslinking points in PBSI-EDT-11 was significantly smaller than that in PBSI-LP-11, i.e., the crosslinking density of PBSI-EDT-11 was higher than that of PBSI-LP-11. Furthermore, the T_m of the PBSI-EDT-11 11 was not detected by DSC analysis.

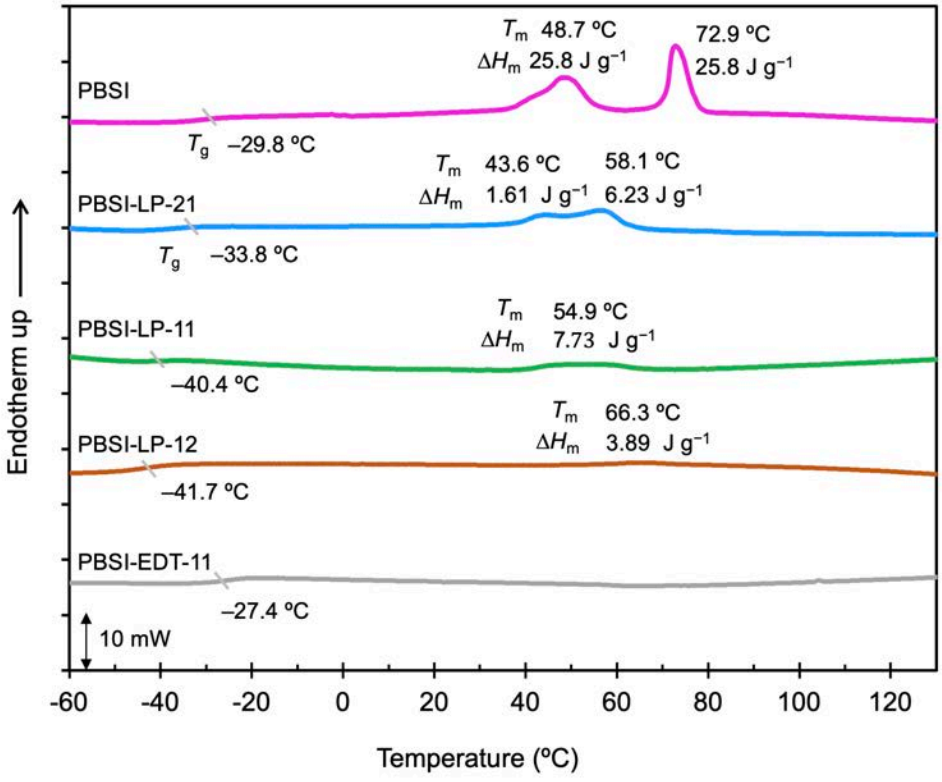

Fig.5. DSC curves of PBSI-LPs and PBSI-EDT-11.

3.3.2.2. DMA

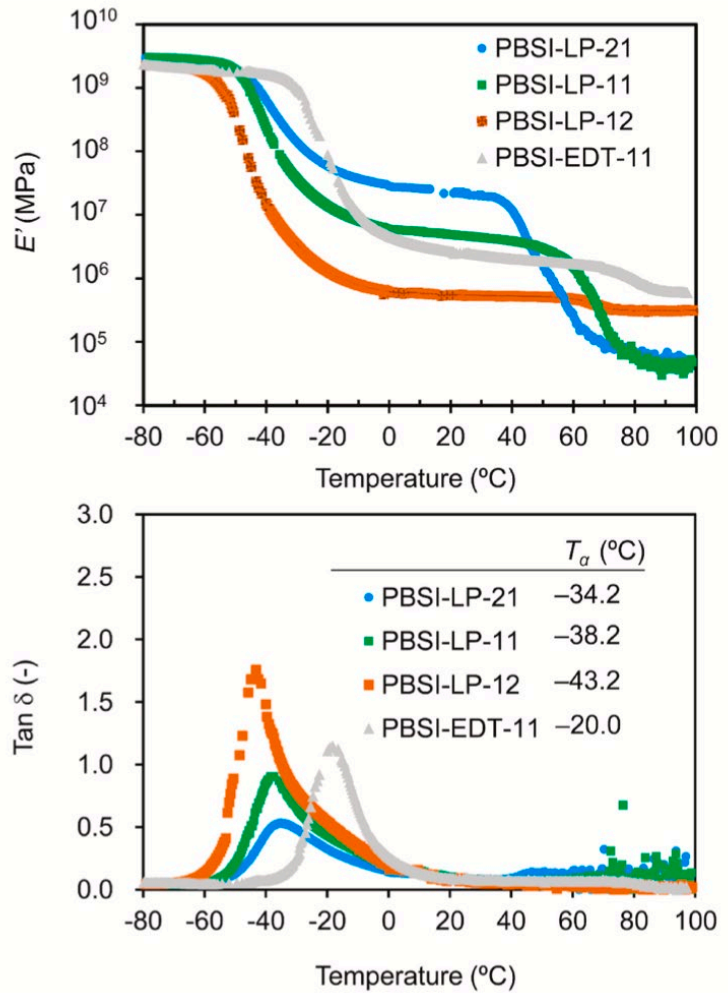

Fig.6. DMA curves of PBSI-LPs and PBSI-EDT-11.

Fig.6. shows DMA curves of the PBSI-LPs and PBSI-EDT-11. In accord with the DSC results, the tan δ peak temperature (T_α) of PBSI-LPs decreased with increasing LP-3 feed fraction and was lower than that of PBSI-EDT-11. According to the DSC experiments, the tan δ peak height of PBSI-LPs increased with increasing LP-3 feed fraction in accordance with the decreasing order of crystallinity (that is, the increasing order of the amorphous region). Two distinct drops in the storage modulus (*E'*) were observed in all crosslinked films. The lower temperature *E'* drop appears to have been caused by glass transition, while the higher temperature *E'* decrease appears to have been caused by the melting of the crystalline PBSI segments. The degree of *E'* reduction at a higher temperature region for PBSI-LPs decreased with increasing LP-3 fraction and

decreasing crystallinity. In addition, all films exhibited the *E'* rubbery plateau region between 10 ℃ and 30 ℃, indicating the formation of a network structure. In accordance with the results of the degree of swelling, the *E'* values in the plateau region for PBSI-LPs decreased as the LP-3 fraction increased. However, the *E'* value of PBSI-EDT-11 at approximately 20 ℃ was lower than that of PBSI-LP-21 and PBSI-LP-11. This result may be due to the possibility that the affinity of PBSI-EDT and PBSI-LPs for the acetone used in the swelling test is different. Furthermore, when the *E'* values at approximately 90 ℃ for each crosslinked film were compared, PBSI-EDT had the highest *E'* value. The T_m of PBSI-EDT-11 was not detected by DSC analysis but can observe its T_m at approximately 80 ℃ in DMA analysis.

3.3.2.3. TGA

The TGA curves of PBSI-LPs and PBSI-EDT-11 are shown in Fig. 7. Table 3 showed $T_{dx\%}$ (x = 5, 10, and 50). The $T_{dx\%}$ of PBSI-LP-11 was significantly lower than that of PBSI-EDT-11, indicating that the disulfide bonds in the LP-3 segments are lower thermal stability than the ether bonds in the EDT segment. The $T_{dx\%}$ of PBSI-LPs decreased as the LP-3 feed fraction increased. This result was due to the lower crosslinking density and thermal stability of LP-3 segments compared to PBSI segments.

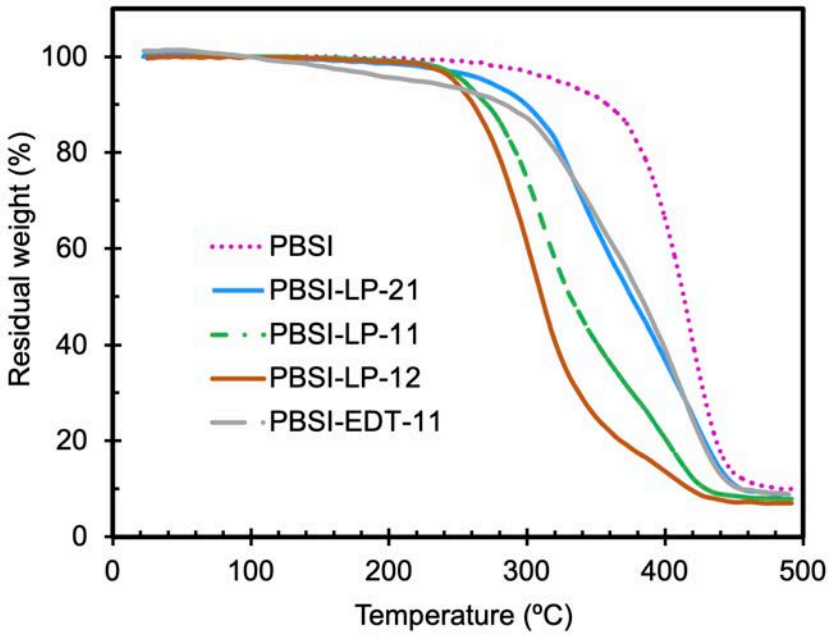

Fig.7. TGA curves of PBSI-LPs and PBSI-EDT-11.

Table 3. $T_{dx\%}$ of PBSI-LPs and PBSI-EDT-11.

Sample	$T_{d5\%}$(°C)	$T_{d10\%}$(°C)	$T_{d50\%}$(°C)
PBSI	366	377	418
LP	288	298	331
EDT	131	144	186
PBSI-LP-21	313	324	393
PBSI-LP-11	275	286	344
PBSI-LP-12	262	271	316
PBSI-EDT-11	307	321	399

3.3.3. Mechanical properties of PBSI-LPs and PBSI-EDT-11

Fig.8 shows tensile strengths, tensile moduli, and elongations at break obtained from the stress-strain curves of PBSI-LPs and PBSI-EDT-11. Tensile strengths and moduli of PBSI-LPs decreased as the LP-3 fraction increased, indicating a decrease in crosslinking density and an increase in flexible LP-3 segments. The elongation at break of PBSI-LPs increased in the following order: PBSI-LP-21 < PBSI-LP-12 < PBSI-LP-11. The lower elongation at break of PBSI-LP-12 compared to PBSI-LP-11 may be attributable to the presence of branched polymers in which the excess SH groups of LP-3 did not react with the C=C groups of PBSI. PBSI-EDT-11 exhibited superior tensile strength, modulus, and lower elongation at break compared to PBSI-LP-11, indicating a higher crosslinking density in the former than the latter.

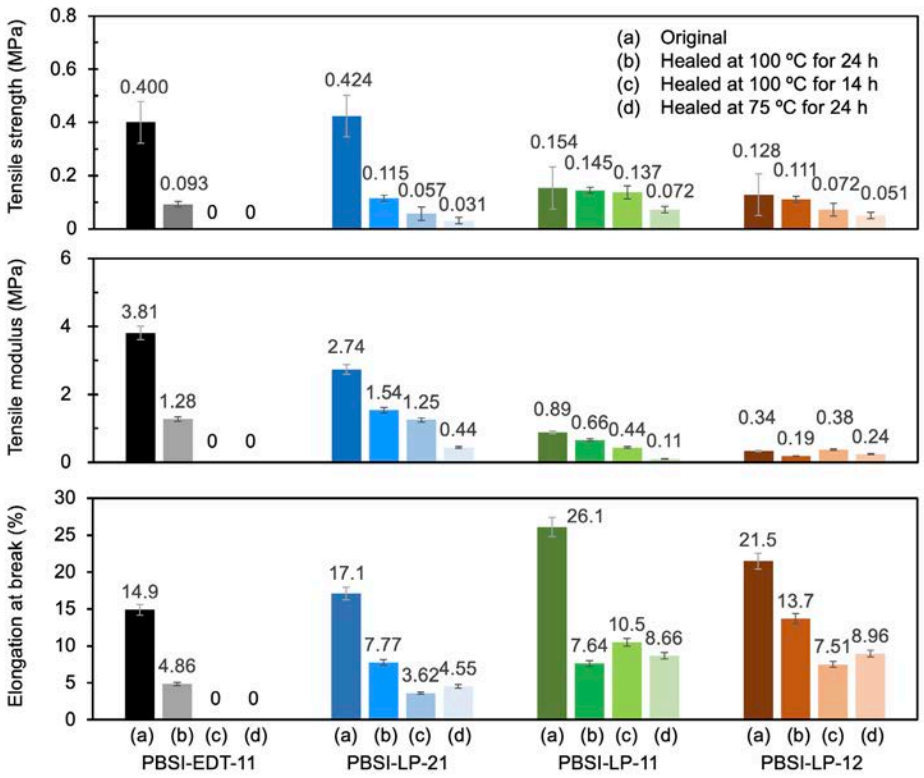

Fig.8. Tensile strengths, tensile moduli, and elongations at break of as-prepared and self-healed PBSI-LPs and PBSI-EDT-11.

3.3.4. Self-healing properties of PBSI-LPs and PBSI-EDT-11

Fig.9 shows the self-healing behavior of the PBSI-LP-11 film. When two cut samples of as-prepared PBSI-LP-11 film were contacted at the cross-section and hot-pressed at 100 ℃ for 24 h, the two pieces adhered to produce a self-healing film (shPBSI-LP-11). Even when loaded with a 50 g weight, the healed sample did not break. With comparable healing treatment, all PBSI-LPs possessed self-healability. The self-healing ability of PBSI-LP-21, PBSI-LP-11, and PBSI-LP-12 were confirmed by hot-pressing at 100 ℃ for 24 h, 100 C for 14 h, and 75 ℃ for 24 h. PBSI-LPs contain 0.5% 1-MI, which was used as a catalyst for the thiol-ene reaction. Since it is known that tributylphosphine and triethylamine catalyze the disulfide metathesis reaction [9], it could not be ruled out that 1-MI in PBSI-LPs promoted the self-healing ability driven by the disulfide metathesis reaction. Furthermore, the self-healing behavior of PBSI-EDT-11 without disulfide bonds was also examined for comparison. However, PBSI-EDT-11 exhibited healing ability only at 100 ℃ for 24 h by the melting and recrystallization of the crystalline phase of the PBSI segment.

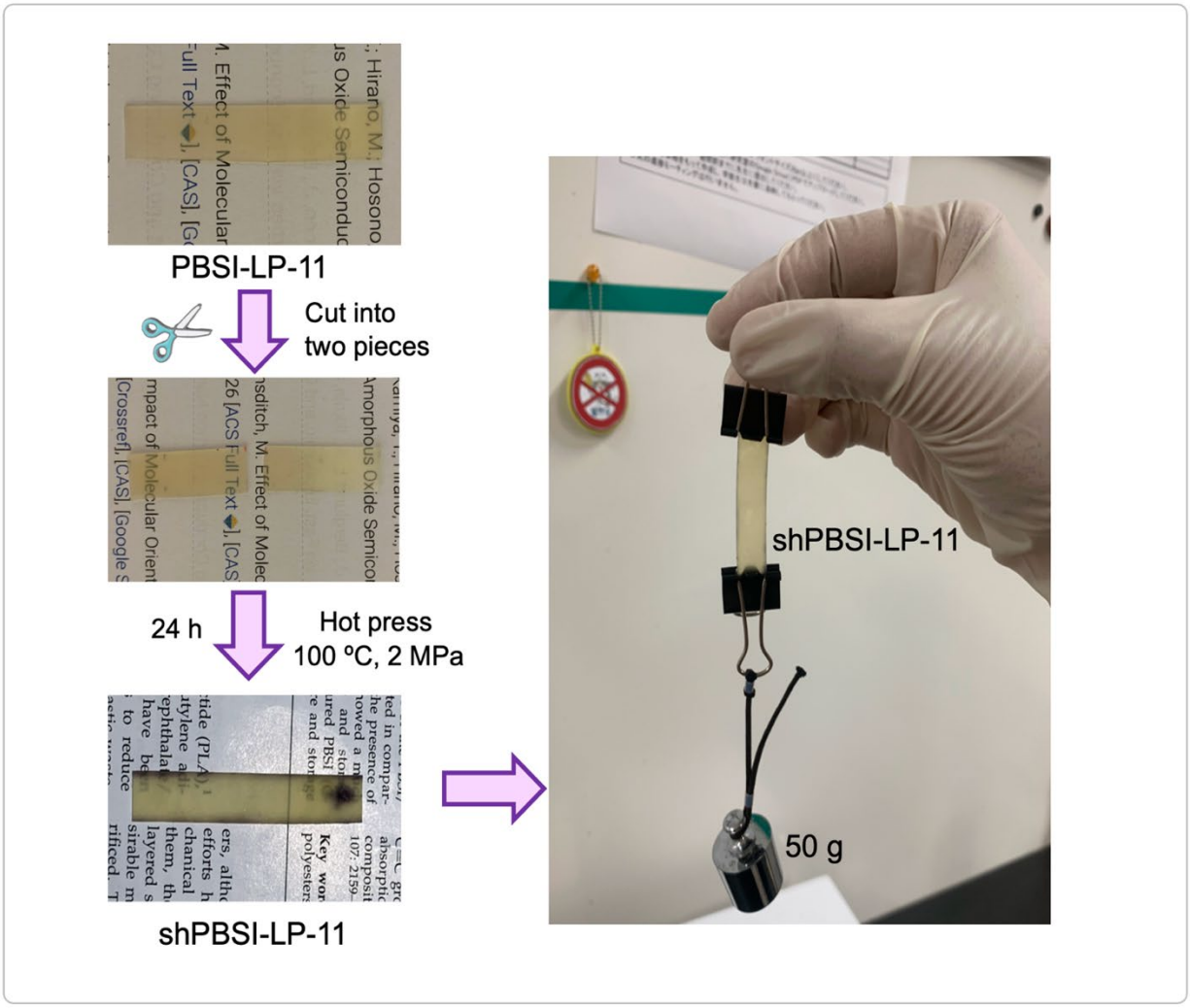

Fig.9. Self-healing behavior of PBSI-LP-11 after hot-pressing at 100 ℃ under 2 MPa.

The stress-strain curves of the original and self-healed PBSI-LPs and PBSI-EDT-11 at 100 ℃ for 24 h, 75 ℃ for 24 h, and 100 ℃ for 14 h are shown in Fig.10. Even though the maximal stresses of all self-healed samples were lower than those of the original samples, the maximal stresses of the self-healed samples increased in the following order: 75 ℃ for 24 h < 100 ℃ for 14 h < 100 ℃ for 24 h. The samples cured at 100 ℃ for 24 h exhibited the highest tensile strength, tensile modulus, and elongation at break, despite some variation in the measured values (Fig.8.).

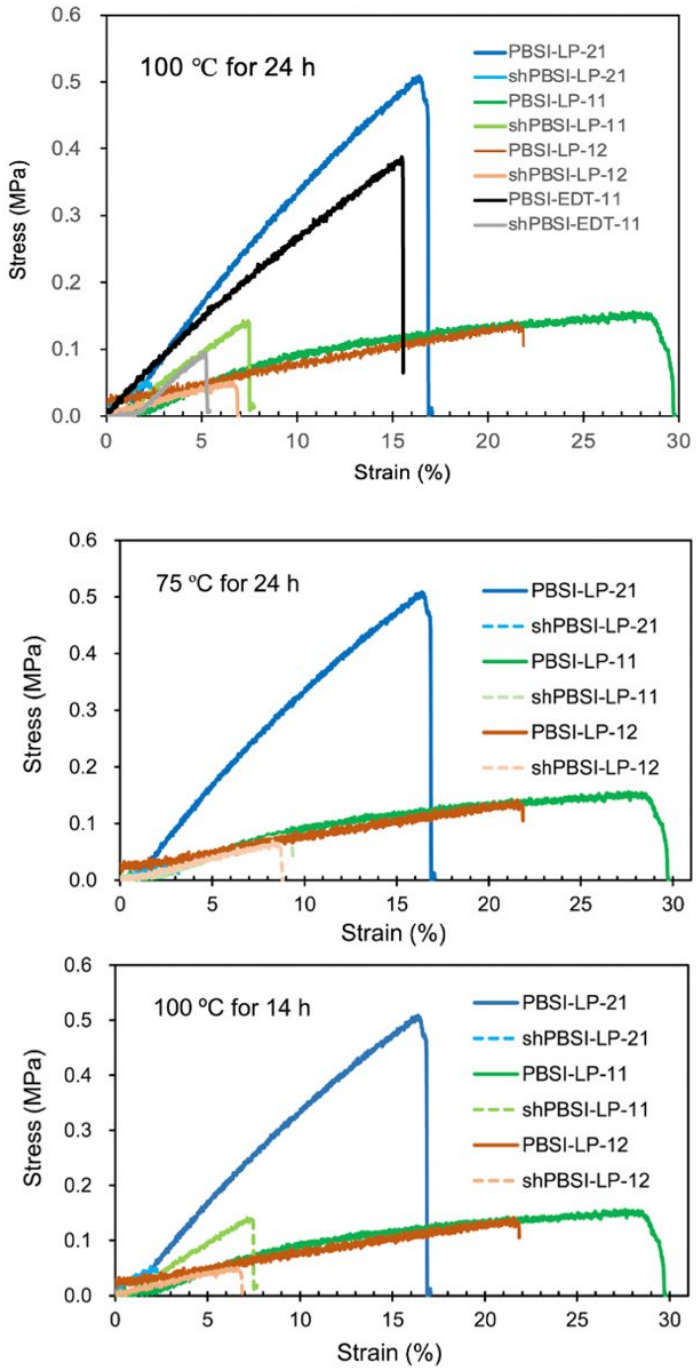

Fig.10. The stress-strain curves of the original and self-healed PBSI-LPs and PBSI-EDT-11 at 100 ℃ for 24 h, 75 ℃ for 24 h, and 100 ℃ for 14 h.

The tensile strengths obtained before and after healing were used to determine the healing efficiencies of all the healed samples, which are shown in Fig.11. The healing efficiencies of PBSI-LP-11 were comparatively higher than those of PBSI-EDT-11, indicating that the introduction of disulfide bonds is a highly efficient method for achieving superior healing properties. The small extent of healability observed in PBSI-EDT-11 may be attributed to the melting of the crystalline phase and its subsequent rearrangement upon cooling. The healing efficiency increased as follows: PBSI-LP-21 < PBSI-LP-12 < PBSI-LP-11. The lower healing efficiency of PBSI-LP-12 with a higher LP-3 fraction than that of PBSI-LP-11 may be due to the following factor: PBSI-LP-12, which has a lower crystallinity than that PBSI-LP11, contributes less to the healing ability through crystalline region melting and recrystallization. The fact that PBSI-LP-11, with lower crystallinity than PBSI-LP-21, exhibited a significantly higher healing efficiency than those of PBSI-LP-21 suggests that the contribution of disulfide bonds to the ability to heal is crucial. Regarding healing conditions, the healing efficiency of PBSI-LPs decreased as follows: 100 ℃ for 24h >100 ℃ for 14h > 75 ℃ for 24h. Because disulfide metathesis reaction and melting of the crystalline region are promoted at a higher temperature, the treatment at 100 ℃ for 14 h resulted in a higher healing efficiency than 75 ℃ for 24 h.

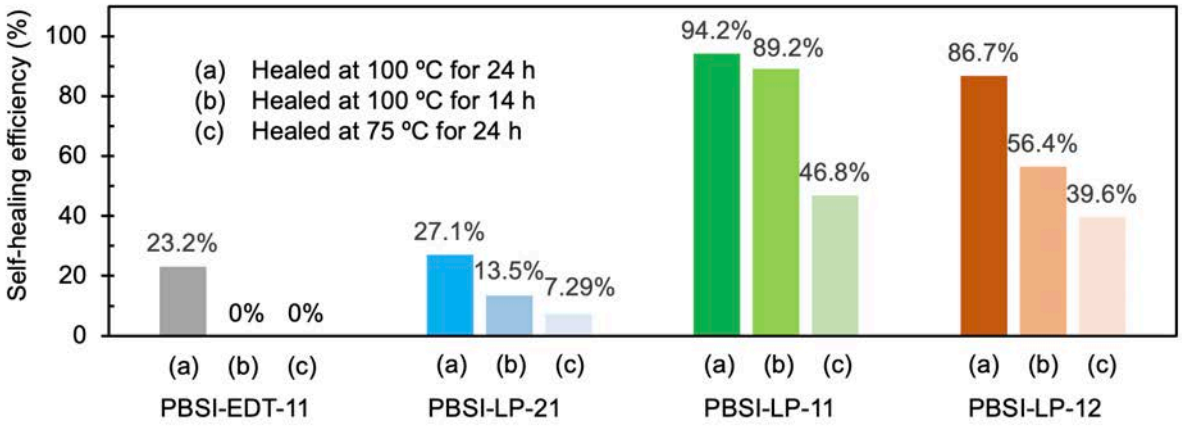

Fig.11. Healing efficiencies of all the self-healed samples.

3.4. Conclusions

Polyester network films containing disulfide bonds (PBSI-LP-21, 11, and 12) were produced by the thermal thiol-ene reaction of PBSI and LP-3 at C=C/SH ratios of 2/1, 1/1, and 1/2, respectively. In addition, the thermal, mechanical, and self-healing properties of PBSI-LPs were compared to those of a polyester network film (PBSI-EDT-11) prepared by reacting PBSI and EDT without disulfide bonds. As the crosslinking density increased, $T_{dx\%}$ (x = 5, 10, and 50), T_g, T_α, tensile strength, and tensile modulus increased for PBSI-LPs as the C=C/SH ratio increased. PBSI-EDT-11 showed higher $T_{dx\%}$, T_g, T_α, tensile strength, and tensile modulus compared to PBSI-LP-11 as a result of the difference in crosslinking density. PBSI-LPs exhibited healing properties when pressed at 100 ℃ for 14～24 h and 75 ℃ for 24 h. For samples healed at 100 ℃ for 24h, PBSI-LP-11 demonstrated the highest healing efficiency (94.2%), which was significantly higher than PBSI-EDT-11 (23.2%), proving the efficiency of incorporating disulfide bonds into the polymer. PBSI-LP-11 proved to be a promising material with superior healing properties. In addition, because PBSI can be synthesized from renewable resources and its PBS segments are biodegradable and biocompatible, it is expected that PBSI-LP-11 could be used as an environmentally friendly and healing biomaterial.

3.5. References

[1] S. RameshKumar, P. Shaiju, K. E. O'Connor, and R. B. P, "Bio-based and biodegradable polymers - State-of-the-art, challenges and emerging trends," *Curr. Opin. Green Sustain. Chem.*, vol. 21, pp. 75–81, Feb. 2020, doi: 10.1016/j.cogsc.2019.12.005.

[2] S. Lambert and M. Wagner, "Environmental performance of bio-based and biodegradable plastics: the road ahead," *Chem. Soc. Rev.*, vol. 46, no. 22, pp. 6855–6871, 2017, doi: 10.1039/C7CS00149E.

[3] J. P. Brutman, P. A. Delgado, and M. A. Hillmyer, "Polylactide Vitrimers," *ACS Macro Lett.*, vol. 3, no. 7, pp. 607–610, Jul. 2014, doi: 10.1021/mz500269w.

[4] K. Sugane, N. Kumai, Y. Yoshioka, A. Shibita, and M. Shibata, "Thermo-responsive alternating conetworks by the Diels-Alder reaction of furan-terminated 4-armed star-shaped ε-caprolactone oligomers and maleimide-terminated 4-armed star-shaped l-lactide oligomers," *Polymer*, vol. 124, pp. 20–29, Aug. 2017, doi: 10.1016/j.polymer.2017.07.038.

[5] S. Cai, Z. Qiang, C. Zeng, and J. Ren, "Multifunctional poly (lactic acid) copolymers with room temperature self-healing and rewritable shape memory properties via Diels-Alder reaction," *Mater. Res. Express.*, vol. 6, no. 4, p. 045701, 2019.

[6] Z. Wang, H. Yang, B. D. Fairbanks, H. Liang, J. Ke, and C. Zhu, "Fast self-healing engineered by UV-curable polyurethane contained Diels-Alder structure," *Prog. Org. Coat.*, vol. 131, pp. 131–136, 2019.

[7] T. Ikezaki, R. Matsuoka, K. Hatanaka, and N. Yoshie, "Biobased poly(2,5-furandimethylene succinate- *co* -butylene succinate) crosslinked by reversible Diels–Alder reaction," *J. Polym. Sci. Part A: Polym. Chem.*, vol. 52, no. 2, pp. 216–222, Feb. 2014, doi: 10.1002/pola.26990.

[8] N. Teramoto, M. Ozeki, I. Fujiwara, and M. Shibata, "Crosslinking and biodegradation of poly(butylene succinate) prepolymers containing itaconic or maleic acid units in the main chain," *J. Appl. Polym. Sci.*, vol. 95, no. 6, pp. 1473–1480, Mar. 2005, doi: 10.1002/app.21393.

[9] S. Nevejans, N. Ballard, J. I. Miranda, B. Reck, and J. M. Asua, "The underlying mechanisms for self-healing of poly(disulfide)s," *Phys. Chem. Chem. Phys.*, vol. 18, no. 39, pp. 27577–27583, 2016, doi: 10.1039/C6CP04028D.

Summary of Contributions

In recent years, environmental pollution caused by the plastic wastes to be discorded in a large quantity and ecological destruction of marine organisms caused by microplastics (plastic fragments less than 5 mm) is becoming a significant social problem. As one means for solving the above problems, biodegradable polyesters, which can be finally decomposed into carbon dioxide and water, are gathering considerable attention. Several biodegradable plastics are biomass-derived polymers (biobased polymers). Especially, the research and development of biodegradable/biobased PLA and PBS contributing to the preservation of oil resources and suppressing global warming are actively carried out. However, one of the drawbacks of PLA is the brittle fracture behavior. In contrast, biodegradable/petroleum-based PCL exhibits a much higher elongation at break (>300%) than PLA (ca. 3%), whereas PCL has a much lower melting temperature (ca. 60 °C) and tensile strength (ca. 20 MPa) than those of PLA (ca.170 °C, ca. 50 MPa). In chapter 1, the improvement of thermal and mechanical properties in addition to the compatibility of the PLA and PCL segments was investigated by changing the ratio of PLA/PCL segments of crosslinking comb-shaped polymers. Recently, as polymer materials reducing environmental load, self-healing polymers having the ability to repair physical damage and cracks, thereby leading to the extension of their lifetime and effective use of resources, are attracting the most attention in addition to biodegradable and biobased polymers. In chapter 2, the introduction of disulfide bonds into the conetworks consisting of 6-armed star-shaped L-lactide and ε-caprolactone oligomers was investigated to provide the self-healing properties driven by the disulfide metathesis reaction. In chapter 3, for biodegradable/biobased PBS having intermediate thermal and mechanical properties of PLA and PCL, disulfide-containing PBS-based network polymers were prepared, and their thermal, mechanical, and self-healing properties were investigated. A more detailed overview of each chapter is described below.

In chapter 1, first, methacrylate-terminated L-lactide and ε-caprolactone oligomers (MALLAO and MACLO) were synthesized by the ring-opening polymerizations of L-lactide (LLA) and ε-caprolactone (CL) initiated with hydroxyethyl methacrylate. Next, the radical copolymerizations of butyl methacrylate/MALLAO and butyl methacrylate/MACLO in a molar ratio of 8/2 generated comb-shaped polymers grafted with hydroxy-terminated lactide and ε-caprolactone oligomers (PBML and PBMC). The crosslinking reaction of PBML/PBMC (weight ratios: 100/0, 75/25, 50/50, 25/75, and 0/100) and hexamethylene diisocyanate (HDI) produced polyurethane networks (PUN-BML/Cs). Analyses of FT-IR spectra and gel fractions verified the formation of a polyurethane network structure. PUN-BML/C 100/0 and PUN-BML/C 0/100 had significantly

higher glass transition and 5% weight loss temperatures (T_g and $T_{d5\%}$) than PBML and PBMC, respectively. The results of scanning electron microscopy (SEM) and dynamic mechanical analysis (DMA) revealed that the oligolactide (LAO) and oligocaprolactone (CLO) segments of PUN-BML/C 75/25, 50/50, and 25/75 conetworks are partially miscible but not fully miscible. In addition, the tensile strength and modulus of PUN-BML/Cs increased with increasing feed PBML content, and PUN-BML/C 75/25 exhibited the highest elongation at break and tensile toughness. It is also noted that this study is the first example of crosslinked comb-shaped polymers.

In chapter 2, hydroxy-terminated 6-armed star-shaped L-lactide and ε-caprolactone oligomers (H6LAO and H6CLO) were synthesized by the ring-opening polymerization reactions of LLA and CL initiated with dipentaerythritol. The disulfide-containing polyester-urethane networks (PN-LC*xy*-DS*z*, weight ratios of H6LAO/H6CLO: *x*/*y* = 1/0, 3/1, 1/1, 1/3, and 0/1, BHEDS/(H6LAO + H6CLO) molar ratios: *z* = 0, 1, and 3) were prepared by the reaction of H6LAO, H6CLO, and bis(2-hydroxyethyl) with HDI. The FT-IR and gel fraction analyses demonstrated that the urethanization reaction proceeded smoothly to form polymer networks. Furthermore, according to the differential scanning calorimetric analysis of PN-LC*xy*-DS*z*s, the CLO segments are crystallized, whereas the LAO segments are not. SEM and DMA results revealed that the LAO and CLO segments of PN-LC31-DS1 are fully compatible and that the conetwork compatibility worsens as the CLO fraction increases. The cut lines on PN-LC*xy*-DS1 (*xy* = 10, 31, 11, and 13) films healed after 24 h at room temperature. Especially, PN-LC31-DS1 demonstrated the highest healing efficiency for tensile strength (98.5%). The cut lines provided to PN-LC10-DS0 and PN-LC01-DS0 without disulfide bonds were not healed at all. It is also noted that this study is the first example of self-healing PLA-based network polymers driven by the disulfide metathesis.

In chapter 3, the nucleophilic thiol-ene reaction of poly(butylene succinate-*co*-butylene itaconate) (PBSI) and a thiol-terminated polyether (LP-3) containing disulfide linkages at C=C/SH ratios of 2/1, 1/1, and 1/2 produced crosslinked polyester networks (PBSI-LPs). For comparison, a PBSI/2,2'-(ethylenedioxy) diethanethiol crosslinked polymer (PBSI-EDT-11, C=C/SH = 1/1) without disulfide bonds was prepared. The crosslinking density, $T_{dx\%}$ (*x* = 5, 10, and 50), T_g, tensile strength, and tensile modulus of PBSI-LPs increased as the C=C/SH ratio increased. PBSI-LPs exhibited healing properties when pressed at 100 °C for 14–24 h or 75 °C for 24 h. PBSI-LP-11 exhibited the highest healing efficiency (94.2%), which was significantly higher than PBSI-EDT-11 (23.2%), indicating the effectiveness of incorporating disulfide bonds into the polymer. It is also noted that this study is the first example of self-healing PBS-based network polymers driven by the disulfide metathesis.

Consequently, chapter 1 and chapter 2 revealed that the formation of conetwork structure by the crosslinking reactions of comb-shaped and star-shaped LAOs and CLOs is very effective to improve the compatibility, thermal, and mechanical properties. the formation of conetwork structure by the crosslinking reactions of comb-shaped and star-shaped polymers enhanced the compatibility of both components of the PLA-PCL conetwork. The PUN-BML/C 75/25, 50/50, and 25/75 conetworks generated by cross-linking the comb-shaped polymers in chapter 1 are partially miscible and compatible. In contrast, the LAO and CLO chains are almost miscible in the star-shaped polymer cross-linked PLA-PCL conetwork (PN-LC31-DS1) discussed in chapter 2, and the compatibility is evident decreases as the CLO content increases. Regarding the difference in compatibility between comb-shaped and star-shaped polymers, it was revealed that star-shaped polymers had high symmetry and formed a regular network that was highly compatible when both components were cross-linked. In contrast, comb-shaped polymers are less symmetrical than star polymers, forming an irregular network, and the grafted LAO or CLO segments readily aggregate., resulting in less compatibility than star polymers. Furthermore, PUN-BML/C 75/25 (Chapter 1) and PN-LC31-DS1 (Chapter 2) showed the highest elongation at break compared to the single composition. Although it is unknown why a synergistic effect was observed elongation at break, it is considered that the compatibility system (partial compatibility) forms a microphase-separated structure not observed in the homogeneous system and that the entangled flexible and rigid components contribute to the strong interfacial adhesion strength. In this study, the entanglement of the flexible caprolactone and rigid lactic acid components contributes significantly to the elongation at break of the PUN-BML/C 75/25 and PN-LC31-DS1 conetworks. The T_{α}s value due to the glass transition of PUN-BML/C 75/25 and PN-LC31-DS1 conetworks in the DMA analysis was observed at approximately 30 ℃. This reveals that the glass transition occurs precisely at the tensile test temperature. In addition, at the glass transition, tan δ (E''/E') reaches its maximum value. Namely, the loss elastic modulus (E'') indicates a high value, which may contribute to the release of tensile stress as thermal energy. Therefore, the compatibility, thermal, and mechanical properties of the star-shaped polymer crosslinked PLA-PCL conetworks (Chapter 2) were found to be superior to those of the comb polymer crosslinked PLA-PCL conetworks (Chapter 1).

Chapter 2 and chapter 3 revealed that introducing dynamic disulfide bonds into the PLA-PCL conetworks and PBS networks was very effective in attaining excellent self-healing properties. Chapter 2 shows that polyester-urethane network polymers (PN-LC*xy*-DS*z*) with reversible disulfide bond was healed PLA-based networks (PN-LC10-DS1) and PLA-PCL conetworks (PN-LC*xy*-DS1; *xy* = 31, 11, and 13) when left at room temperature. On the other hand, the crystalline

PCL-based network (PN-LC01-DS3) was healed at temperatures above the crystalline phase melting temperature (60 °C). The crystalline PBS-based network (PBSI-LP) in chapter 3 was healed by pressurization (2 MPa) at temperatures 75～100 °C above the crystalline phase melting temperature of the PBSI segment. The self-healing results evaluated in chapters 2 and 3 indicate that introducing a disulfide bond effectively improves the self-healing efficiency of network polymers and that the recombination of the disulfide bond is easier for low T_g material and depends on the softness of the material. In the case of crystalline network polymers, in the temperature variation of storage modulus (*E'*), it was seen that disulfide bond recombination took place after crystalline phase melting (*E'* decrease) of the network polymer. Furthermore, the self-healing efficiency or disulfide bond exchange reaction is enhanced at temperatures above the crystal melting temperature, indicating that melting and recrystallization of the crystalline phase of the polymer contribute to the self-healing property.

In this thesis, we were successful in synthesizing and improving the thermal and mechanical properties, as well as the self-healability driven by the disulfide metathesis reaction, of various polymer networks composed of the polymer chains of the popular biodegradable polyesters polylactic acid (PLA), poly(ε-caprolactone) (PCL), and poly(butylene succinate) (PBS). The developing self-healing materials in this thesis contribute to resource and energy conservation and extend the service life of materials by adding self-healing properties to biodegradable network polymers. Furthermore, even after the materials are used, they will slowly biodegrade if released into the environment, contributing to solving the marine plastic problem. Furthermore, polycaprolactone is a biodegradable polymer derived from petroleum, while polylactic acid (PLA) and polybutylene succinate (PBS) are biodegradable polymers derived from biomass. Therefore, polymers containing PLA and PBS components are carbon-neutral materials and can contribute to the prevention of global warming.

List of Publications

1. Publications

(1) W. Ussama, S. Matsuda, M. Shibata, Synthesis and properties of polyurethane networks composed of comb-shaped polymers grafted with L-lactide and ε-caprolactone oligomers, ***Polymer***, 174, 178-186 (2019) (on line 2019.4.30, Elsevier, 2018/2019 Impact factor: 3.771)

(2) W. Ussama, M. Shibata, Self-healingpolyester-urethanenetworkscomposedof6-armedstar-shaped oligolactide and oligocaprolactone segments and disulfide bonds, ***Journal of Polymer Research***, 28(1),5 (2021) (Online 2021.01.05, Springer Nature, 2020/2021 Impact factor: 3.097).

(3) W. Ussama and M. Shibata, Self-healing polyester networks prepared from poly(butylene succinate-*co*-butylene itaconate) and thiol-terminated polyether containing disulfide linkages, ***Polymer***, 244, 124668 (2022) (Online 2022.02.20, Elsevier, 2021 Impact factor: 4.432)

2. Conferences

a. International conferences

(1) Self-healing polyester networks prepared from poly(butylene succinate-*co*-butylene itaconate) and thiol-terminated polyether containing disulfide linkages, W. Ussama, M. Shibata, POLY-CHAR,Halle-Siegen 2022 (Online, Germany), 2022.05.25

b. Domestic conferences

(1) Synthesis and properties of Polyester-urethane networks by use of comb-shaped polymers processing lactide and caprolactone oligomer chains, W. Ussama, S. Matsuda, T. Shimasaki, N. Teramoto, M. Shibata, 27th SPSJ Polymer Materials Forum, Tower Hall Funabori, 2018.11.21

(2) Synthesis and properties of polyester-urethane networks by use of comb-shaped polymers processing lactide and caprolactone oligomer chains, S. Matsuda, T. Shimasaki, N. Teramoto, M. Shibata, 36th SPSJ Chiba Regional Seminar for Young Researchers, Tokyo University of Science (Noda Campus), 2019.3.11

(3) Self-healabledisulfide-containing polyester urethane networks composed 6-armedstar-shaped polylactide and polycaprolactone, W. Ussama, N. Teramoto, M. Shibata, 28th SPSJ Polymer Materials Forum, Winc Aichi (Nagoya), 2019.11.21

(4) Self-healing polyester networks prepared from poly(butylene succinate-*co*-butylene itaconate) and thiol-terminated polyether containing disulfide linkages, W. Ussama, N. Teramoto, M. Shibata 71st SPSJ Annual Meeting (Online), 2022.05.27

Acknowledgments

"In the name of God, the Merciful, the Compassionate"

I would like to convey all praise to Almighty god, who gave me the inside will and guidance toward the completion of the research. The completion of the research works, and dissertation would only be possible with continuous guidance and contribution from supervisors, friends, and family.

First of all, I would like to express my deepest gratitude to my advisor, Prof. Dr. Mitsuhiro Shibata for the support of my Ph.D. studies at Polymer Chemical Materials Research Laboratory and for starting my journey into the world of Bio-based polymer. I have been fortunate to have an advisor who cared so much about my work and responded promptly to my questions and queries. There would not have been possible without his continued patience and endless support. It is a privilege to work with him and have him as my advisor. His wisdom and experiences will always be the guidance for my future work and life.

I would like to express my heartfelt appreciation to Dr. Kaito Sugane, my senior, for his kind support, motivation, constructive comment, and guidance. He has always been available to advise and provide the ideal solution to all the problems I have faced in my research. I truly appreciate all his help and continuous support.

I also would like to express my most profound appreciation to my committee members, Prof. Dr.Itaru Tsukushi, Prof. Dr. Naozumi Teramoto, Prof. Dr. Hirobumi Shibata, and Prof. Dr. Norifumi Yamamoto, who gave helpful advice and numerous invaluable discussions throughout the doctoral dissertation review committee. I truly appreciate all the essential concepts from their perspectives.

I would like to thank my friends in the lab for all their help and support from beginning to end. I am really lucky to know them all.

I would like to thank Mr. Amir, Dr. Kornkanok, and Asst. Prof. Dr. Yutthasak and Dr. Chayanis, Ms. Waranrach, Ms. Yanika, and all the people who have supported me during the period of my life in Japan for providing wonderful moments, keeping me going through life, and always pushing and encouraging me to get through all obstacles not only in research but also in my personal life.

I owe my sincere gratitude to my parents for supporting my decision to leave the homeland to pursue my Ph.D. in Japan and for their unconditional love, understanding, patience and support throughout my life. In addition, I thank my little sister Nurhana Ussama for taking her time to video call me on the weekends to give me an update on her exciting teenage life.

Last but definitely not least, I would like to thank my husband, Mr. Kamal Baha, for all his help and support in the past ten years. I would not have been able to complete this thesis without his encouragement and support. Thank you so much from the bottom of my heart.

This list is far from exhaustive; I pray for forgiveness from those I did not mention by name and include them in my heartfelt gratitude.